Molecular Simulation of Liquid Crystals

Phase Equilibrium and the Solubility of Gases in Ordered Fluids

Molecular Simulation of Liquid Crystals

Phase Equilibrium and the Solubility of Gases in Ordered Fluids

Proefschrift

ter verkrijging van de graad van doctor
aan de Technische Universiteit Delft,
op gezag van de Rector Magnificus prof. ir. K.C.A.M. Luyben,
voorzitter van het College voor Promoties,
in het openbaar te verdedigen op
vrijdag, 5 februari, 2016 om 12:30 uur

door

Bernardo Andrés OYARZÚN RIVERA

Diplom-Ingenieur, Technische Universtät Berlin,
geboren te Viña del Mar, Chili.

This dissertation has been approved by the

promotor: Prof. dr. ir. T.J.H. Vlugt

Composition of the doctoral committee:

Rector Magnificus,	chairman
Prof. dr. ir. T.J.H. Vlugt,	Technische Universiteit Delft, promotor
Independent members:	
Dr. S.K. Schnell	NTNU: Norges teknisk-naturvitenskapelige universitet
Prof. dr. C. Filippi	Universiteit Twente
Dr. D. Dubbeldam	Universiteit van Amsterdam
Prof. dr. J. Meuldijk	Technische Universiteit Eindhoven
Prof. dr. ir. B.J. Boersma	Technische Universiteit Delft
Prof. dr. D.J.E.M. Roekaerts	Technische Universiteit Delft

This research was supported by the Stichting voor Technische Wetenschappen (Dutch Technology Foundation, STW), applied science division of the Nederlandse organisatie voor Wetenschappelijk Onderzoek (Netherlands Organization for Scientific Research, NWO) and the Technology Program of the Ministry of Economic Affairs. In addition, this work was sponsored by the Stichting Nationale Computerfaciliteiten (National Computing Facilities Foundation, NCF) for the use of supercomputing facilities, with financial support from NWO-EW.

Keywords: Liquid crystals, Molecular Simulation, Monte Carlo, Nematic, Gas solubility

Printed by: Wöhrmann Print Service

Front & Back: B.A. Oyarzún Rivera & I.N. Spînu

Copyright © 2015 by B.A. Oyarzún Rivera

ISBN/EAN 978-94-6186-563-2

An electronic version of this dissertation is available at
`http://repository.tudelft.nl/`.

This thesis is dedicated to my parents
for all their love and support.

Contents

1 Introduction **1**
- 1.1 Background . . . 2
- 1.2 Structured solvents for CO_2 capture. . . . 3
- 1.3 Molecular models for ordered phases . . . 5
- 1.4 Molecular simulation . . . 6
- 1.5 Scope and outline . . . 8

2 Molecular simulation methods for chain fluids **11**
- 2.1 Chain fluids and ordered phases . . . 12
  - 2.1.1 Hard-sphere chain fluids . . . 12
  - 2.1.2 Lennard-Jones chain fluids . . . 13
- 2.2 Order parameters . . . 13
  - 2.2.1 Nematic order parameter . . . 13
  - 2.2.2 Smectic order parameter . . . 14
- 2.3 Monte Carlo simulations . . . 14
  - 2.3.1 Configurational-bias Monte Carlo . . . 14
  - 2.3.2 *NPT* ensemble . . . 15
  - 2.3.3 Gibbs ensemble . . . 16
- 2.4 Expanded Gibbs ensemble . . . 22
  - 2.4.1 *NVT* expanded Gibbs ensemble . . . 23
  - 2.4.2 *NPT* expanded Gibbs ensemble . . . 28
  - 2.4.3 Wang-Landau algorithm . . . 29
- 2.5 Solubility of gases . . . 29
  - 2.5.1 Henry's law . . . 29
  - 2.5.2 Widom's test-particle insertion method . . . 30

3 Liquid crystal phase behavior of hard-sphere chain fluids **33**
- 3.1 Introduction . . . 34
- 3.2 Simulation details . . . 34
- 3.3 Linear hard-sphere chain fluids . . . 36
- 3.4 Partially flexible hard-sphere chain fluids . . . 43
- 3.5 Solubility of hard spheres in hard-sphere chain fluids . . . 47
- 3.6 Conclusions . . . 50

4 Isotropic-nematic phase equilibrium of hard-sphere chain fluids **53**
- 4.1 Introduction . . . 54
- 4.2 Simulation details . . . 54
- 4.3 Linear hard-sphere chain molecules. . . . 55
- 4.4 Binary mixtures of linear hard-sphere chain fluids. . . . 56
- 4.5 Binary mixtures of linear and partially-flexible hard-sphere chain fluids . . . 62
- 4.6 Solubility of hard spheres in hard-sphere chain fluids . . . 64
- 4.7 Conclusions . . . 66

5 Isotropic-nematic phase equilibrium of Lennard-Jones chain fluids 67
5.1 Introduction 68
5.2 Simulation details and theory 69
5.3 Linear Lennard-Jones chains 70
5.4 Partially-flexible Lennard-Jones chains 76
5.5 Binary mixture of linear Lennard-Jones chains 76
5.6 Solubility of gases in Lennard-Jones chains 79
5.7 Conclusions 81

Bibliography 83

Summary 93

Samenvatting 95

Curriculum Vitæ 97

List of Journal Publications 99

Acknowledgement 101

1

Introduction

The phase behavior of liquid crystals and the solubility of gases in them are studied in this thesis using molecular simulation techniques. The aim of this study is twofold: (1) to provide a basic understanding of molecular principles behind the phase behavior of liquid crystals and the solubility of gases in them, and (2) to contribute with state-of-the-art simulation data on the liquid crystal phase behavior of chain fluids. The importance of this study is rooted on the potential use of liquid crystals as solvents for CO_2 capture. Results obtained in this work are used to understand the effect of molecular structure on gas solubility. Furthermore, simulation data is used to validate a recently developed equation of state for nematic liquid crystal phases. The nature of liquid crystal phases and the principle behind their use as solvents for CO_2 capture is shown in section 1.1 and section 1.2 respectively. Molecular models used for the simulation of liquid crystals together with an introduction to molecular simulation techniques are presented in section 1.4. Finally, the outlook and scope of this thesis are described in section 1.5.

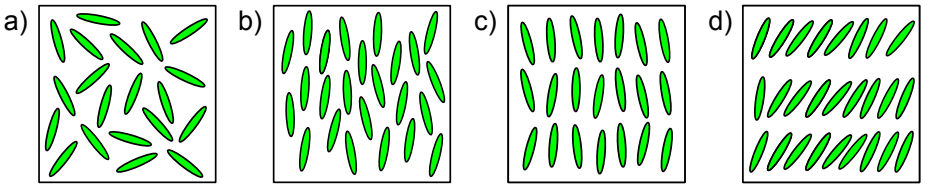

Figure 1.1: Schematic representation of liquid crystal phases: a) Isotropic, b) Nematic, c) Smectic-A, d) Smectic-C.

1.1 Background

Liquid crystals are fluids with a certain degree of molecular order between the liquid and the crystal state [1]. Liquid crystal phases are identified depending on the orientational and positional order of their constituents. Fig. 1.1 shows schematically liquid crystal phases with their molecular ordering and classification. In the isotropic phase (*Iso*), molecules are distributed randomly in space without any preferred long-range orientational nor positional order. In the nematic phase (*Nem*), molecules are oriented around a preferred direction but with positions randomly distributed in space. The preferred direction that molecules follow in the nematic phase is defined as the nematic director (**n**). In smectic phases, molecules are distributed in layers showing both long-range orientational (nematic ordering) and positional order. In smectic-A phases (*SmA*), the nematic director and the normal vector of the smectic layers lay in parallel directions. In smectic-C phases (*SmC*) the nematic director is tilted with respect to the normal vector of the smectic layers.

Molecular order in liquid crystal phases is a consequence of the balance between translational and orientational entropy. In the transition from the isotropic to the nematic phase, the entropy loss by the formation of an orientational ordered phase is more than compensated by the gain in translational entropy. The orientational ordering of molecules in the nematic phase allows an increase in the number of accessible translational configurations for the molecules in the fluid. A similar argument can be used to explain the formation of smectic phases.

A necessary condition for the emergence of liquid crystal phases is shape anisotropy, *i.e.* molecular elongation and rigidity [1, 2]. Typically, liquid crystal molecules showing nematic and smectic phases have a backbone formed by two or more aromatic (or aliphatic) rings (rigid core) decorated with terminal groups which can vary from monoatomic substituents to long alkyl chains (flexible tail) [2]. As an example, Fig. 1.2 shows the molecular structure of the nematic forming 4-trans-4-pentyl-cyclohexyl-benzonitrile (PCH5).

The molecular order of liquid crystal phases confers specific physical properties to these fluids. For instance, circularly birefringence of twisted nematic liquid crystals is widely used for modulating light polarization in visual display devices [3]. Strong intermolecular interactions in a nematic electron-donor liquid crystal fluid can improve charge mobility in organic photovoltaic cells [4]. Ordering in liquid crystal complexes can modulate the immune response in dendritic cells [5]. Of particular interest for this thesis is the solubility of gases in liquid crystals and their use as solvents for gas separation applications [6–10].

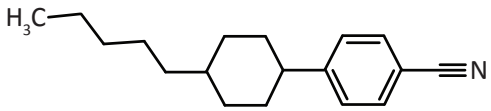

Figure 1.2: Liquid Crystal 4-(trans-4-Pentylcyclohexyl) Benzonitrile (PCH5). Transition temperatures at 1 atm: solid-nematic $T^{S\text{-}N}$=303.05 K, nematic-isotropic $T^{N\text{-}I}$=328.14 [11].

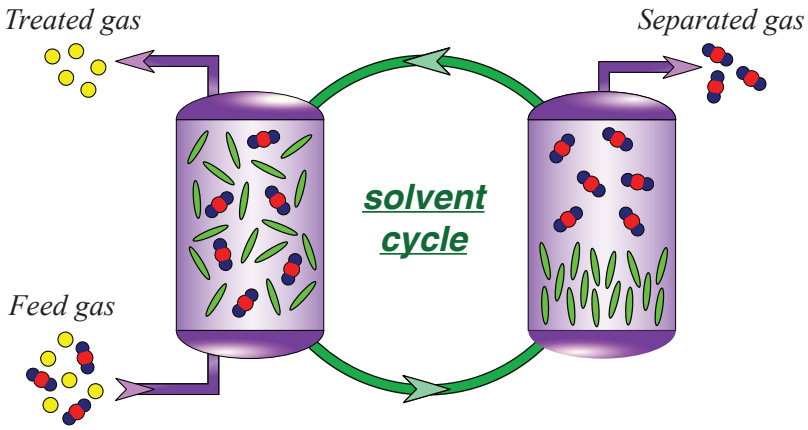

Figure 1.3: Schematic representation of an absorption-desorption process for the separation of gases with liquid crystal solvents. In the absorption stage (left), the gas of interest is separated from a mixture of gases by the liquid crystal solvent. In the desorption stage (right), the liquid crystal solvent is cooled down for a phase transition to an ordered phase, releasing the separated gas. The depleted solvent is recirculated to the absorption stage to complete the solvent cycle.

1.2 Structured solvents for CO_2 capture

The fluid-fluid transition from the isotropic to the nematic phase causes a sudden drop in the solubility of gases in liquid crystal fluids [7, 12, 13]. This phase change is associated with a very low enthalpy of transition $\Delta H^{N\text{-}I}$~1−10 kJ/mol, taking place at a broad range of temperature and pressure conditions [14]. Moreover, liquid crystals are scarcely volatile with reported vapor pressures as low as 0.1−10 Pa at relatively high temperatures ~373 K [15]. Gas solubility and physical properties of liquid crystal fluids have attracted the attention to their use as new solvents for CO_2 capture processes [6, 7, 16]. Furthermore, the rich phase behavior observed in liquid crystals fluids offers the potential of highly tailorable solvents [14, 15].

Fig. 1.3 shows schematically the use of liquid crystals as solvents for gas separation in an absorption-desorption process. Absorption-desorption processes are widely used in the chemical industry and represent the reference scheme for post-combustion CO_2 capture processes [17, 18]. In the absorption stage, CO_2 is separated from a gas mixture by the liquid crystal solvent in its isotropic state. In the desorption stage, a temperature drop causes a phase change of the liquid crystal fluid from its isotropic to the nematic state reducing the solubility of the gas in the fluid. This temperature drop originates a two-phase region of the separated gas and the depleted liquid crystal solvent. The depleted solvent is heated up and recirculated to the absorption column in its isotropic state completing the solvent

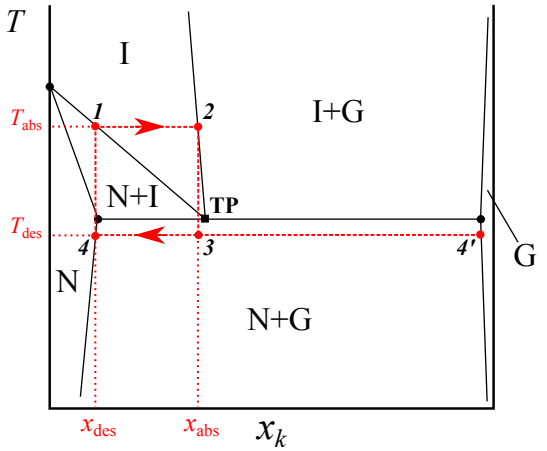

Figure 1.4: Schematic phase diagram, temperature T *vs.* solute composition x_k, for a gas solute k diluted in a liquid crystal solvent. Isotropic (I), nematic (N) and gas phase (G) are single-phase regions. Two-phase regions are identified with a plus sign. Numbers and dashed lines represent the solvent cycle of a simplified absorption-desorption process: *(1)-(2)* absorption, *(3)-(4)* desorption, the gas is separated at *(4')*. T_{abs} is the temperature in the absorption stage and T_{des} is the temperature in the desorption stage. x_{abs} is the mole fraction of the solute in the loaded liquid crystal solvent after absorption. x_{des} is the mole fraction of the solute in the depleted liquid crystal solvent after desorption. TP is the gas-isotropic-nematic triple point.

cycle. The energy consumed in this process is principally due to: (1) cooling of the solvent in the desorption stage for the phase transition from the isotropic to the nematic phase Q_{cooling}; (2) heating up the solvent after the desorption stage for recovering the isotropic phase Q_{heating}; and (3) the energy required for a pump to recirculate the solvent W_{pump}. The solvent performance is defined as the energy consumed in the process per amount of solvent used in the cycle $(Q_{\text{cooling}} + Q_{\text{heating}} + W_{\text{pump}})/m_{\text{solvent}}$ [19]. It can be observed that the total energy consumption, and therefore the solvent performance, depends directly on the amount of solvent recirculated. A larger solubility difference of the gas between the absorption (isotropic) and desorption (nematic) stages reduces the amount of solvent employed in the cycle, improving the performance of the solvent. The solubility difference between the isotropic and the nematic phase can be used as an indication of the performance of liquid crystal solvents in an absoprtion-desorption process.

In Fig. 1.4, the absorption-desorption process is shown together with a schematic phase diagram for the mixture of gas solute with a liquid-crystal solvent. The solvent cycle is represented by the dashed lines. The stages of the solvent cycle are represented as follows: *(1)-(2)*: the gas is absorbed in the isotropic liquid crystal solvent at constant temperature T_{abs} until the solvent is saturated with the gas at a concentration x_{abs}. *(2)-(3)*: the solvent loaded with the gas is cooled down to the desorption temperature T_{des} below the triple point (TP) to promote a phase split between a nematic and a gas phase. *(3)-(4)*: the gas is separated in the gas phase (4') from the depleted liquid crystal solvent in the nematic phase (4) with a remaining gas concentration of x_{des}. *(4)-(1)*: the depleted solvent is heated up from T_{des} to T_{abs} for a phase change in the solvent from the nematic to the isotropic phase and in that state it is recirculated back to the absorption stage. The solubility difference

x_{abs} - x_{des} is directly related to the performance of the solvent as stated before.

Determining the solubility difference $x_{abs} - x_{des}$ would require the knowledge of a large part of the phase diagram for a specific liquid crystal solvent and solute (as schematically represented in Fig. 1.4). However, a similar indication of the solvent performance can be obtained from the width of the isotropic-nematic region. In this work, the width of the isotropic-nematic region, *i.e.* the isotropic-nematic solubility difference, is used as a simple criteria for comparing the potential solvent performance of different liquid crystal fluids.

1.3 Molecular models for ordered phases

A certain degree of shape anisotropy is a necessary molecular condition for the appearance of ordered phases [1, 2]. Shape anisotropy introduces anisotropic repulsive and attractive interactions between molecules in a liquid crystal fluid. Repulsive interactions are responsible for excluded volume effects while attractive interactions induce molecular aggregation.

Nematic ordering in a fluid was first predicted by Onsager as early as 1949 considering anisotropic hard repulsive interactions only [20]. Almost a decade later, Maier and Saupe described the isotropic-nematic phase transition using an average angle-dependent attractive potential derived from a mean-field approach [21–23]. In this mean-field approach repulsive forces are neglected assuming spherical symmetry in the distribution of the centers of mass. Quantitative deviations between theory and experiments have led to criticism on the validity of the basic assumptions made in the Maier-Saupe theory [24–28]. Specifically, it has been shown that including angle dependent short-range repulsive interactions improve the description of this mean-field approach [25, 29]. Therefore, it is assumed that a certain degree of anisotropic repulsive interactions is essential for the appearance of liquid crystal phases [29–32]. Molecular simulation studies have shown the existence of liquid crystal phases in fluids made of molecules with a broad range of hard anisotropic shapes: hard disks [33, 34], hard ellipsoids [35–38], hard spherocylinders [39–44], cut hard spheres [45] and hard-sphere chains [46]. Frenkel [47] and Allen [48] provide excellent reviews on molecular simulation of anisotropic hard molecules forming athermal liquid crystal phases.

Molecular models including both anisotropic attractive and repulsive interactions have been used in the simulation of thermotropic liquid crystals [49, 50]. From these, the Gay-Berne potential is a popular model based on an anisotropic form of the Lennard-Jones potential [51–56]. Other more elaborated anisotropic interaction models including attractive and repulsive interactions are: hard-spherocylinder with an attractive square-well potential [57–60], hard-spherocylinder with an attractive Lennard-Jones potential [61], hard-disc with an anisotropic square-well attractive potential [62], anisotropic soft-core spherocylinder potential [63], and copolymers [64–66].

In this work, tangent chain molecules are used for the simulation of liquid crystal phases as described in section 2.1. Chain molecules are molecules formed by a sequence of tangent bonded segments that interact with a defined form of the pair potential, *e.g* hard-sphere, Lennard-Jones or square-well potentials. The use of a segment-based approach is justified from a multi-scale description of fluids, connecting molecular information summarized in a coarse-grained model with a molecular-based theory for the description of liquid crystal phases. In a coarse-grained model, the information of the molecular structure (based on chemical groups, or small molecules, or in general a collection of atoms) is reduced to the pair potential parameters of a force-field [67, 68]. Simulations based on coarse-grained

1

models reach longer time and length scales than their atomistic counterparts, allowing a bulk description of fluids. Moreover, molecular-based fluid theories as the family of theories derived from the statistical association fluid theory (SAFT) are based on a segment-based description of molecules [69–76]. A common form of the interaction potential between both theory and molecular simulations allow a direct comparison of theoretical results with simulation data. Recently, an analytical equation of state describing nematic liquid crystal phases based on a SAFT approach was developed [77–79]. In this context, the study of segment-based chain molecules is meaningful in the sense that this type of model offers the structural form required for a coarse-grained description of liquid crystal molecules providing, at the same time, a basis for validating the predictions obtained from a molecular-based equation of state.

1.4 Molecular simulation

Molecular simulations are used to calculate the physical properties (macrostate) of a molecular system from statistical mechanics principles. A system is defined by a number N of interacting molecules at some defined thermodynamic state. The statistical nature of a molecular system determines that an observed macrostate is an average of a series of instantaneous states or microstates in which the system can exist. In a classical approach, a microstate is defined by the instantaneous set of positions and momenta $(\mathbf{r}^N, \mathbf{p}^N)$ of all molecules in the system, representing coordinates in the phase space $\mathbb{P}$. The collection of all possible microstates is identified as an ensemble.

The physical properties of a system at thermal equilibrium can be determined from the ensemble average [80],

$$\langle \mathcal{A} \rangle = \frac{\int_{\mathbb{P}} d\mathbf{r}^N d\mathbf{p}^N \exp\left[\mathcal{H}(\mathbf{r}^N, \mathbf{p}^N)/k_B T\right] \mathcal{A}(\mathbf{r}^N, \mathbf{p}^N)}{\int_{\mathbb{P}} d\mathbf{r}^N d\mathbf{p}^N \exp\left[\mathcal{H}(\mathbf{r}^N, \mathbf{p}^N)/k_B T\right]}. \tag{1.1}$$

in which $\langle \mathcal{A} \rangle$ stands for the ensemble average of an observable macroscopic property $\mathcal{A}(\mathbf{r}^N, \mathbf{p}^N)$. The Hamiltonian $\mathcal{H}$ corresponds to the total energy of the system considering the potential and kinetic contributions. T is the temperature and k_B is the Boltzmann factor. In Eq. 1.1, the integration over momenta can be carried out analytically and independently from the integration over positions since the forces between particles are momentum independent. Therefore, equilibrium properties of a system made of N molecules at constant volume V and temperature T can be determined by the configurational average,

$$\langle \mathcal{A} \rangle = \frac{\int_V d\mathbf{r}^N \exp\left[-U(\mathbf{r}^N)/k_B T\right] \mathcal{A}(\mathbf{r}^N)}{\int_V d\mathbf{r}^N \exp\left[-U(\mathbf{r}^N)/k_B T\right]}. \tag{1.2}$$

The Boltzmann factor $\exp\left[-U(\mathbf{r}^N)/k_B T\right]$ is proportional to the probability of the system to be in a specific configuration $\mathbf{r}^N$ as a function of the configuration's potential energy $\mathcal{U}(\mathbf{r}^N)$ and temperature T.

The denominator of Eq. 1.2 is proportional to the partition function of the a system at constant number molecules, volume, and temperature, *i.e.* the *NVT* ensemble,

$$Q^{NVT} = \frac{1}{\Lambda^{3N} N!} \int_V d\mathbf{r}^N \exp\left[-U(\mathbf{r}^N)/k_B T\right], \tag{1.3}$$

where Λ is the thermal de Broglie wavelength. The partition function is related to the macroscopic or thermodynamic properties of a system. In the case of the *NVT* ensemble, the partition function is directly related to the Helmholtz energy $A(N, V, T)$ of the system,

$$A(N, V, T) = -k_B T \ln Q^{NVT}. \tag{1.4}$$

All thermodynamic properties of a system could be in principle determined from Eq. 1.4, however, the integration over all possible microstates required by Eq. 1.3 is in practice impossible. Random sampling over a finite space would in principle approximate macroscopic properties calculated from configurational averages as in Eq. 1.2. This method is known as Monte Carlo simulation and is the principle that is used in this work for determining thermodynamic properties. However, direct random sampling with equal probability for all configurations has the problem that most of the configurations have a very large energy and consequently a Boltzmann factor close to 0, resulting in an undefined division 0/0 for the configurational average in Eq. 1.2. Metropolis *et al.* [81] provided a solution to this problem, proposing an algorithm in which configurations are generated with a probability proportional to the Boltzmann factor, sampling therefore the Boltzmann distribution:

> "...the method we employ is actually a modified Monte Carlo scheme, where, instead of choosing configurations randomly, then weighting them with $\exp(-E/k_B T)$, we choose configurations with a probability $\exp(-E/k_B T)$ and weight them evenly." [81]

Using the Metropolis sampling scheme, configurational averages can be calculated by,

$$\langle \mathcal{A} \rangle = \frac{\sum_{i=1}^{n} \mathcal{A}\left(\mathbf{r}_i^N\right)}{n}, \tag{1.5}$$

where n is the number of configurations visited during sampling.

Different configurations are obtained by performing molecular trial moves, *e.g* molecular translation or rotation. Every trial move is an attempt of changing the configuration of the system from a configuration α to β.

In Monte Carlo molecular simulations, obeying detailed balance is a sufficient condition for sampling a correct distribution [80, 82]. The condition of detailed balance is given by,

$$\mathcal{P}_\alpha \, \mathcal{P}_{\alpha\beta}^{\text{move}} \, \mathcal{P}_{\alpha\beta}^{\text{acc}} = \mathcal{P}_\beta \, \mathcal{P}_{\beta\alpha}^{\text{move}} \, \mathcal{P}_{\beta\alpha}^{\text{acc}}, \tag{1.6}$$

where,

$\mathcal{P}_\alpha$: probability of the system to be in configuration α. In the *NVT* ensemble, Eq. 1.3, this probability is proportional to $\exp\left[-U(\mathbf{r}^N)/k_B T\right]$.

1

$\mathcal{P}_{\alpha\beta}^{\text{move}}$: probability for attempting a change in the configuration of the system from α to β.

$\mathcal{P}_{\alpha\beta}^{\text{acc}}$: probability that a change in the configuration of the system from α to β is accepted.

The probabilities of the backward move from configuration β to α are analogous. Usually the probability of attempting a forward and backward move is selected to be the same, simplifying Eq. 1.6 to,

$$\mathcal{P}_\alpha \, \mathcal{P}_{\alpha\beta}^{\text{acc}} = \mathcal{P}_\beta \, \mathcal{P}_{\beta\alpha}^{\text{acc}}. \tag{1.7}$$

The criterion $\mathcal{C}_{\alpha\beta}$ for the transition from a configuration α to β is given by,

$$\mathcal{C}_{\alpha\beta} = \frac{\mathcal{P}_{\alpha\beta}^{\text{acc}}}{\mathcal{P}_{\beta\alpha}^{\text{acc}}} = \frac{\mathcal{P}_\alpha}{\mathcal{P}_\beta}. \tag{1.8}$$

In the Metropolis scheme the probability of accepting a change in the configuration of the system from α to β is chosen as follows [81],

$$\mathcal{P}_{\alpha\beta}^{\text{acc}} = \min\left(1, \mathcal{C}_{\alpha\beta}\right). \tag{1.9}$$

For accepting a trial move, a random number R obtained from an uniform distribution is generated. The probability that this number is less than $P_{\alpha\beta}^{\text{acc}}$ is equal to $P_{\alpha\beta}^{\text{acc}}$. Therefore, a trail move is accepted when $R < P_{\alpha\beta}^{\text{acc}}$. This method assures that microstates are sampled following the Boltzmann distribution.

The criterion for accepting a trial change from configuration α to β in the *NVT* ensemble is given by,

$$\mathcal{C}_{\alpha\beta} = \frac{\mathcal{P}_{\alpha\beta}^{\text{acc}}}{\mathcal{P}_{\beta\alpha}^{\text{acc}}} = \frac{\mathcal{P}_\alpha}{\mathcal{P}_\beta} = \exp\left[-\frac{U(\beta) - U(\alpha)}{k_B T}\right] = \exp\left[-\frac{\Delta U}{k_B T}\right]. \tag{1.10}$$

where $U(\alpha)$ and $U(\beta)$ are the potential energies of configuration α and β, and $\Delta U = U(\beta) - U(\alpha)$ is the energy difference between both configurations.

It can be observed that a configuration change, in the *NVT* ensemble, associated with a negative difference in the potential energy ($\Delta U < 0$) will be always accepted. Changes carrying out a positive difference in energy ($\Delta U > 0$) will be accepted with a probability proportional to $\exp\left[-\Delta U / k_B T\right]$.

1.5 Scope and outline

The scope of this thesis is to contribute with simulation data to the understanding of the behavior of liquid crystal phases and the solubility of gases in them. Linear and partially-flexible chain molecules are used for simulating the behavior of liquid crystal phases. The effect of molecular elongation is studied by linear chain molecules of different lengths and the effect of flexibility is studied by partially-flexible molecules made of a linear and a freely-jointed part. The pair interaction between segments is accounted by hard-sphere and Lennard-Jones potentials. The use of these potentials allows to study the effect of purely

repulsive (excluded volume effects) and soft-attractive interactions (aggregation) on the liquid crystal behavior of chain fluids. The molecular model and pair interaction potentials are presented in chapter 2 together with the simulation techniques used in this work. Chapter 2 includes a detailed description of the expanded Gibbs ensemble method used for the calculation of liquid-crystal fluid phase equilibria. The liquid crystal behavior of single component hard-sphere chain fluids is reported in chapter 3. In this chapter, the effect of molecular elongation and flexibility on the phase behavior (packing fraction and pressure) and its relation with solubility is determined. Chapter 4 shows the isotropic-nematic phase equilibria of single component and binary mixtures of hard-sphere chain fluids. The effects of mixing on the coexisting isotropic-nematic phases and on the solubility of gases in them are determined in this chapter. Temperature effects for Lennard-Jones systems are studied in chapter 5. In this chapter, isotropic-nematic phase equilibria are determined for single component systems with different degrees of molecular anisotropy and for a binary mixture of linear Lennard-Jones chains. Isotropic-nematic phase equilibria simulation results are compared with predictions obtained from the recently developed analytical equation of state by van Westen *et al.*: for hard-sphere chain fluids Refs. 77, 78, 83, and Lennard-Jones chain fluids Refs. 79, 84. Assumptions made in the development of the equation of state are directly evaluated by comparing analytical results with simulation data. A large amount of simulation data on the liquid crystal behavior of chain fluids and on the solubility of gases in liquid crystal phases is presented in this work.

2

Molecular simulation methods for chain fluids

Linear and partially-flexible chain molecules are used to study the phase behavior of liquid crystal fluids using Monte Carlo simulations. The properties defining these molecular models are introduced in section 2.1 together with the pair potentials defining their interactions. Ordered phases are identified by nematic and smectic order parameters as described in section 2.2. Monte Carlo algorithms for the calculation of single-phase and two-phase systems are presented in section 2.3. Phase equilibria calculations of large chain molecules are difficult to perform using classical methods due to the very low acceptance rate for the molecular exchange between phases. In section 2.4, an expanded version of the Gibbs ensemble is presented which improves the efficiency of phase equilibria calculations compared to classical methods. Solubilities of gases in liquid crystal phases are calculated using the Widom test-particle insertion method and are presented here as Henry coefficients. Section 2.5 presents the Widom test-particle insertion method for determining Henry coefficients.

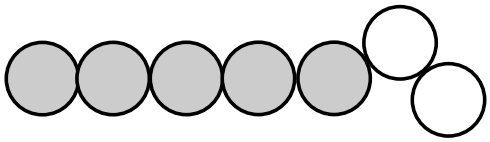

Figure 2.1: Partially-flexible chain molecule m–m_R–mer made of a linear part (gray area) and a freely-jointed flexible part (white area). This specific model molecule is denoted as a 7-5-mer.

2.1 Chain fluids and ordered phases

The molecular models used in this work are rigid linear chain and partially-flexible chain molecules. A chain molecule is defined as a molecule made of spherical segments connected tangentially by a rigid bond with fixed length equal to the segment diameter σ. A linear chain is a molecule with all segments laying on the same molecular axis. Partially-flexible molecules are made of a linear part and a freely-jointed flexible part as shown in Fig. 2.1. The linear part introduces rigidity while the flexible part incorporates flexibility to the model. The freely-jointed part does not have any bond-bending or torsional potential, therefore it is free to move between any possible molecular configuration limited only by the rigid bond length constraint and the pair potential interaction between segments. The partially-flexible model is proposed in similarity with real liquid crystal molecules, formed by a rigid core and a flexible tail. The linear chain is a special case of the partially-flexible model where no segments are present in the freely-jointed part. A linear chain with a number of m segments is identified as a linear m-mer. A partially-flexible chain molecule made of m segments in total and m_R segments in the rigid part is denoted as a partially-flexible m-m_R-mer. Two types of pair interactions between segments, denoted here as u_{ij}, are used in this study: the hard-sphere potential (section 2.1.1), and the Lennard-Jones potential (section 2.1.2).

2.1.1. Hard-sphere chain fluids

Hard-sphere segments are defined by a rigid sphere with diameter σ. Hard repulsions are the only interactions present in this model with an infinite repulsion energy at distances r_{ij} lower than the segment diameter,

$$u_{ij} = \begin{cases} \infty & ; \quad r_{ij} < \sigma \\ 0 & ; \quad r_{ij} \geq \sigma \end{cases} . \tag{2.1}$$

Vega *et al.* [85] studied the phase behavior of linear hard-sphere chain fluids with a length of 3, 4, 5, 6 and 7 segments from constant pressure Monte Carlo simulations. These authors observed that hard-sphere chain fluids with a length of 5 segments and higher are able to form liquid crystal phases, while shorter chains experience a direct transition from the isotropic to the crystal state [85–87]. A more detailed simulation study on the phase behavior of the linear hard-sphere 7-mer was performed by Williamson and Jackson [88]. The isotropic-nematic phase behavior of the linear hard-sphere 8-mer and 20-mer chain fluids was obtained by Yethiraj and Fynewever [89]. Whittle and Masters [90] studied the phase behavior of 6 and 8 segment linear fused hard-sphere molecules with length-to-width ratios ranging from 3.5 to 5.2, observing a nematic phase only for the longest molecule.

A partially-flexible model was employed by McBride and Vega *et al.* [91–93] for fused hard-sphere molecules composed of a linear and a freely-jointed part with a total length of 15 beads and with 8 to 15 segments in the linear part, observing isotropic, nematic, and smectic phases, in all but the most flexible molecule where a nematic phase was not detected. Escobedo and de Pablo [94] calculated the isotropic-nematic phase transition of 8 and 16 hard-sphere chain molecules with finite and infinite (linear chains) bond-bending potentials.

2.1.2. Lennard-Jones chain fluids

The Lennard-Jones pair potential between two segments separated a distance r_{ij} is defined by,

$$u_{ij} = 4\epsilon\left[\left(\frac{\sigma}{r_{ij}}\right)^{12} - \left(\frac{\sigma}{r_{ij}}\right)^{6}\right], \tag{2.2}$$

where ϵ is the depth of the potential well, and σ is the segment diameter defined as the distance at which the potential between two segments is zero. Intermolecular pair interactions take place between segments of different molecules and intramolecular pair interactions between segments of the same molecule separated by two or more bonds. In this work, the Lennard-Jones pair potential is truncated at a cutoff radius $r_c = 2.5\sigma$ and the usual long-range tail corrections are applied [37, 80].

Simulation results for the liquid crystal behavior of Lennard-Jones chains could not be found in any other previous study. Galindo *et al.* [95] studied the phase behavior of linear Lennard-Jones chains of 3 and 5 segments, however, no liquid crystalline phases were observed due to the short length of the chains.

2.2 Order parameters

2.2.1. Nematic order parameter

Orientational order is determined by the nematic order parameter and it is used for monitoring the transition from the isotropic to the nematic phase. It has a value of 0 in the isotropic fluid and experiences a near-step change at the isotropic-nematic phase transition approaching 1 in the nematic fluid.

The nematic order parameter S_2 is defined by the second-order Legendre polynomial [34],

$$S_2 = \frac{1}{N}\left\langle \sum_{i=1}^{N} P_2(\cos\theta_i)\right\rangle = \frac{1}{N}\left\langle \sum_{i=1}^{N}\left(\frac{3}{2}\cos^2\theta_i - \frac{1}{2}\right)\right\rangle, \tag{2.3}$$

where θ_i is the angle between the molecular axis and the nematic director $\mathbf{n}$ of each molecule in the system. For partially-flexible molecules, the molecular axis is defined as the eigenvector corresponding to the lowest eigenvalue of the moment of inertia tensor [89].

In molecular simulations when a nematic phase is formed, molecules do not necessary align across the largest dimension of the simulation box and knowledge *a priori* of the direction of the nematic director is in general not possible. In practice, the orientation of the liquid crystal phase with respect to the laboratory framework is identified with the eigenvectors of the so-called *de Gennes* $\mathbf{Q}$-tensor [1], $\mathbf{Q} = \frac{1}{N}\sum_{i=1}^{N}(\mathbf{q}_i\mathbf{q}_i - \frac{1}{3}\mathbf{I})$, where $\mathbf{q}$ is

a unit vector identifying the direction of the molecular axis with respect to the laboratory frame. In the case that two of the eigenvalues of $\mathbf{Q}$ are equal, an uniaxial nematic phase is identified and the nematic director is associated with the eigenvector corresponding to the different eigenvalue, *i.e.* the largest eigenvalue of $\mathbf{Q}$. In the case that all three eigenvalues are the same, the system is found in an isotropic state. For an uniaxial nematic phase, $\mathbf{Q} = S(\mathbf{n} \otimes \mathbf{n} - \frac{1}{3}\mathbf{I})$, where $\mathbf{n} \otimes \mathbf{n}$ is the tensor product of the nematic director $\mathbf{n}$. The eigenvalues of the $\mathbf{Q}$-tensor are $\lambda_+ = \frac{2}{3}S$ and $\lambda_0 = \lambda_- = -\frac{1}{3}S$, where $S = \sum_{i=1}^{N}(\frac{3}{2}\cos^2\theta - \frac{1}{2})$ [96]. The order parameter S_2 is estimated as $S_2 = \frac{3}{2}\langle\lambda_+\rangle$. It has to be noticed that the $\mathbf{Q}$ tensor is diagonalized for every configuration considered in the ensemble average. An average phase direction can also be obtained by the average $\langle\mathbf{Q}\rangle$, whereby the $\mathbf{Q}$ tensor is diagonalized only at the end of the simulation run. However, this approach requires that fluctuations in the direction of the nematic director with respect to the laboratory frame are negligible, which is in principle not the general case and therefore this approach is not implemented here. In this work, the order parameter is obtained from the ensemble average $\langle\lambda_+\rangle$ calculated every 10^3 Monte Carlo cycles.

2.2.2. Smectic order parameter

Positional ordering is detected by the smectic order parameter, which is defined by the magnitude of the first Fourier component of the normalized density wave along the nematic director [97, 98],

$$\tau = \frac{1}{N}\left\langle\left|\sum_{j=1}^{N} e^{ik_z z_j}\right|\right\rangle. \tag{2.4}$$

where N is the total number of molecules and k_z=$2\pi/\lambda_z$. The periodicity of the smectic layers is λ_z and z_j are the coordinates of the center of mass of the j-th molecule in the direction of the nematic director. Values of the smectic order parameter, which differ significantly from zero indicate the presence of smectic layers.

2.3 Monte Carlo simulations

In this section classical methods for the simulation of fluid systems are presented. The general principles of Monte Carlo simulation methods were presented in section 1.4 together with the isobaric-isothermal *NVT* ensemble. Changes in the configuration of partially-flexible chain molecules are obtained using the configurational-bias method. The isobaric-isothermal *NPT* ensemble is described for the calculation of properties of single phase systems. Direct phase equilibrium calculations of simple fluids are performed in the Gibbs-ensemble. The methods and algorithms presented here are general independent of the form of the pair interaction potential. The specific cases of hard-sphere or Lennard-Jones potentials are obtained by replacing the form of the interaction potential u_{ij} by Eq. 2.1 or Eq. 2.2 respectively.

2.3.1. Configurational-bias Monte Carlo

In the configurational-bias method [99–102], the configuration of a partially-flexible molecule is changed by regrowing the freely-jointed part attempting a change from configuration α to

β. In this method, the flexible part is regrowth segment by segment attempting each time a number of trail orientations with coordinates $\{\mathbf{b}_1, ..., \mathbf{b}_k\}$ for every regrown segment. For the chain molecules with fixed bond length studied here, the trial orientations are distributed around a sphere with radius equal to the segment diameter. Each trail orientation experiences pair interactions with the other segments of the same molecule (excepting the segment from which the trail segment is regrown from) and with the segments of all other molecules in the system. For the actual regrown segment i, the Boltzmann factor is calculated for each trail orientation k, and one of those, denoted by n, is selected with a probability,

$$p_i(\mathbf{b}_n) = \frac{\exp\left[-u_i(\mathbf{b}_n)/k_BT\right]}{\sum_{j=1}^{k} \exp\left[-u_i(\mathbf{b}_j)/k_BT\right]}. \tag{2.5}$$

For each regrown segment, the statistical weight of the segment in the regrowing process of the flexible part is the denominator of Eq. 2.5,

$$w_i = \sum_{j=1}^{k} \exp\left[-u_i(\mathbf{b}_j)/k_BT\right]. \tag{2.6}$$

In partially-flexible molecules, only the configuration of the flexible part is changed, *i.e* from segment $m_R + 1$ to m. After the whole chain is regrown, the Rosenbluth factor of the new configuration β is obtained,

$$W_\beta = \prod_{i=m_R+1}^{m} w_i. \tag{2.7}$$

The Rosenbluth factor of the old configuration α is also calculated using the old configuration as the first trial direction. Considering the condition of microscopic reversibility, Eq. 1.7, the criterion for accepting a change in the configuration of a chain molecule by configurational-bias regrowth is given by,

$$\mathcal{C}_{\alpha\beta} = \frac{W_\alpha}{W_\beta}. \tag{2.8}$$

A trial change in the configuration of a chain molecule from α to β is accepted with a probability given by Eq. 1.9.

2.3.2. *NPT* ensemble

The phase behavior of single phase system made of N molecules at constant pressure P and temperature T are obtained in the isobaric-isothermal *NPT* ensemble [80],

$$Q^{NPT} = \left(\frac{P}{k_BT}\right) \frac{1}{\Lambda^{3N} N!} \int_0^\infty dV\, V^N \exp\left[-\frac{PV}{k_BT}\right] \int_0^1 d\mathbf{s}^N \exp\left[-\frac{U(\mathbf{s}^N)}{k_BT}\right]. \tag{2.9}$$

The scaled coordinates, $\mathbf{s} = \mathbf{r}/L$ where $L = V^{1/3}$, are introduced here to perform a random walk in a sampling space that is independent of the actual size of the simulation

box. These coordinates refer to the position of every segment of all molecules in the system accounting therefore for the molecular configuration and orientation of molecules. The partition function of the *NPT* ensemble for configurational changes in the logarithm of the volume V is derived as follows,

$$Q^{NPT} = \left(\frac{P}{k_B T}\right) \frac{1}{\Lambda^{3N} N!} \int_{-\infty}^{\infty} d \ln V \, V^{N+1} \exp\left[-\frac{PV}{k_B T}\right] \int_0^1 d\mathbf{s}^N \exp\left[-\frac{U(\mathbf{s}^N)}{k_B T}\right]. \tag{2.10}$$

The probability that the system is in a determined configuration α with volume $\ln V$ and coordinates $\mathbf{s}^N$ is proportional to,

$$\mathcal{P}_\alpha \propto V^{N+1} \exp\left[-\frac{PV}{k_B T}\right] \exp\left[-\frac{U(\mathbf{s}^N)}{k_B T}\right]. \tag{2.11}$$

Changes in the configuration of the system are performed by trial changes in the position/orientation of molecules, the molecular configuration of partially-flexible molecules, and the volume of the system (the size of the simulation box). Trial changes that do not involve a change in volume of the system are equivalent to a change in the *NVT* ensemble and the acceptance criterion for a trail change from a configuration α to a configuration β is equivalent to the one presented in section 1.4,

$$\mathcal{C}_{\alpha\beta} = \exp\left[-\frac{\Delta U}{k_B T}\right], \tag{1.10}$$

where ΔU is the difference in potential energy between both configurations.

Volume change
The acceptance criterion for a trial change in $\ln V$ is given by,

$$\mathcal{C}_{\alpha\beta} = \exp\left[\frac{P\Delta V}{k_B T} + (N+1)\ln\left(\frac{V+\Delta V}{V}\right) - \frac{\Delta U}{k_B T}\right]. \tag{2.12}$$

where ΔV is the change in the volume of the system.

2.3.3. Gibbs ensemble

Direct phase equilibria simulations are performed in the method proposed by Panagiotopoulos [103, 104], denoted as the Gibbs ensemble. The basis of this method are presented in this section as a preamble of the expanded Gibbs ensemble simulation method developed in the next section. In the Gibbs ensemble method two phases, subsystems a and b, are brought into contact to achieve thermal, mechanical, and chemical potential equilibrium:

$$\begin{array}{rcll} T_a & = & T_b & = T \\ P_a & = & P_b & (= P) \\ \mu_{a,i} & = & \mu_{b,i}. & \end{array} \tag{2.13}$$

Two forms of the method can be identified: simulations at constant total volume V and temperature T conditions (*NVT* Gibbs ensemble), or simulations at constant pressure P and temperature T conditions (*NPT* Gibbs ensemble). In both cases, simulations are performed

for a total number of molecules $N = N_a + N_b$.

The *NVT* Gibbs ensemble is used to calculate the phase equilibria of pure component systems. In this case, only one thermodynamic variable, the temperature, is required for determining the thermodynamic state of the system. The total volume of the system $V = V_a + V_b$ is selected in order to match a density in the two-phase region. The volume of one of the phases is varied independently until both phases reach the same pressure.

The *NPT* version of the Gibbs ensemble is used in the case of mixtures where two thermodynamic variables, in this case temperature and pressure, are required for determining the thermodynamic state of the system.

In both cases, thermal equilibration is achieved by rotation/displacement of molecules and partial-regrowth of partially-flexible molecules. Mechanical equilibrium is obtained by: volume changes of one subsystem in the *NVT* Gibbs ensemble, or by volume changes in both subsystems in the *NPT* Gibbs ensemble. Equality in the chemical potential of every component i is achieved by molecular exchange between both subsystems.

***NVT* Gibbs ensemble**

The partition function of the *NVT* Gibbs ensemble is given by [80],

$$\begin{aligned} Q^{NVT-\text{Gibbs}} &= \frac{1}{N!\Lambda^{3N}V}\sum_{N_a=0}^{N}\frac{N!}{N_a!N_b!}\int_0^V dV_a V_a^{N_a}V_b^{N_b} \\ &\times \int_0^1 d\mathbf{s}_a^{N_a}\exp\left[-\frac{U_a(\mathbf{s}_a^{N_a})}{k_BT}\right]\int_0^1 d\mathbf{s}_b^{N_b}\exp\left[-\frac{U_b(\mathbf{s}_b^{N_b})}{k_BT}\right]. \end{aligned} \tag{2.14}$$

Similarly as in the previous section, reduced coordinates are introduced, $\mathbf{s}_j = \mathbf{r}_j/L_j$ where $L_j = V_j^{1/3}$ is the box length of either subsystem a or b. N_a and N_b are the number of molecules in each subsystem.

The probability of finding the system in a configuration α with coordinates $(\mathbf{s}_a^{N_a}, \mathbf{s}_b^{N_b})$ and volume ratio V_a and V_b is proportional to,

$$\mathcal{P}_\alpha \propto \frac{N!}{N_a!N_b!}\frac{V_a^{N_a}V_b^{N_b}}{V}\exp\left[-\frac{U_a(\mathbf{s}_a^{N_a})}{k_BT}\right]\exp\left[-\frac{U_b(\mathbf{s}_b^{N_b})}{k_BT}\right]. \tag{2.15}$$

Volume change

Volume changes are performed by a random walk in the logarithm of the ratio between the volume of both subsystems $\ln(V_a/V_b)$. The partition function changes then to,

$$\begin{aligned} Q^{NVT-\text{Gibbs}} &= \frac{1}{N!\Lambda^{3N}V}\sum_{N_a=0}^{N}\frac{N!}{N_a!N_b!}\int_{-\infty}^{\infty} d\ln\left(\frac{V_a}{V_b}\right)\frac{V_aV_b}{V}V_a^{N_a}V_b^{N_b} \\ &\times \int_0^1 d\mathbf{s}_a^{N_a}\exp\left[-\frac{U_a(\mathbf{s}_a^{N_a})}{k_BT}\right]\int_0^1 d\mathbf{s}_b^{N_b}\exp\left[-\frac{U_b(\mathbf{s}_b^{N_b})}{k_BT}\right]. \end{aligned} \tag{2.16}$$

The acceptance criterion for a trial change in the configuration of the system from α to β by a volume change trial move in the phase space $\ln(V_a/V_b) = \ln(V_a/(V - V_a))$ is then given by,

$$\mathcal{C}_{\alpha\beta} = \exp\left[(N_a + 1)\ln\left(\frac{V_a + \Delta V_a}{V_a}\right) + (N_b + 1)\ln\left(\frac{V_b - \Delta V_a}{V_b}\right) - \frac{\Delta U_a}{k_B T} - \frac{\Delta U_b}{k_B T}\right], \quad (2.17)$$

where ΔV_a indicates the magnitude of the volume change in subsystem a, and ΔU_a and ΔU_b indicate the related energy change in both subsystems.

Algorithm for molecular exchange in the Gibbs ensemble
The algorithm for molecular exchange as originally proposed by Panagiotopoulos [103] is used in this work. The algorithm is described as follows:

1. The molecular donor and recipient subsystems are first chosen randomly, $\mathcal{P}^{\text{sub}\,a} = \mathcal{P}^{\text{sub}\,b} = 1/2$.
2. The component to be exchanged is chosen randomly with same probability for all components in the mixture, $\mathcal{P}^{\text{comp}\,1} = \mathcal{P}^{\text{comp}\,2} = ... = \mathcal{P}^{\text{comp}\,i}$.
3. A random molecule of component i in the donor subsystem (a in this case) is selected with probability, $\mathcal{P}_\alpha^{\text{mol}\,i,a} = 1/N_{a,i}$. If $N_{a,i} = 0$, then the trail move is immediately rejected.
3. The molecule is transferred to a random position in the recipient subsystem (b in this case).
4. A new configuration β is accepted with a probability given by $\min(1, \mathcal{C}_{\alpha\beta})$.

A different form of the algorithm satisfying detailed balance can be obtained by selecting first the molecule to exchange regardless the subsystem in which it is in. This choice leads to a different acceptance criterion for the molecular exchange move as the one presented in this section [105].

Molecular exchange, pure components
The transfer of a particle between both subsystems will transform the overall configuration of the system from configuration α to configuration β. The probability of such a transfer is then equal to,

$$\mathcal{P}_{\alpha\beta} = N_a! N_b!\, \mathcal{P}_\alpha\, \mathcal{P}^{\text{sub},\,a}\, \mathcal{P}_\alpha^{\text{mol},\,a}\, \mathcal{P}^{\text{pos},\,b}\, \mathcal{P}_{\alpha\beta}^{\text{acc}}, \quad (2.18)$$

where,

$\mathcal{P}_{\alpha\beta}$	:	probability to change the configuration of the system from α to β.
$\mathcal{P}_\alpha$	:	probability of the system to be in configuration α, Eq. 2.15.
$\mathcal{P}^{\text{sub},\,a}$	:	probability of choosing subsystem a as molecular donor.
$\mathcal{P}_\alpha^{\text{mol},\,a}$	:	probability that a specific molecule is chosen from the N_a molecules in subsystem a in configuration α.
$\mathcal{P}^{\text{pos},\,b}$	:	probability of selecting a position for insertion in subsystem b.
$\mathcal{P}_{\alpha\beta}^{\text{acc}}$	:	acceptance criterion for the particle transfer.

The probability of the backward move, *i.e.*, the probability of a particle exchange from subsystem b to a and therefore to change the configuration of the system from α to β is equal to,

$$\mathcal{P}_{\beta\alpha} = (N_a - 1)!(N_b + 1)!\, \mathcal{P}_\beta\, \mathcal{P}^{\mathrm{sub},\,b}\, \mathcal{P}_\beta^{\mathrm{mol},\,b}\, \mathcal{P}^{\mathrm{pos},\,a}\, \mathcal{P}_{\beta\alpha}^{\mathrm{acc}}. \tag{2.19}$$

The probability of the total system to be in configuration β is given by,

$$\mathcal{P}_\beta \propto \frac{N!}{(N_a - 1)!(N_b + 1)!} \frac{V_a^{N_a-1} V_b^{N_b+1}}{V} \times \exp\left[-\frac{U_a(\mathbf{s}_a^{(N_a-1)})}{k_B T}\right] \exp\left[-\frac{U_b(\mathbf{s}_b^{(N_b+1)})}{k_B T}\right]. \tag{2.20}$$

The condition of microscopic reversibility states that the probability of the forward $\mathcal{P}_{\alpha\beta}$ and backward $\mathcal{P}_{\beta\alpha}$ move has to be the same,

$$\mathcal{P}_{\alpha\beta} = \mathcal{P}_{\beta\alpha}. \tag{2.21}$$

The probability of choosing any of both subsystem as molecular donor is the same, therefore $\mathcal{P}^{\mathrm{sub},\,a} = \mathcal{P}^{\mathrm{sub},\,b} = 1/2$. The probability of choosing a molecule from subsystem a in configuration α is proportional to $\mathcal{P}_\alpha^{\mathrm{mol},\,a} = 1/N_a$ for the forward move and the probability of choosing a molecule in subsystem b is proportional to $\mathcal{P}_\beta^{\mathrm{mol},\,b} = 1/(N_b + 1)$ for the backward move. The probability of choosing a position for the insertion of a molecule is equal for both subsystems $\mathcal{P}^{\mathrm{pos},\,a} = \mathcal{P}^{\mathrm{pos},\,b}$. Considering this, from Eq 2.18 and Eq. 2.19, the following acceptance criterion is derived from Eq. 2.21,

$$\begin{aligned} \mathcal{C}_{\alpha\beta} &= \frac{\mathcal{P}_{\alpha\beta}^{\mathrm{acc}}}{\mathcal{P}_{\beta\alpha}^{\mathrm{acc}}} \\ &= \frac{(N_a - 1)!(N_b + 1)!}{N_a! N_b!} \frac{\mathcal{P}^{\mathrm{sub},\,b}}{\mathcal{P}^{\mathrm{sub},\,a}} \frac{\mathcal{P}_\beta^{\mathrm{part},\,b}}{\mathcal{P}_\alpha^{\mathrm{part},\,a}} \frac{\mathcal{P}^{\mathrm{pos},\,a}}{\mathcal{P}^{\mathrm{pos},\,b}} \frac{\mathcal{P}_\beta}{\mathcal{P}_\alpha} \\ &= \exp\left[\ln\left(\frac{N_a V_b}{(N_b + 1) V_a}\right) - \frac{\Delta U_a}{k_B T} - \frac{\Delta U_b}{k_B T}\right], \end{aligned} \tag{2.22}$$

where ΔU_a and ΔU_b are the change in energy in both subsystems due to molecular exchange.

***NPT* Gibbs ensemble**

The *NPT* version of the Gibbs ensemble is used for the calculation of the phase equilibria of mixtures. Here, the partition function and algorithms are developed for the case of a binary mixture. The general case of a multicomponent mixture is presented at the end of the section. The partition function for phase equilibria calculations in the Gibbs ensemble at constant number of molecules N, pressure P and temperature T, for a binary mixture of components 1 and 2 is given by,

$$
\begin{aligned}
Q^{NPT-\text{Gibbs}} = & \frac{1}{N_1!\Lambda^{3N_1}V_0}\frac{1}{N_2!\Lambda^{3N_2}V_0}\sum_{N_{a,1}=0}^{N_1}\frac{N_1!}{N_{a,1}!N_{b,1}!}\sum_{N_{a,2}=0}^{N_2}\frac{N_2!}{N_{a,2}!N_{b,2}!} \\
& \times \int_0^\infty dV_a V_a^{N_a}\exp\left[-\frac{PV_a}{k_BT}\right]\int_0^\infty dV_b V_b^{N_b}\exp\left[-\frac{PV_b}{k_BT}\right] \\
& \times \int_0^1 d\mathbf{s}_{a,1}^{N_{a,1}}\int_0^1 d\mathbf{s}_{a,2}^{N_{a,2}}\exp\left[-\frac{U_a(\mathbf{s}_{a,1}^{N_{a,1}},\mathbf{s}_{a,2}^{N_{a,2}})}{k_BT}\right] \\
& \times \int_0^1 d\mathbf{s}_{b,1}^{N_{b,1}}\int_0^1 d\mathbf{s}_{b,2}^{N_{b,2}}\exp\left[-\frac{U_b(\mathbf{s}_{b,1}^{N_{b,1}},\mathbf{s}_{b,2}^{N_{b,2}})}{k_BT}\right],
\end{aligned}
\tag{2.23}
$$

where $N_1 = N_{a,1} + N_{b,1}$ is the total number of molecules of component 1, and $N_{a,1}$ and $N_{b,1}$ are the number of molecules of component 1 present in subsystem a and b respectively. As before, reduced coordinates are introduced, where $\mathbf{s}_{a,1}^{N_{a,1}}$ are the coordinates of the segments of all molecules of component 1 in subsystem a. All other coordinates are represented in a similar manner. V_0 is a reference volume introduced here for making the partition function dimensionless.

The probability that the system is in configuration α is proportional to,

$$
\begin{aligned}
\mathcal{P}_\alpha \propto & \exp\left[\ln\left(\frac{N_1!}{N_1^a!N_1^b!}\right)+\ln\left(\frac{N_2!}{N_2^a!N_2^b!}\right)+N_a\ln V_a+N_b\ln V_b\right. \\
& \left.-\frac{PV_a}{k_BT}-\frac{PV_b}{k_BT}-\frac{U_a(\mathbf{s}_{a,1}^{N_{a,1}},\mathbf{s}_{a,2}^{N_{a,2}})}{k_BT}-\frac{U_b(\mathbf{s}_{b,1}^{N_{b,1}},\mathbf{s}_{b,2}^{N_{b,2}})}{k_BT}\right].
\end{aligned}
\tag{2.24}
$$

Volume change

Volume changes are performed in an independent manner in both subsystems. As before, a random walk in the logarithm of the volume is preferred and the criterion for accepting a trial change in $\ln V_j$, where j is either subsystem a or b, is equivalent to Eq. 2.12.

Molecular exchange, binary mixtures

The equality of chemical potentials is obtained by the exchange of particles of component 1 and 2 between both subsystems a and b at constant temperature and pressure. The transfer of a molecule, *e.g.* of component 1, between both subsystems will transform the overall configuration of the system from configuration α to configuration β. The probability of such a transfer is then proportional to,

$$
\mathcal{P}_{\alpha\beta} = N_{a,1}!N_{b,1}!N_{a,2}!N_{b,2}!\,\mathcal{P}^{\text{sub}\,a}\,\mathcal{P}^{\text{comp}\,1}\,\mathcal{P}_\alpha^{\text{mol}\,1,a}\,\mathcal{P}^{\text{pos}\,b}\,\mathcal{P}_\alpha\,\mathcal{P}_{\alpha\beta}^{\text{acc}},
\tag{2.25}
$$

where,

$\mathcal{P}_{\alpha\beta}$	:	probability of changing the overall configuration of the system from α to β due to molecular exchange.
$\mathcal{P}^{\text{sub}\,a}$	:	probability of choosing subsystem a as particle donor.
$\mathcal{P}^{\text{comp}\,1}$	:	probability of choosing component 1 for molecular exchange.

$\mathcal{P}_{\alpha}^{\text{mol}\,1,a}$: probability that a specific molecule of component 1 is chosen from the $N_{a,1}$ molecules in subsystem a.
$\mathcal{P}^{\text{pos}\,b}$: probability of selecting a position for insertion in subsystem b.
$\mathcal{P}_{\alpha}$: probability of the total system to be in configuration α, Eq 2.24.
$\mathcal{P}_{\alpha\beta}^{\text{acc}}$: acceptance criterion for the particle transfer.

The probability of the reverse move, *i.e.* the probability of transferring a molecule of component 1 from subsystem b to a, changing therefore the configuration of the system from configuration α to β, is equal to,

$$\begin{aligned}\mathcal{P}_{\beta\alpha} &= (N_{a,1}-1)!(N_{b,1}+1)!N_{a,2}!N_{b,2}! \\ &\quad \times \mathcal{P}^{\text{sub}\,b}\,\mathcal{P}^{\text{comp}\,1}\,\mathcal{P}_{\beta}^{\text{mol}\,1,b}\,\mathcal{P}^{\text{pos}\,a}\,\mathcal{P}_{\beta}\,\mathcal{P}_{\beta\alpha}^{\text{acc}},\end{aligned} \tag{2.26}$$

where now,

$$\begin{aligned}\mathcal{P}_{\beta} \propto \exp\Bigg[&\ln\left(\frac{N_1!}{(N_{a,1}-1)!(N_{b,1}+1)!}\right)+\ln\left(\frac{N_2!}{N_{a,2}!N_{b,2}!}\right) \\ &+N_a\ln V_a+(N_b+2)\ln V_b-\frac{PV_a}{k_BT} \\ &-\frac{PV_b}{k_BT}-\frac{U_a(\mathbf{s}_{a,1}^{N_{a,1}-1},\mathbf{s}_{a,2}^{N_{a,2}})}{k_BT}-\frac{U_b(\mathbf{s}_{b,1}^{N_{b,1}+1},\mathbf{s}_{b,2}^{N_{b,2}})}{k_BT}\Bigg].\end{aligned} \tag{2.27}$$

The acceptance criterion $\mathcal{C}_{\alpha\beta}$ is obtained from the condition of microscopic reversibility Eq. 2.21. The probability of choosing any of both subsystems is the same $\mathcal{P}^{\text{sub}\,a}=\mathcal{P}^{\text{sub}\,b}=1/2$. The probability of choosing component 1 or 2 for molecular exchange is also symmetric $\mathcal{P}^{\text{comp}\,1}=\mathcal{P}^{\text{comp}\,1}=1/2$. The probability of choosing a molecule of component 1 in subsystem a in configuration α is $\mathcal{P}_{\alpha}^{\text{mol}\,a}=1/N_{a,1}$ and the probability of choosing a molecule of component 1 in subsystem b in configuration β is $\mathcal{P}_{\alpha}^{\text{mol}\,b}=1/(N_{b,1}+1)$. If $N_{a,1}=0$ then the trial move is immediately rejected. The probability of selecting a position for insertion is the same in both subsystems $\mathcal{P}^{\text{pos}\,a}=\mathcal{P}^{\text{pos}\,b}$. Therefore, the acceptance criterion for a trial move involving molecular exchange is given by,

$$\begin{aligned}\mathcal{C}_{\alpha\beta} &= \frac{\mathcal{P}_{\alpha\beta}^{\text{acc}}}{\mathcal{P}_{\beta\alpha}^{\text{acc}}} \\ &= \frac{(N_{a,1}-1)!(N_{b,1}-1)!N_{a,2}!N_{b,2}!}{N_{a,1}!N_{b,1}!N_{a,2}!N_{b,2}!}\,\frac{\mathcal{P}^{\text{sub}\,b}}{\mathcal{P}^{\text{sub}\,a}}\,\frac{\mathcal{P}^{\text{comp}\,1}}{\mathcal{P}^{\text{comp}\,1}}\,\frac{\mathcal{P}_{\beta}^{\text{mol}\,1,b}}{\mathcal{P}_{\alpha}^{\text{mol}\,1,a}}\,\frac{\mathcal{P}^{\text{pos}\,a}}{\mathcal{P}^{\text{pos}\,b}}\,\frac{\mathcal{P}_{\beta}}{\mathcal{P}_{\alpha}} \\ &= \exp\left[\ln\left(\frac{N_{a,1}V_b}{(N_{b,1}+1)V_a}\right)-\frac{\Delta U_a}{k_BT}-\frac{\Delta U_b}{k_BT}\right].\end{aligned} \tag{2.28}$$

ΔU_a and ΔU_b are the changes in energy in both subsystems due to the molecular exchange of a molecule of component i from subsystem a to b.

Molecular exchange, multicomponent mixtures
After inspection of Eq. 2.28 and Eq. 2.22, the following acceptance criterion can be deduced for the molecular exchange of any component i in a multicomponent system following the selection algorithm described in the beginning of this section,

$$\mathcal{C}_{\alpha\beta} = \exp\left[\ln\left(\frac{N_{a,i}V_b}{(N_{b,i}+1)V_a}\right) - \frac{\Delta U_a}{k_B T} - \frac{\Delta U_b}{k_B T}\right]. \tag{2.29}$$

2.4 Expanded Gibbs ensemble

Phase equilibria of simple systems can be directly calculated using the Gibbs ensemble as shown in the previous section. In Gibbs ensemble simulations, the equilibrium of chemical potentials is achieved by the exchange of whole molecules between both phases. While transfer of whole molecules between phases is effective only for short and simple molecules, highly anisotropic or complex molecules have a very low probability of transfer acceptance [101, 104, 106]. This condition results in poor ergodic sampling of systems made of non-simple molecules within reasonable simulation time. Advanced techniques have been developed to overcome this difficulty. Configurational-bias sampling [100, 107] was implemented in the Gibbs ensemble for improving the simulation of vapor-liquid equilibria of non-simple fluids [102, 108–111]. Although configurational-bias Monte Carlo shows an improved molecular transfer efficiency over the traditional Gibbs ensemble scheme, it is computational expensive and its efficiency is decreased as molecular complexity increases [112–114]. Even improvements of the configurational-bias Monte Carlo technique as the Recoil Growth method show to be inefficient for dense systems [115, 116].

Either in the traditional or in the configurational-bias implementation of the Gibbs ensemble, molecular transfers are attempted by insertion/deletion of whole molecules. Intuitively, molecular transfer efficiency can be improved by attempting at every step the transfer of molecular segments rather than of whole molecules. Expanded ensemble techniques are based on this principle [117–119]. In these methods, the ensemble of a system of whole molecules is expanded into a series of sub-ensembles covering for one fractional molecule, the range between a "ghost" molecule (a molecule without any intermolecular interactions) to a fully coupled molecule (a molecule where all intermolecular interactions are present). In expanded Gibbs ensemble simulations, molecular transfer between phases is achieved by gradually coupling a fractional molecule in one phase while, at the same time, a complementary fractional molecule is decoupled from the other [120, 121]. Gradual coupling/decoupling is performed by a random walk over sub-ensembles, each one of them corresponding to a defined fractional state that determines the degree of intermolecular coupling of the fractional molecules. In the traditional Metropolis sampling scheme [81], a random walk over fractional states results in an uneven distribution of the relative probability of visiting fractional states. This condition restricts molecular transfer between phases, limiting the efficiency of the method. A smooth transition between all fractional states is desired, striving ideally to the same relative probability for visiting any fractional state. For this aim, the partition function of the expanded ensemble is modified by a weight function for each fractional state, changing the Boltzmann statistics of the original system [122–124]. Numerical values for these weight functions are not known *a priori* and an iterative method for determining them is required, see section 2.4.3 and Refs. [117–119].

Simulation of chain molecules are performed in this study in an expanded version of the Gibbs ensemble [125]. The method is based on the gradual exchange of molecules between phases by the coordinated coupling/decoupling of segments of a fractional molecule . There is one fractional molecule present in each subsystem for each component. The simulation method is based on the ideas of Lyubartsev *et. al.* [117, 126, 127] on expanded ensembles and is similar in spirit to the Continuous Fractional Component Monte Carlo method of Maginn and co-workers [121, 128–140]. Instead of the continuous insertion presented in their work, here a segment-wise insertion of chain molecules is proposed. Similarly, Escobedo and de Pablo developed the expanded ensemble ideas for the calculation of phase equilibria of polymer molecules [119, 120, 141]. However, in their method, configurational-bias is used for stepwise insertion/deletion of molecular segments. Furthermore, in that method, fractional molecules in their end-states are counted as whole molecules, changing the form of the partition function every time an end-state is visited [119]. In the method presented here, the total number of whole molecules and therefore the form of the partition function remain unchanged during the simulation.

Constant volume expanded Gibbs ensemble simulations are used for determining the phase equilibria of pure components. A constant pressure formulation of the expanded Gibbs ensemble is used for the calculation of the phase equilibria of binary mixtures.

2.4.1. *NVT* expanded Gibbs ensemble

The partition function for a multicomponent system made of n components with a total number of N whole molecules and one fractional molecule per component in each subsystem, a and b, for a constant total volume $V = V_a + V_b$, at constant temperature T, is given by,

$$\begin{aligned} Q^{NVT-\mathrm{EG}} &= \frac{1}{\Lambda^{3(N+2n)}V}\prod_{i=1}^{n}\frac{1}{N_i!}\sum_{N_{a,i}=0}^{N_i}\sum_{\lambda_i=0}^{m_i}\frac{N_i!}{N_{a,i}!N_{b,i}!}\exp\left[w_i(\lambda_i)\right] \\ &\times\int_0^V dV_a\,(V_a)^{(N_a+n)}\,(V_b)^{(N_b+n)} \\ &\times\int_0^1 d\mathbf{s}_a^{N_a}d\mathbf{s}_a^n\exp\left[-\frac{U_a(\mathbf{s}_a^{N_a},\mathbf{s}_a^n,\lambda_1,...,\lambda_n)}{k_BT}\right] \\ &\times\int_0^1 d\mathbf{s}_b^{N_b}d\mathbf{s}_b^n\exp\left[-\frac{U_b(\mathbf{s}_b^{N_b},\mathbf{s}_b^n,\lambda_1,...,\lambda_n)}{k_BT}\right]. \end{aligned} \tag{2.30}$$

Here Λ is the de Broglie wavelength and k_B is the Boltzmann factor. $N_i = N_{a,i} + N_{b,i}$ is the total number of whole molecules of component i, and $N_a = \sum_i^n N_{a,i}$ and $N_b = \sum_i^n N_{b,i}$ are the total number of whole molecules in subsystem a and b respectively. A molecule is defined by a chain of interacting segments with a total length m_i for a molecule of component i. The dimensionless coordinates $\mathbf{s}_a^{N_a}$ and $\mathbf{s}_b^{N_b}$ describe the positions of all segments of the N_a and N_b whole molecules. The dimensionless coordinates $\mathbf{s}_a^n$ and $\mathbf{s}_b^n$ describe the positions of all beads of the n fractional molecules in subsystem a and b respectively. Each subsystem has one fractional molecule per component with fractional states defined by the coupling parameter λ_i. The coupling parameter determines the fractional state (number of interacting

segments) of the fractional molecules in both subsystems simultaneously, *i.e.* λ_i coupled segments in subsystem a and $(m_i - \lambda_i)$ in subsystem b. Therefore, $\lambda_i = 0$ defines an ideal chain molecule in subsystem a (a molecule where only bonded interactions are present) and a fractional molecule identical (but not equal) to a whole molecule in subsystem b. Here, discrete values of the coupling parameter in the range $\lambda_i = [0, ..., m_i]$ are considered, leading to a total of $m_i + 1$ possible fractional states. Note that only whole molecules of a specific component are indistinguishable from each other and can be permuted between subsystems. This explains the factors $1/N_i!$ and $N_i!/N_{a,i}!N_{b,i}!$ expressed in terms of the number of whole molecules. The weight functions $w_i(\lambda_i)$ are introduced to modify the Boltzmann statistics of the system in order to improve the sampling efficiency of all fractional states. The weight functions of each component are considered to be independent of each other, which is exact in the thermodynamic limit. Weight functions are determined iteratively using the Wang-Landau sampling method [142, 143] as explained below. The total energy of a subsystem U^a (the same for subsystem b), is the sum of the bonded interactions U_a^{bond} for all molecules in the subsystem, plus the intermolecular $U_a^{\text{inter}}(\mathbf{s}_a^{N_a}, \mathbf{s}_a^n, \lambda_1, ..., \lambda_n)$ and intramolecular interactions $U_a^{\text{intra}}(\mathbf{s}_a^{N_a}, \mathbf{s}_a^n, \lambda_1, ..., \lambda_n)$ for the N_a whole and n fractional molecules in the subsystem, $U_a = U_a^{\text{non-bonded}} + U_a^{\text{bonded}} = U_a^{\text{inter}} + U_a^{\text{intra}} + U_a^{\text{bond}}$. Only non-bonded interactions (intermolecular and intramolecular) are a function of the fractional state. Bonded interactions do not depend on the fractional state and are equivalent to those of whole molecules.

The probability that the system is in configuration α is proportional to,

$$\begin{aligned}\mathcal{P}_\alpha \quad \propto \quad & \exp\left[\sum_{i=1}^{n}\left(\ln\left(\frac{N_i!}{N_{a,i}!N_{b,i}!}\right) + w_i(\lambda_i)\right)\right. \\ & +(N_a + n)\ln V_a + (N_b + n)\ln V_b \\ & \left. -\frac{U_a(\mathbf{s}_a^{N_a}, \mathbf{s}_a^n, \lambda_1, ..., \lambda_n)}{k_B T} - \frac{U_b(\mathbf{s}_b^{N_b}, \mathbf{s}_b^n, \lambda_1, ..., \lambda_n)}{k_B T}\right]. \end{aligned} \tag{2.31}$$

A Markow chain in the space of fractional states can be organized by random changes in the coupling parameter, λ_i. Two different cases can be identified: changes without molecule transfer, and changes with molecule transfer. A coupling parameter change without molecule transfer will occur when the new fractional state $\lambda_i^{\text{new}} = \lambda_i^{\text{old}} + \Delta\lambda_i$ has a value within the range $[0, ..., m_i]$ and a change with molecule transfer takes place when λ_i^{new} is outside this range. The end-states, $\lambda_i = 0$ and $\lambda_i = m_i$, deserve special attention. A fractional molecule with coupling parameter $\lambda_i = m_i$ is fully coupled to the system, however, this molecule will become equal to a whole one only when a further change in the fractional state takes place (see Fig. 2.2). A molecule transfer is therefore defined as the state transition $\lambda_i = m_i \rightarrow 0$ from the old to a new randomly inserted fractional molecule. Strictly, only configurations with fractional molecules in their end-states have a clear physical meaning equivalent to that of a system without fractional molecules. However, sampling only when an end-state is visited has the inconvenience of observables averaged over a reduced number of samples. For a pure component system this is not truly a limitation, but for multicomponent systems the probability of visiting an end-state for all components at the same time is reduced to the joint probability of visiting those states. Nevertheless, in the thermodynamic limit, the fractional state does not affect the properties of the system. Therefore, all thermo-

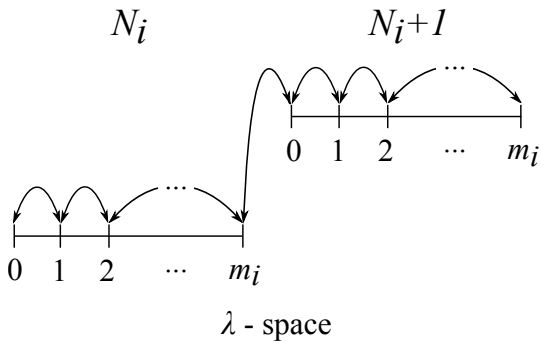

Figure 2.2: Schematic representation of changes in the coupling parameter space λ for component i. When a change in λ_i reaches the end-state m_i, the fractional molecule has the same interactions as a whole molecule but it is still not considered as a whole one. A new whole molecule is transferred to the subsystem, $N_i + 1$, only when a further change in the coupling parameter reaches a state beyond the full fractional state m_i.

dynamic properties are calculated based on the number of whole molecules present in the system independent of the fractional state.

Volume change
As in the case of the Gibbs ensemble, volume changes are performed by a random walk in the logarithm of the relative volume $\ln[V_a/V_b]$. Taking this into account, the partition function takes the form,

$$\begin{aligned} Q^{NVT-\mathrm{EG}} &= \frac{1}{\Lambda^{3(N+2n)}V}\prod_{i=1}^{n}\frac{1}{N_i!}\sum_{N_{a,i}=0}^{N_i}\sum_{\lambda_i=0}^{m_i}\frac{N_i!}{N_{a,i}!N_{b,i!}}\exp\left[w_i(\lambda_i)\right] \\ &\times\int_{-\infty}^{\infty}d\ln\left(\frac{V_a}{V_b}\right)\frac{V_aV_b}{V}(V_a)^{N_a+n}(V_b)^{N_b+n} \\ &\times\int_0^1 d\mathbf{s}_a^{N_a}d\mathbf{s}_a^n\exp\left[-\frac{U_a(\mathbf{s}_a^{N_a},\mathbf{s}_a^n,\lambda_1,...,\lambda_n)}{k_BT}\right] \\ &\times\int_0^1 d\mathbf{s}_b^{N_b}d\mathbf{s}_b^n\exp\left[-\frac{U_b(\mathbf{s}_b^{N_b},\mathbf{s}_b^n,\lambda_1,...,\lambda_n)}{k_BT}\right]. \end{aligned} \tag{2.32}$$

The criterion for a reversible change in the volume by a random walk in $\ln[V^a/(V-V^a)]$ is then equal to,

$$\begin{aligned} \mathcal{C}_{\alpha\beta} &= \exp\left[(N_a+n+1)\ln\left(\frac{V_a+\Delta V_a}{V_a}\right)+(N_b+n+1)\ln\left(\frac{V_b-\Delta V_a}{V_b}\right)\right. \\ &\left.-\frac{\Delta U_a}{k_BT}-\frac{\Delta U_b}{k_BT}\right], \end{aligned} \tag{2.33}$$

where ΔU_a and ΔU_b are the change in energy related to the volume change in in both subsystems.

Algorithm for a coupling parameter change in the expanded Gibbs ensemble
The algorithm for performing a trail change in the coupling parameter is described as follows:

1. The subsystem in which the fractional state is incremented is first chosen randomly with equal probability, $\mathcal{P}^{\text{sub}\,a} = \mathcal{P}^{\text{sub}\,b} = 1/2$.
2. The component i which experiences a change in the coupling parameter is chosen randomly with same probability for all components in the mixture, $\mathcal{P}^{\text{comp}\,1} = \mathcal{P}^{\text{comp}\,2} = ... = \mathcal{P}^{\text{comp}\,i}$.
3. A positive discrete change in the coupling parameter $\Delta\lambda_i$ is chosen randomly from $[1, 2, ..., \Delta\lambda_i^{\max}]$, where $\Delta\lambda_i^{\max}$ is adjusted depending on the acceptance ratio required for this trial move.
4. If the coupling parameter change $\Delta\lambda_i$ is not related with a molecular exchange, the criterion for accepting a trial change in the coupling parameter is given by Eq. 2.36.
5. If the coupling parameter change $\Delta\lambda_i$ is related with a molecular exchange, a new fractional molecule with random configuration is inserted randomly in the subsystem where the coupling parameter is increased and the the criterion for accepting a trial change in the coupling parameter is given by Eq. 2.39.
6. A new configuration β is accepted with a probability given by $\min(1, \mathcal{C}_{\alpha\beta})$.

The acceptance criterion for a change in the coupling parameter without and with molecular exchange is derived based on this form of the algorithm.

Coupling parameter change without molecular exchange
Every attempt of changing the configuration of the system from a configuration α to a configuration β by a change in the coupling parameter $\Delta\lambda_i$ for component i has to satisfy the condition of microscopic reversibility [105],

$$\mathcal{P}_{\alpha\beta} = \mathcal{P}_{\beta\alpha}. \tag{2.34}$$

For a change in the coupling parameter $\lambda_i^{\text{new}} = \lambda_i^{\text{old}} + \Delta\lambda_i$ *without* molecular exchange, the condition of microscopic reversibility is given by,

$$\mathcal{P}^{\text{sub}\,a}\ \mathcal{P}^{\text{comp}\,i}\ \mathcal{P}_\alpha\ \mathcal{P}^{\text{acc}}_{\alpha\beta} = \mathcal{P}^{\text{sub}\,b}\ \mathcal{P}^{\text{comp}\,i}\ \mathcal{P}_\beta\ \mathcal{P}^{\text{acc}}_{\beta\alpha}, \tag{2.35}$$

where,

$\mathcal{P}^{\text{sub}\,a}$	:	probability of selecting subsystem a for an increase in the fractional state.
$\mathcal{P}^{\text{comp}\,i}$	:	probability of selecting component i for an change in the coupling parameter.
$\mathcal{P}_\alpha$	:	probability of the system to be in configuration α, Eq. 2.31.
$\mathcal{P}^{\text{acc}}_{\alpha\beta}$	:	acceptance probability for a configurational change from α to β.

The probability of selecting any of both subsystems for a change in the coupling parameter is the same, $\mathcal{P}^{\text{sub}\,a} = \mathcal{P}^{\text{sub}\,b} = 1/2$, and the probability of selecting a component i is the same for all components in the system $\mathcal{P}^{\text{comp}\,1} = \mathcal{P}^{\text{comp}\,2} = ... = \mathcal{P}^{\text{comp}\,i} = 1/n$. The criterion for a reversible change in λ_i without molecular exchange is given by,

$$\mathcal{C}_{\alpha\beta} = \frac{\mathcal{P}^{\text{acc}}_{\alpha\beta}}{\mathcal{P}^{\text{acc}}_{\beta\alpha}} = \frac{\mathcal{P}_\beta}{\mathcal{P}_\alpha} = \exp\left[w_i(\lambda_i^{\text{new}}) - w_i(\lambda_i^{\text{old}}) - \frac{\Delta U_a}{k_B T} - \frac{\Delta U_b}{k_B T}\right], \tag{2.36}$$

where ΔU_a and ΔU_b indicate the change in energy in both subsystems due to a change in the coupling state of component i. It has to be noticed that for the case of chain molecules with constant bond length considered here, the change in energy considers the intermolecular U^{inter} as well as the intramolecular U^{intra} contributions. A new configuration β is accepted with a probability given by $\min(1, \mathcal{C}_{\alpha\beta})$.

Coupling parameter change with particle transfer
For a change in the coupling parameter $\Delta\lambda_i$ of component i *with* particle exchange (from subsystem a to b), the condition of microscopic reversibility is given by,

$$\begin{aligned} &N_{a,i}!N_{b,i}!\ \mathcal{P}^{\text{sub}\,b}\ \mathcal{P}^{\text{comp}\,i}\ \mathcal{P}^{\text{mol}\,i,a}_\alpha\ \mathcal{P}^{\text{pos}\,b}_\alpha\ \mathcal{P}_\alpha\ \mathcal{P}^{\text{acc}}_{\alpha\beta} = \\ &(N_{a,i}-1)!(N_{b,i}+1)!\ \mathcal{P}^{\text{sub}\,b}\ \mathcal{P}^{\text{comp}\,i}\ \mathcal{P}^{\text{mol}\,i,b}_\alpha\ \mathcal{P}^{\text{pos}\,a}_\beta\ \mathcal{P}_\beta\ \mathcal{P}^{\text{acc}}_{\beta\alpha}, \end{aligned} \tag{2.37}$$

where,

$\mathcal{P}^{\text{sub}\,b}$	:	probability of selecting subsystem b as the subsystem where the coupling state of the particle is increased.
$\mathcal{P}^{\text{comp}\,i}$	:	probability of selecting component i for a coupling state change.
$\mathcal{P}^{\text{mol}\,i,a}_\alpha$	:	probability of choosing a molecule of component i in subsystem a as the new fractional molecule, $1/N_{a,i}$.
$\mathcal{P}^{\text{pos}\,b}_\alpha$	:	probability of choosing a position in subsystem b for the insertion of a new fractional molecule $\lambda = 0$.
$\mathcal{P}_\alpha$	:	probability of the system to be in configuration α, Eq. 2.31.
$\mathcal{P}^{\text{acc}}_{\alpha\beta}$	:	probability of accepting a change in the configuration of the system from α to β.
$\mathcal{P}^{\text{mol}\,i,b}_\beta$	:	probability of choosing a molecule in subsystem b as the new fractional molecule, $1/(N_{b,i}+1)$.

The probability of the new configuration β is proportional to,

$$\begin{aligned} \mathcal{P}_\beta \propto \exp\Bigg[&\sum_{j\neq i}^{n}\left(\ln\left(\frac{N_j!}{N_{a,j}!N_{b,j}!}\right) + w_j(\lambda_j)\right) + \ln\left(\frac{N_i!}{(N_{a,i}-1)!(N_{b,i}+1)!}\right) + w_i(\lambda_i) \\ &+(N_a+n-1)\ln V_a + (N_b+n+1)\ln V_b \\ &-\frac{U_a(\mathbf{s}_a^{N_a-1}, \mathbf{s}_a^n, \lambda_1, ..., \lambda_n)}{k_B T} - \frac{U_b(\mathbf{s}_b^{N_b+1}, \mathbf{s}_b^n, \lambda_1, ..., \lambda_n)}{k_B T}\Bigg]. \end{aligned} \tag{2.38}$$

Therefore, for component type i the criterion for a reversible change in λ_i *with* particle exchange is given by,

$$\begin{aligned}
\mathcal{C}_{\alpha\beta} &= \frac{\mathcal{P}^{\rm acc}_{\alpha\beta}}{\mathcal{P}^{\rm acc}_{\beta\alpha}} \\
&= \frac{(N_{a,i}-1)!(N_{b,i}+1)!}{N_{a,i}!N_{b,i}!}\frac{\mathcal{P}^{{\rm mol}\,i,b}_{\beta}}{\mathcal{P}^{{\rm mol}\,i,a}_{\alpha}}\frac{\mathcal{P}_\beta}{\mathcal{P}_\alpha} \\
&= \exp\left[\ln\left(\frac{N_{a,i}}{N_{b,i}+1}\frac{V_b}{V_a}\right) + w_i(\lambda_i^{\rm new}) - w_i(\lambda_i^{\rm old}) - \frac{\Delta U_a}{k_BT} - \frac{\Delta U_b}{k_BT}\right], \qquad (2.39)
\end{aligned}$$

where ΔU_a and ΔU_b indicate the change in energy in both subsystems due to a change in the coupling state of component i with molecular transfer. As in the case of molecular exchange without particle transfer, the change in energy for chain molecules with constant bond length, the change in the energy of both subsystems considers the intermolecular $U^{\rm inter}$ as well as the intramolecular $U^{\rm intra}$ contributions to the energy. Here, the coupling state of the new inserted fractional molecule is equal to $\lambda_i^{\rm new} = \lambda_i^{\rm old} + \Delta\lambda_i - (m_i + 1)$. The particle transfer step $(m_i + 1) \rightarrow 0$ does not carry out any weight function change. A new configuration β is accepted with a probability given by $\min(1, \mathcal{C}_{\alpha\beta})$.

2.4.2. *NPT* expanded Gibbs ensemble

The partition function for constant pressure *NPT* expanded Gibbs ensemble simulations is given by (see section 2.3.3 for the constant pressure Gibbs ensemble),

$$\begin{aligned}
Q_{NPT} &= \left(\frac{P}{k_BT}\right)^2 \frac{1}{\Lambda^{3(N+2n)}} \prod_{i=1}^{n}\frac{1}{N_i!}\sum_{N_{a,i}=0}^{N_i}\sum_{\lambda_i=0}^{m_i}\frac{N_i!}{N_{a,i}!N_{b,i}!}\exp\left[w_i(\lambda_i)\right] \\
&\quad\times\int_0^\infty dV_a\,\exp\left[-\frac{PV_a}{k_BT}\right]V_a^{N_a+n} \\
&\quad\times\int_0^\infty dV_b\exp\left[-\frac{PV_b}{k_BT}\right]V_b^{N_b+n} \\
&\quad\times\int_0^1 d\mathbf{s}_a^{N_a}d\mathbf{s}_a^{n}\exp\left[-\frac{U_a(\mathbf{s}_a^{N_a},\mathbf{s}_a^{n},\lambda_1,...,\lambda_n)}{k_BT}\right] \\
&\quad\times\int_0^1 d\mathbf{s}_b^{N_b}d\mathbf{s}_b^{n}\exp\left[-\frac{U_b(\mathbf{s}_b^{N_b},\mathbf{s}_b^{n},\lambda_1,...,\lambda_n)}{k_BT}\right]. \qquad (2.40)
\end{aligned}$$

The constant value $(P/k_BT)^2$ is introduced to keep the partition function dimensionless [80]. Volume changes are performed for each system independently, in the logarithm of the volume. The criterion for accepting a trial change in the volume of each subsystem is given by Eq. 2.12. The acceptance criterion for a trial change in the coupling state of a component i is given by Eq. 2.36 for a change without molecular exchange and by Eq. 2.39 for a change with molecular exchange.

2.4.3. Wang-Landau algorithm

Ideally, an equal probability of visiting any fractional state is desired. For this aim, a weight function for every fractional state $w_i(\lambda_i)$ is introduced in the partition function (Eq. 2.30 and Eq. 2.40) to bias the statistics of the system. It is clear that in the modified system, the magnitude of the weight functions has to be inversely proportional to the density of states of the fractional state of the non-modified system. However, the magnitude of these weight functions cannot be know *a priori* and an iterative method is required for their determination. Wang and Landau proposed an iterative algorithm for estimating the density of states of systems in energy space [142, 143]. Similarly, this algorithm can be used for estimating the density of states in any other parameter space. Here, it is used for estimating the density of states in the coupling parameter space and therefore determining the values of the weight functions. The method is based on modifying the density of states of the system every time a fractional state is visited to produce a flat probability distribution in the coupling parameter space (flat histogram). The density of states is changed through the weight function $w_i(\lambda_i)$ by a modification factor ν that reduces the weight of a fractional state each time it is visited,

$$w_i(\lambda_i) \rightarrow w_i(\lambda_i) - \nu. \tag{2.41}$$

When a flat histogram is obtained, the value of the modification factor ν is reduced, $\nu \rightarrow \nu/2$, and the histograms are set to zero. A complete flat histogram is not possible and a flat histogram is identified when the difference between the largest and smallest frequency is smaller than 10% of the largest frequency. Changing the density of states at each step alters the Markowian chain and only a modification factor as small as the number precision of the computing machine will strictly obey detailed balance [144]. This condition is practically impossible and the iteration proceeds until the modification factor is reduced to a very small value. A final value of 1×10^{-9} is considered satisfactory in this work. A starting value of 1×10^{-5} was sufficient for reaching fast convergence avoiding large oscillations in the value of the weight functions.

2.5 Solubility of gases

2.5.1. Henry's law

The solubility of sligthly soluble gases in fluids is usually described using Henry's law, which establishes a proportional relation between the partial pressure of a gas and its concentration in the fluid solvent. The constant of proportionality is called the Henry coefficient and it is formally defined as [145],

$$H_k = \lim_{x_k \rightarrow 0} \frac{\hat{f}_k}{x_k}, \tag{2.42}$$

here $\hat{f}_k$ is the fugacity of the diluted gas in the fluid mixture. The subindex k is introduced to identify the gas as the diluted solute and x_k is the mole fraction of the diluted gas in the fluid.

The fugacity of component k is related to its chemical potential by,

$$\mu_k = \mu_k^0 + RT \ln \frac{\hat{f}_k}{f_k^0}, \tag{2.43}$$

where μ_k is the chemical potential of component k. The reference state is identified with the superscript 0. A similar equation can be written for an ideal gas,

$$\mu_k^{\mathrm{IG}} = \mu_k^0 + RT \ln \frac{\hat{f}_k^{\mathrm{IG}}}{f_k^0}. \tag{2.44}$$

The fugacity of component k in the ideal gas state is equal to its partial pressure, which at same temperature T and density ρ conditions as in the non-ideal fluid is equal to, $\hat{f}_k^{\mathrm{IG}} = x_k \rho k_B T$. Subtracting Eq 2.43 from Eq 2.44 leads to the residual chemical potential of component k [146],

$$\mu_k^{\mathrm{res}}(T, \rho, \mathbf{x}) = \mu_k(T, \rho, \mathbf{x}) - \mu_k^{\mathrm{IG}}(T, \rho, \mathbf{x}) = k_B T \ln \frac{\hat{f}_k(T, \rho, \mathbf{x})}{x_k \rho k_B T}, \tag{2.45}$$

where $\mathbf{x}$ indicates the mole fraction of the fluid.

The relationship between Henry coefficient and the residual chemical potential at defined temperature and density is obtained by replacing Eq. 2.45 into Eq. 2.42 [146, 147],

$$H_k(T, \rho, \mathbf{x}) = \rho k_B T \exp\left[\frac{\mu_k^{\mathrm{res}}(T, \rho, \mathbf{x})}{k_B T}\right]. \tag{2.46}$$

This expression is obtained in the infinite dilution limit of component k, where the composition of the fluid $\mathbf{x}$ is not changed by the presence of the solute.

A dimensionless Henry coefficient that is directly related to the residual chemical potential is defined as following,

$$\ln H_k^*(T, \rho, \mathbf{x}) = \ln \frac{H_k(T, \rho, \mathbf{x})}{\rho k_B T} = \frac{\mu_k^{\mathrm{res}}(T, \rho, \mathbf{x})}{k_B T}. \tag{2.47}$$

The relative effect of connectivity and molecular anisotropy in chain fluids is studied by relative Henry coefficients, defined as the ratio between the Henry coefficient for the solubility in a chain fluid H_k to the Henry coefficient for the solubility in a monomer (single-segment) fluid H_2^0 at same temperature and density conditions.

$$\frac{H_k}{H_k^0} = \exp\left[\frac{\mu_k^{\mathrm{res}}(T, \rho, \mathbf{x})}{k_B T} - \frac{\mu_k^{\mathrm{res},0}(T, \rho)}{k_B T}\right]. \tag{2.48}$$

2.5.2. Widom's test-particle insertion method

In the test-particle insertion method proposed by Widom [148], the chemical potential of a component k in a fluid with mole fraction $\mathbf{x}$ is calculated by the energy change of a virtual insertion of a molecule of component k in the fluid. The method is derived from the relation between chemical potential and the partition function of the system.

The chemical potential of a component k in a mixture with mole fraction $\mathbf{x}$ at constant temperature T and density ρ is defined by the partial molar property [149],

$$\mu_k(T,\rho,\mathbf{x}) = \left.\frac{\partial A(T,\rho,\mathbf{x})}{\partial N_k}\right|_{T,\rho,N_{j\neq k}}, \tag{2.49}$$

where $A(T,\rho,\mathbf{x})$ is the Helmholtz free energy which is related to the canonical partition (NVT ensemble, Eq. 1.3) as following,

$$A(T,\rho,\mathbf{x}) = -k_B T \ln Q^{NVT}. \tag{2.50}$$

The canonical partition function is defined by Eq. 1.3, which in reduced coordinates is expressed as,

$$Q^{NVT} = \frac{V^N}{\Lambda^{3N} N!}\int d\mathbf{s}^N \exp\left[-\frac{\mathcal{U}(\mathbf{s}^N)}{k_B T}\right]. \tag{2.51}$$

In the Widom's test particle method, a test-particle is temporary inserted in the fluid. The partition function of the actual system is identified as Q_N^{NVT} and the partition function of the system with the inserted test-particle is denoted as Q_{N+1}^{NVT}. Replacing Eq. 2.50 into Eq. 2.49, the chemical potential of component k is given by,

$$\begin{aligned}
\mu_k &= -k_B T \ln\left(\frac{Q_{N+1}^{NVT}}{Q_N^{NVT}}\right) \\
&= -k_B T \ln\left(\frac{V}{\Lambda^3(N+1)}\right) - k_B T \ln\left\langle \exp\left[-\frac{\Delta\mathcal{U}_k^{\text{test}}}{k_B T}\right]\right\rangle \\
&= \mu^{\text{IG}} + \mu_k^{\text{res}},
\end{aligned} \tag{2.52}$$

where $\Delta\mathcal{U}_k^{\text{test}}$ is the energy change in the system by the temporary insertion of a test-particle of component k. From this last equation, it can be identified that the residual chemical potential of component k in the fluid is obtained from the ensemble average of the Boltzmann factor related to the energy of insertion of the test-particle [146, 148, 150],

$$\frac{\mu_k^{\text{res}}(T,\rho,\mathbf{x})}{k_B T} = -\ln\left\langle \exp\left[-\frac{\Delta\mathcal{U}^{\text{test}}}{k_B T}\right]\right\rangle. \tag{2.53}$$

In the case of hard-sphere fluids Eq. 2.53 reduces to,

$$\frac{\mu_k^{\text{res,HS}}(T,\rho,\mathbf{x})}{k_B T} = -\ln\langle p\rangle, \tag{2.54}$$

where the parameter p takes the value of 1 for a virtual test-particle insertion without overlap or 0 for a virtual insertion with overlap.

Calculation of the residual chemical potential in the *NPT* ensemble is derived from the partition function given in Eq. 2.9,

$$\begin{aligned} Q^{NPT} &= \left(\frac{P}{k_B T}\right) \frac{1}{\Lambda^{3N} N!} \int_0^\infty dV\, V^N \exp\left[-\frac{PV}{k_B T}\right] \int_0^1 d\mathbf{s}^N \exp\left[-\frac{U(\mathbf{s}^N)}{k_B T}\right] \\ &= \frac{P}{k_B T} \int_0^\infty dV\, \exp\left[-\frac{PV}{k_B T}\right] Q^{NVT}. \end{aligned} \tag{2.55}$$

The chemical potential of component k can be then obtained from,

$$\begin{aligned} \mu_k &= -k_B T \ln\left(\frac{Q_{N+1}^{NPT}}{Q_N^{NPT}}\right) \\ &= -k_B T \ln\left(\frac{\langle V\rangle}{\Lambda^3 (N+1)}\right) - k_B T \ln \frac{\left\langle V \exp\left[-\Delta\mathcal{U}_k^{\text{test}}/k_B T\right]\right\rangle}{\langle V\rangle} \\ &= \mu^{\text{IG}} + \mu_{NPT}^{\text{res}}. \end{aligned} \tag{2.56}$$

Therefore, the residual chemical potential of component k is calculated in the *NPT* ensemble from [132, 151, 152],

$$\frac{\mu^{\text{res}}(T, \rho', \mathbf{x})}{k_B T} = -\ln \frac{\left\langle V \exp\left[-\Delta\mathcal{U}_k^{\text{test}}/k_B T\right]\right\rangle}{\langle V\rangle}. \tag{2.57}$$

It has to be noticed that in this equation calculations are performed at constant temperature and pressure conditions and the density in Eq. 2.57 is obtained from the ensemble average $\rho' = \langle\rho\rangle = \langle N/V\rangle$. In the case of hard-sphere systems, this expression reduces to,

$$\frac{\mu_k^{\text{res,HS}}(T, \rho', \mathbf{x})}{k_B T} = -\ln \frac{\langle V p\rangle}{\langle V\rangle}, \tag{2.58}$$

where the parameter p takes the value of either 1 or 0 as explained before.

3

Liquid crystal phase behavior of hard-sphere chain fluids

The liquid crystal phase behavior of linear and partially-flexible hard-sphere chain fluids and the solubility of a hard-sphere gas in them are studied using constant pressure Monte Carlo simulations (NPT ensemble). An extensive study on the liquid crystal phase behavior of linear hard-sphere 7-mer to 16-mer, 18-mer, and 20-mer chain fluids is shown in this chapter. The phase behavior of partially-flexible fluids with a total length of 8, 10, 14 and 15 segments with different lengths in the linear part was also determined. For linear fluids, a maximum in the isotropic to nematic packing fraction change is observed for the linear 15-mer and 16-mer chain fluids. The infinite dilution solubility of hard spheres in linear and partially-flexible hard-sphere chain fluids is calculated using the Widom test-particle insertion method. To identify the effect of chain connectivity and molecular anisotropy, solubility is expressed as relative Henry coefficients, defined as the ratio between the Henry coefficient of a gas in the chain fluid to Henry coefficient of a gas in a monomer fluid at same packing fraction. A linear relationship between relative Henry coefficients and packing fraction is observed for all linear fluids. Furthermore, this linearity is independent of liquid crystal ordering and seems to be independent of chain length for the linear hard-sphere 10-mer and longer chains. A similar trend was observed for the solubility of hard spheres in partially-flexible fluids. At higher packing fractions, the small flexibility of these fluids seems to improve solubility in comparison with their linear counterparts.

This chapter is based on:
B. Oyarzún, T. van Westen, and T.J.H. Vlugt *J. Chem. Phys.* **138** (2013) 204905 [46].

3.1 Introduction

Fluids made of linear hard-sphere chain molecules can show liquid crystal phase for chain molecules with sufficient elongation. Vega *et al.* [85] studied the phase behavior of linear hard-sphere chain fluids with a length of 3, 4, 5, 6 and 7 segments (3-mer to 7-mer) from constant pressure Monte Carlo simulations. These authors observed that the linear hard-sphere 5-mer and longer chains form liquid crystal phases, while shorter chains experience a direct transition from the isotropic to the crystal state [85–87]. Williamson *et al.* [88] investigated the phase behavior of the linear hard-sphere 7-mer fluid in all phases from the isotropic to the crystal state. The isotropic-nematic phase behavior of the linear hard-sphere 8-mer and 20-mer chain fluid was obtained by Yethiraj *et al.* [89]. Whittle *et al.* [90] studied the phase behavior of linear 6-mer and 8-mer fused hard-sphere chain molecules with length-to-width ratios ranging from 3.5 to 5.2, observing a nematic phase only for the longest molecule.

Real liquid crystal molecules have a certain degree of flexibility which is mainly provided by alkyl terminal substituents [2]. It has been shown that increasing flexibility destabilizes the nematic and smectic phases favoring the isotropic state [91, 153]. Introducing molecular flexibility into hard-sphere chain molecules can be done either homogeneously by semi-flexible molecules where a bond-bending and torsional potential is defined for the whole molecule, or heterogeneously by partially-flexible molecules where potentials are defined for different parts of the molecule. The first approach was used by Wilson *et al.* [153, 154] for a fluid made of semi-flexible hard-sphere 7-mer chain molecules bonded by potential wells, as well as by Yethiraj *et al.* [89] who determined the isotropic and nematic phase behavior of semi-flexible hard-sphere 8-mer and 20-mer chain molecules with bending potentials of varying stiffness. A partially-flexible model was employed by McBride *et al.* [91, 91, 93] for fused hard-sphere molecules composed of a linear and a freely-jointed part with a total length of 15 segments and with 8 to 15 segments in the linear part. Escobedo *et al.* [94] used the expanded Gibbs ensemble and the pseudo-Gibbs ensemble for calculating the isotropic-nematic phase transition of hard-sphere 8-mer and 16-mer chain molecules with finite and infinite bond bending potentials (linear chains).

In this chapter, simulation results are presented for the liquid crystal phase behavior of linear and partially-flexible hard-sphere chain fluids. Simulation details are described in section 3.2. The phase behavior of linear hard-sphere chain fluids is presented in section 3.3 and the effect of flexibility is studied in section 3.4 from liquid crystal phase behavior of partially-flexible hard-sphere chain fluids. The infinite dilution solubility of hard spheres in hard-sphere chain fluids is described in section 3.5. Results of this chapter are summarized in section 3.6.

3.2 Simulation details

The phase behavior of linear and partially-flexible hard-sphere chain fluids was obtained by Monte Carlo simulations in the isobaric-isothermal *NPT* ensemble. Periodic boundary conditions were used in a rectangular simulation box with varying orthogonal dimensions. The following Monte Carlo trial moves were used: displacement, rotation, volume change, and partial-regrowth of the freely-jointed part using the Configurational-bias Monte Carlo method [80, 100, 101, 155]. In the Configurational-bias Monte Carlo method 10 trail direc-

tions were attempted for regrowing each segment in the freely-jointed part. A system size of N=350 molecules was used for all simulations except for the linear hard-sphere 7-mer and 8-mer chain fluids in which a larger number of 576 molecules was employed. The latter was done in order to compare actual simulation results with previous simulation data, especially with that obtained by Williamson *et al.* [88] for the linear hard-sphere 7-mer chain fluid. Simulations with 216 and 350 molecules were also performed for the linear 7-mer in order to study the system size effect. In the equilibration period, the maximum displacement and rotation angle were adjusted in order to obtain an acceptance ratio of 20%. Rotation around every Cartesian axes was considered separately due to the orientation of molecules around the nematic director in nematic and smectic phases. Volume changes were performed in an anisotropic manner by choosing independently the box side which is expanded/contracted [89, 91]. In this way, the natural anisotropy introduced by a rectangular box is decoupled from the phase anisotropy inherent to ordered systems. Displacement and rotation trial moves were selected with the same probability, while the probability of attempting a volume change was set to 2%. In the case of partially-flexible molecules, 15% of the trial moves were attempted to regrow the freely-jointed part. The anisotropic expansion of the simulation box may result in the contraction of one of its dimensions to zero due to the finite size of the system. This event is avoided by using large system sizes but at the cost of long simulation runs. A good balance between a very low occurrence of this event and short simulation runs was obtained for a system size of 350 molecules. A typical simulation run comprises 1×10^6 Monte Carlo cycles in the equilibration period and 1×10^6 cycles in the production period. Every Monte Carlo cycle consisted of a total of N Monte Carlo trial moves. However, close to the isotropic-nematic transition region, the required number of simulation cycles in the equilibration and production periods was normally doubled due to large fluctuations in the observed variables.

Initial isotropic and nematic configurations were used for the simulation of linear hard-sphere chain fluids. For partially-flexible systems, however, only nematic initial configurations were used, since for these systems simulations starting from an isotropic configuration required very long equilibration periods, typically larger than 5×10^6 Monte Carlo cycles. For linear chains, simulation starting from an isotropic configuration were obtained for a region close to the isotropic-nematic phase transition in order to verify that results in the isotropic and nematic phases are independent of the initial configuration, and to determine the hysteresis at the isotropic-nematic phase transition. Isotropic initial configurations were obtained by placing molecules in the simulation box randomly without a preferred orientation. A nematic configuration was generated by placing molecules in random positions but perfectly aligned on the direction of the largest dimension of the simulation box. In the case of partially-flexible molecules, an initial linear molecular configuration was chosen. The initial dimensions of the simulation box were selected in order to ensure that the initial packing fraction of the system is located in either the isotropic or nematic regions. Every simulation run was started from an independent initial configuration in order to avoid correlation between results.

Simulations were performed at constant reduced pressure defined as $P^* = P\,v_{\mathrm{mol}}/k_BT$, where P is pressure, k_B is the Boltzmann constant, T is temperature, and $v_{\mathrm{mol}} = m\pi d^3/6$ is the volume of a molecule made of m beads with diameter d set to unity. The density is expressed dimensionless by the packing fraction $\eta = Nv_{\mathrm{mol}}/V$, where N is the number

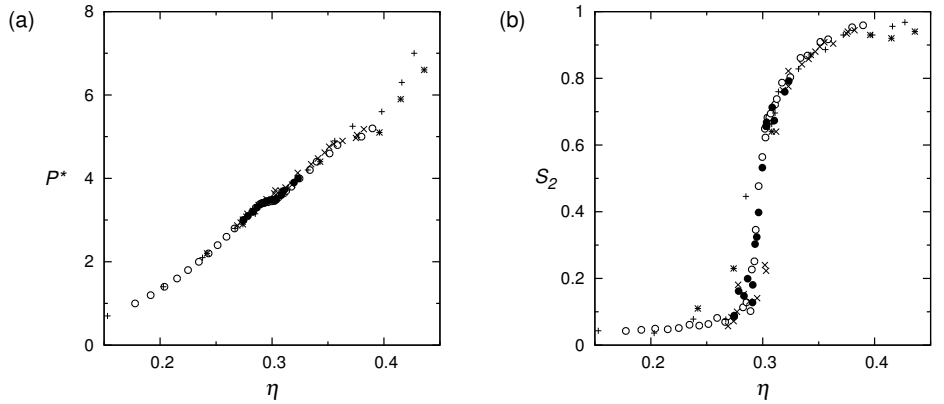

Figure 3.1: Liquid crystal phase behavior of the linear hard-sphere 7-mer chain fluid: (a) reduced pressure P^*, (b) order parameter S_2 as a function of packing fraction η. Results obtained from initial isotropic and nematic configurations are denoted by closed (•) and open circles (◦) respectively. Previous data from Williamson and Jackson [88] are denoted by crosses (×) for initial isotropic configurations and by pluses (+) for initial crystal configurations. In addition, results of Vega *et al.* [85] started from a crystal structure are indicated by an asterisk (∗). The size of the symbols is larger than the relative error in the packing fraction (1-2%) and the relative error in the order parameter (2-5%) .

of molecules. The orientational order of the system is measured by the order parameter S_2 Eq. 2.3, which has a value of 0 in an isotropic fluid and a value of 1 for a completely aligned nematic phase.

The solubility of hard spheres in hard-sphere chain fluids at infinite dilution is described by Henry coefficients defined by Eq. 2.46. The residual chemical potential is calculated by the Widom test-particle insertion method [148], which for Monte Carlo simulations of hard spheres at constant pressure takes the form of Eq. 2.54 [152]. A total of 100 test-particle insertions are performed for each configuration sampled every 1×10^3 Monte Carlo cycles.

3.3 Linear hard-sphere chain fluids

A systematic study on the liquid crystal phase behavior was performed for linear 7-mer to 16-mer, 18-mer, and 20-mer hard-sphere chain fluids. Previous simulation data for the linear 7-mer [85, 88], 8-mer and 20-mer [89] are present in literature. Compared to previous studies, simulation runs in this work were significantly longer (typically by a factor of 2 to 10) in particular close to the isotropic-nematic phase transition. In addition, a large number of simulations was performed close to the isotropic-nematic phase transition in order to describe the transition region with high accuracy. The phase behavior of the 7-mer was already determined by Williamson *et al.* [88] and Vega *et al.* [85]. Due to the large collection of data existing for this system, the linear hard-sphere 7-mer molecule can be considered as a suitable reference system. Nevertheless, new and more precise simulation data for the 7-mer was obtained. Fig. 3.1 shows the liquid crystal phase behavior of the linear hard-sphere 7-mer chain fluid compared to literature data. It can be observed that all simulation data are comparable with slight differences at reduced pressures of 5.0 and higher. From the extensive results obtained in this work the isotropic-nematic phase transition is found at a

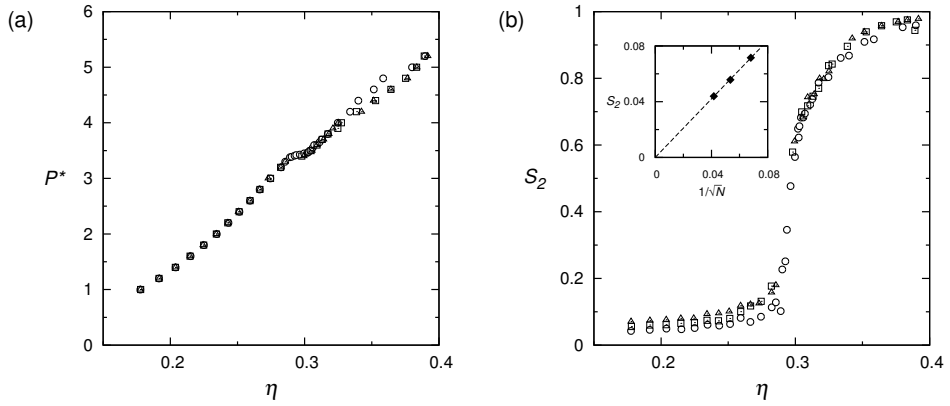

Figure 3.2: Finite size effect on: (a) reduced pressure P^*, (b) order parameter S_2 for the linear hard-sphere 7-mer chain fluid as a function of packing fraction η. All results were obtained from initial nematic configurations with system sizes of 216 (△), 350 (□) and 576 (○) molecules. The inset in figure (b) shows the system size dependence of the order parameter for the linear 7-mer in the isotropic region at a reduced pressure of P^*=1 and at a packing fraction η∼0.178 for systems sizes of 216, 350 and 576 molecules. In this sub-figure, values are the average of four independent simulation results and the symbol size is larger than one standard deviation. The solid line is a linear fit with $R^2 = 0.999$.

reduced pressure of P^*∼3.39−3.49 at a packing fraction of η^I∼0.289−0.291 for the isotropic phase and of η^N∼0.302−0.303 for the nematic phase. These values lie in between the ranges P^*∼3.15−3.78, η^I∼0.266−0.303 and η^N∼0.285−0.312 reported by Williamson *et al.* [88], and it is in agreement with the reduced pressure range P^*∼2.9−3.7 and packing fractions η^I≈0.274 and η^N≈0.308 reported by Vega *et al.* [85]. The large hysteresis at the isotropic-nematic phase transition observed by Williamson *et al.* [88] was not detected here. It is suspected that close to the isotropic-nematic phase transition, where fluctuations are large, the simulations results of Williamson and Jackson may either not be well equilibrated or their sampling period was too short (4×10^5 compared to 2×10^6 of this work). Nevertheless, a narrow hysteresis of 0.1 in reduced pressure was detected for the linear 7-mer. A phase transition to the smectic-A phase was observed at a reduced pressure P^*∼4.80−5.00 and η^N≈0.359, η^S≈0.380.

The system size effect of the linear 7-mer was also studied and results for systems sizes of 216, 350 and 576 molecules are compared in Fig. 3.2. It can be observed that results for reduced pressure versus packing fraction at the isotropic and nematic regions for all three systems are comparable. However, the precise location of the nematic-smectic phase transition seems to be system size dependent. For the larger 576 molecules system, a first-order phase transition to a smectic-A phase is detected at a reduced pressure between 4.8 and 5.0. On the contrary, for the smaller 350 and 216 molecules systems, partial smectic ordering with no clear defined smectic layers was observed for lower reduced pressure between 4.0 and 5.0. For all three system sizes, smectic-A layers were clearly recognized only at reduced pressures of 5.0 and higher. This system size dependence on the nematic-smectic phase transition was already pointed out by Polson *et al.* [98] for the nematic to smectic phase transition of hard spherocylinders in the limit of infinite aspect ratio. In their study, the free-energy profile at the nematic-smectic phase transition was calculated for different

system sizes (928, 540 and 280 molecules) as a function of smectic ordering. These authors found that a large Gibbs energy barrier between the nematic and the smectic state exists only for the larger system. The Gibbs energy barrier was negligible for the intermediate system size and vanishing for the smaller one. In their work, Polson *et al.* concluded that, in the thermodynamic limit, the nematic to smectic phase transition of spherocylinders seems to be of first-order for all aspect ratios. Similarly, here, a first order nematic-smectic phase transition was observed only for the larger system size of 576 molecules and the partial smectic ordering observed in the smaller systems can be a consequence of a low Gibbs energy barrier caused by the reduced system size.

Another effect of the finite size of the system can be identified in Fig. 3.2 from the order parameter in the isotropic region. It can be observed that in the isotropic region all three systems show a positive value different than zero for the order parameter, approaching a system-size dependent limiting value as the packing fraction is reduced. The origin of this finite order in the isotropic phase and its corresponding finite order parameter value was described by Eppenga *et al.* [34]. For isotropic systems of finite size, these authors demonstrated the largest eigenvalue of the **Q**-tensor (from which the order parameter is estimated) deviates from zero by $1/\sqrt{N}$. The inset in Fig. 3.2 (b) shows the relation between order parameter values and system size at same packing fraction. It can be observed that the $1/\sqrt{N}$ dependence is almost exact leading to a vanishing value of the order parameter on the thermodynamic limit.

The phase behavior of the linear hard-sphere 8-mer to 16-mer, 18-mer, and 20-mer chain fluids is shown in Figs. 3.3-3.5. Literature data for the linear 8-mer and 20-mer from Yethiraj *et al.* [89] are also included. These authors used a slightly different definition for the order parameter, based on the middle eigenvalue of the **Q**-tensor instead of the largest one used here. The middle eigenvalue leads to values of the order parameter that fluctuate around zero in the isotropic phase. Although both definitions are directly related (as shown in the previous section), the definition based on the largest eigenvalue is considered to be more consistent with the mathematical framework of the **Q**-tensor. Initial isotropic and nematic configurations led to hysteresis in the isotropic-nematic phase transition. The magnitude of the hysteresis showed to be dependent of the packing fraction difference at the isotropic-nematic transition, varying from a difference in reduced pressure of ~0.04 for the linear 7-mer to ~0.17 for the linear 15-mer fluid.

Fig. 3.2 and Table 3.1 summarize the reduced pressure and packing fraction change at the isotropic-nematic transition for all linear systems studied. Reduced transition pressures were calculated at the middle-point of the hysteresis, which was estimated by the average of the reduced pressure at coexistence for results starting from an initial isotropic and nematic configurations. Packing fractions were obtained by fitting a third order polynomial on the packing fraction as a function of reduced pressure for each isotropic and nematic branches separately. The isotropic and nematic packing fraction at phase transition were obtained using the previous calculated reduced transition pressures in the fitted equations. Fig. 3.2 also includes the available literature data for the isotropic-nematic phase transition of linear hard-sphere chain fluids. It is observed that the literature data is comparable with the results for the reduced pressure at coexistence but no systematic behavior can be identified from literature data for the packing fraction difference. From Fig. 3.2 (a), it can be observed that with increasing chain length, the transition pressure decreases in a continuous manner.

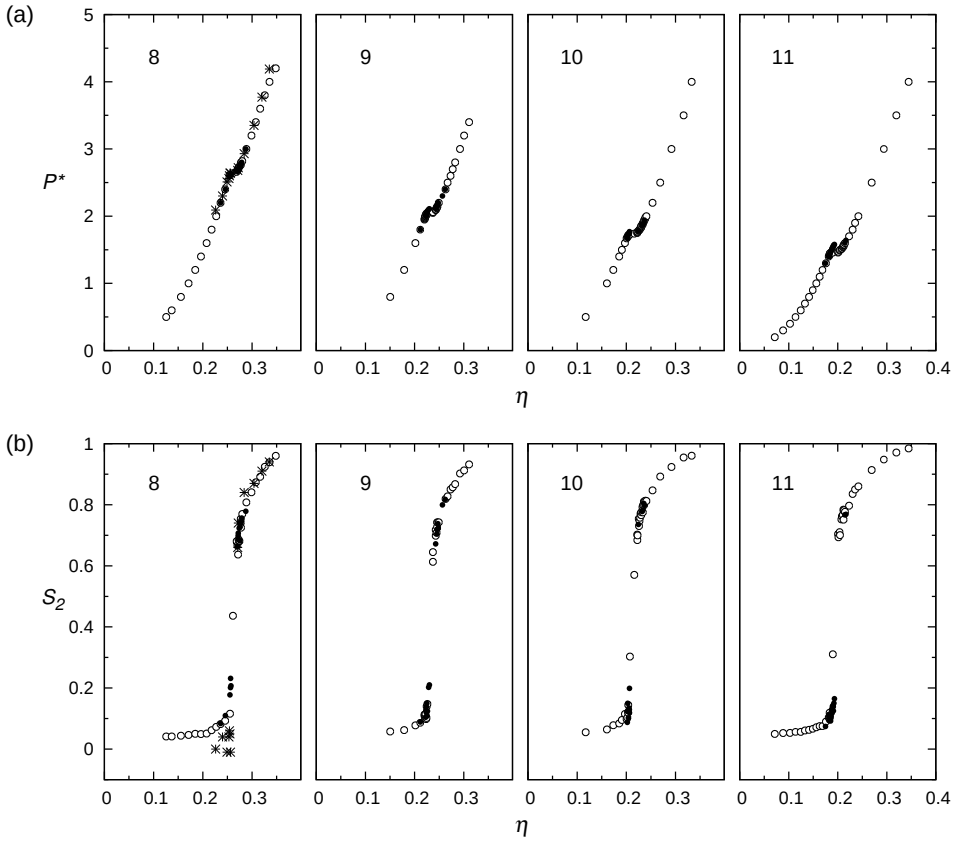

Figure 3.3: Liquid crystal phase behavior of linear hard-sphere 8-mer to 11-mer chain fluids: (a) reduced pressure P^*, (b) order parameter S_2 as a function of packing fraction η. Results obtained from initial isotropic and nematic configurations are denoted by closed (•) and open circles (○) respectively. Previous simulation data from Yethiraj *et al.* [89] for the 8 linear chain are indicated by an asterisk (∗).

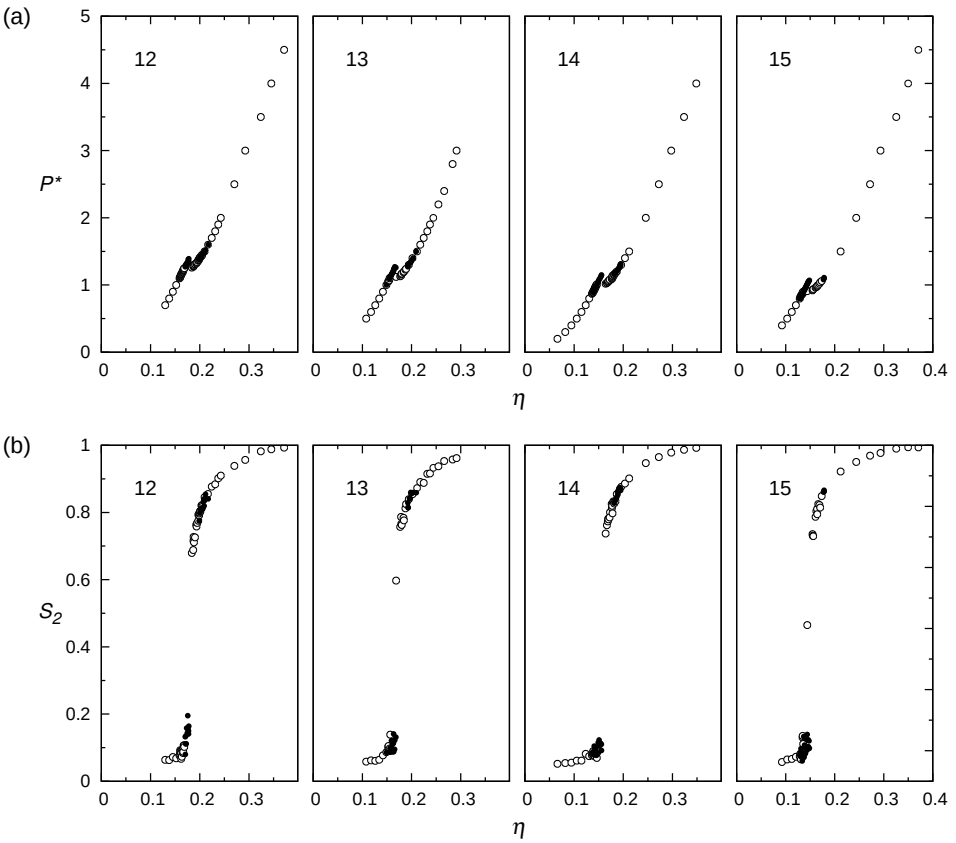

Figure 3.4: Liquid crystal phase behavior of linear hard-sphere 12-mer to 15-mer chain fluids: (a) reduced pressure P^*, (b) order parameter S_2 as a function of packing fraction η. Results obtained from initial isotropic and nematic configurations are denoted by closed (•) and open circles (○) respectively.

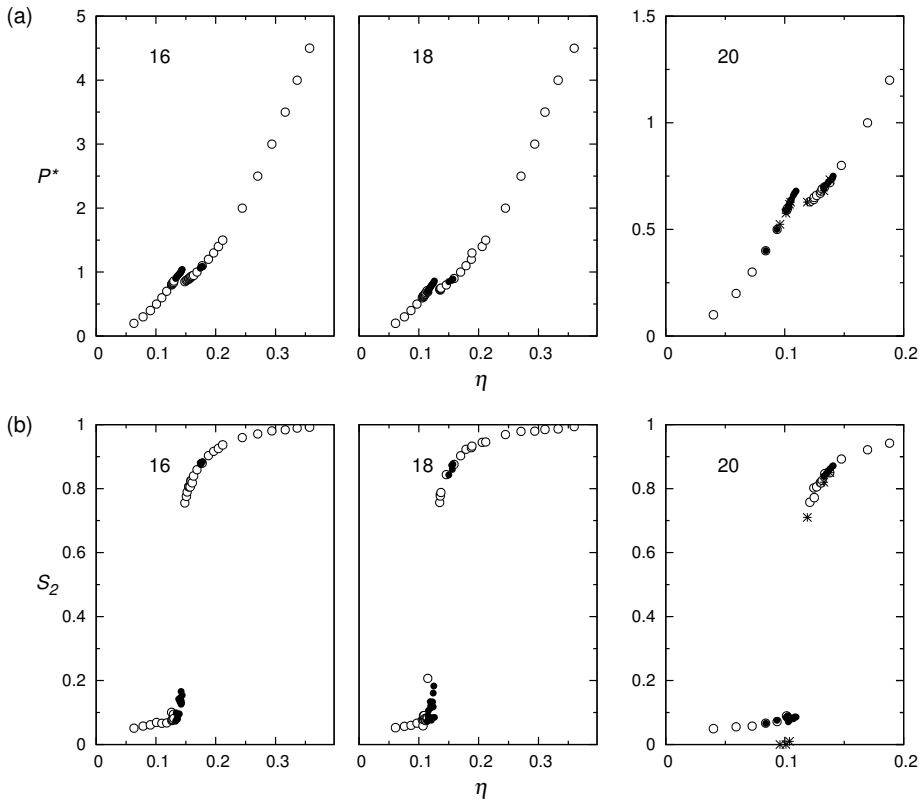

Figure 3.5: Liquid crystal phase behavior of linear hard-sphere 16-mer, 18-mer, and 20-mer chain fluids" (a) reduced pressure $P*$, (b) order parameter S_2 as a function of packing fraction η. Results obtained from initial isotropic and nematic configurations are denoted by closed (•) and open circles (○) respectively. Previous simulation data from Yethiraj *et al.* [89] are indicated by an asterisk (∗).

Table 3.1: Reduced pressure P^*, packing fraction of the isotropic phase η^I, packing fraction of the nematic phase η^N and packing fraction change at the isotropic-nematic phase transition $\Delta\eta^{N-I}$ for linear molecules with a length of linear hard-sphere 7-mer to 16-mer, 18-mer, and 20-mer chain fluids.

m	P^*	η^I	η^N	$\Delta\eta^{N-I}$
7	3.47	0.2941	0.3009	0.0068
8	2.65	0.2560	0.2678	0.0118
9	2.08	0.2269	0.2415	0.0146
10	1.76	0.2065	0.2231	0.0166
11	1.53	0.1900	0.2083	0.0183
12	1.32	0.1733	0.1935	0.0202
13	1.20	0.1625	0.1838	0.0213
14	1.09	0.1528	0.1747	0.0219
15	0.99	0.1429	0.1649	0.0220
16	0.94	0.1388	0.1610	0.0220
18	0.78	0.1207	0.1425	0.0218
20	0.65	0.1073	0.1250	0.0177

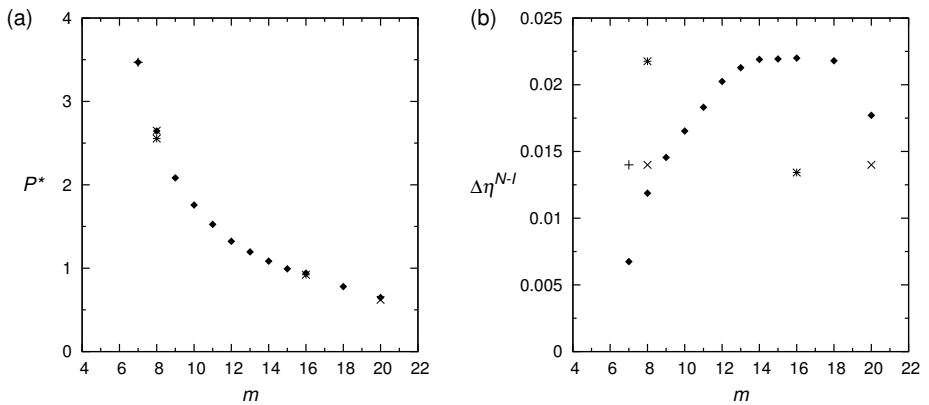

Table 3.2: (a) Transition pressures P^*, and (b) packing fraction change $\Delta\eta^{N-I}$ at the isotropic-nematic coexistence for linear hard-sphere 8-mer to 16-mer, 18-mer, and 20-mer chain fluids. Previous data from Williamson *et al.*[88] for the linear 7-mer (+), Yethiraj *et al.* [89] for the linear 8-mer and 20-mer (×) and from Escobedo and *et al.* [94] for the linear 8-mer and 16-mer (∗) are also indicated.

Table 3.3: Reduced pressure P^*, packing fraction of the isotropic phase η^I, packing fraction of the nematic phase η^N and packing fraction change at the isotropic-nematic phase transition η^{N-I} for partially-flexible hard-sphere 15-14-mer, 15-13-mer, 15-12-mer, 14-13-mer and 14-12-mer chain fluids.

$m - m_R$	P^*	η^I	η^N	$\Delta\eta^{N-I}$
15-14	1.28	0.1577	0.1740	0.0163
15-13	1.77	0.1788	0.1906	0.0118
15-12	2.54	0.2071	0.2174	0.0103
14-13	1.44	0.1689	0.1841	0.0152
14-12	2.12	0.2034	0.2139	0.0105

On the other hand, from Fig. 3.2 (b) it can be observed that the packing fraction difference shows a maximum for the linear 15-mer and the 16-mer. This is a rather surprising result that has not been explicitly reported in the simulation of hard-sphere chain systems before. Bolhuis *et al.* [44] obtained for spherocylinders the isotropic and nematic densities at coexistence as a function of shape anisotropy L/D by a modified Gibbs-Duhem integration method. From their data, it can be identified that a maximum is reached in the isotropic-nematic density difference at coexistence for a shape anisotropy between 15 and 20. From an Onsager type density functional theory, Fynewever *et al.* [156] show a similar behavior of the packing fraction difference for linear hard-sphere chain fluids as a function of chain length, with a maximum at a chain length close to 10. However, neither of these studies mentions the existence of a maximum in the packing fraction difference explicitly.

3.4 Partially flexible hard-sphere chain fluids

The liquid crystal phase behavior of partially-flexible molecules is investigated for different molecular lengths with varying degree of flexibility. Results for this section were obtained from an initial nematic configuration only, since simulations started from an initial isotropic configuration required excessively long equilibration periods. In Fig. 3.6, the phase behavior of the partially-flexible hard-sphere 15-12-mer, 15-13-mer, and 15-14-mer chain fluids is shown. It can be observed that increasing flexibility destabilizes the nematic phase with respect to the isotropic phase, leading to higher transition pressures at higher coexistence packing fractions. The isotropic to nematic phase transition is driven by a difference in the orientational average of the excluded volume between the isotropic and nematic phase [20]. Flexibility reduces this difference [157], therefore a higher pressure is required in order to induce the transition to the nematic state. Reduced pressures and packing fraction changes at the isotropic-nematic phase transition are summarized in Table 3.3. It can be identified that flexibility increases the transition pressure and reduces the isotropic-nematic packing fraction difference. A transition to a smectic-A phase is identified at a reduced pressure in the range of $3.0 - 3.5$ for the partially-flexible hard-sphere 15-14-mer and 15-13-mer chain fluids and between $3.40 - 3.60$ for the partially-flexible 15-12-mer.

The average end-to-end length in the isotropic and nematic regions for the partially-flexible hard-sphere 15-14-mer, 15-13-mer and 15-12-mer chain fluids is shown in Fig. 3.7 as a function of pressure. It can be clearly identified that in the isotropic region the average end-to-end length decreases as pressure increases. This behavior is a consequence of the

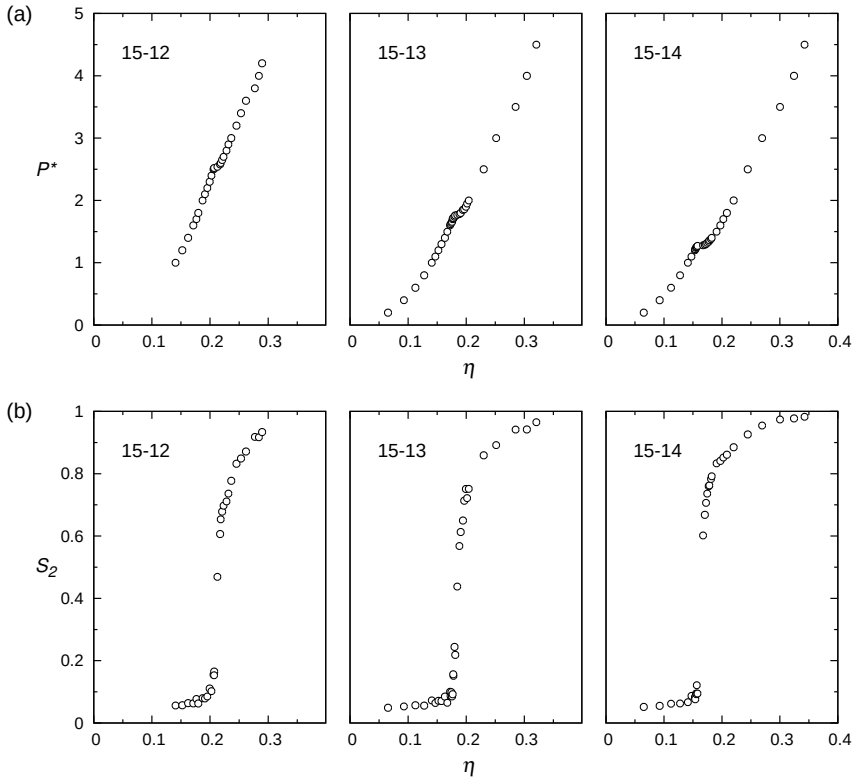

Figure 3.6: Liquid crystal phase behavior of partially-flexible hard-sphere 15-12-mer, 15-13-mer and 15-14-mer chain fluids: (a) reduced pressure P^*, (b) order parameter S_2 as a function of packing fraction η.

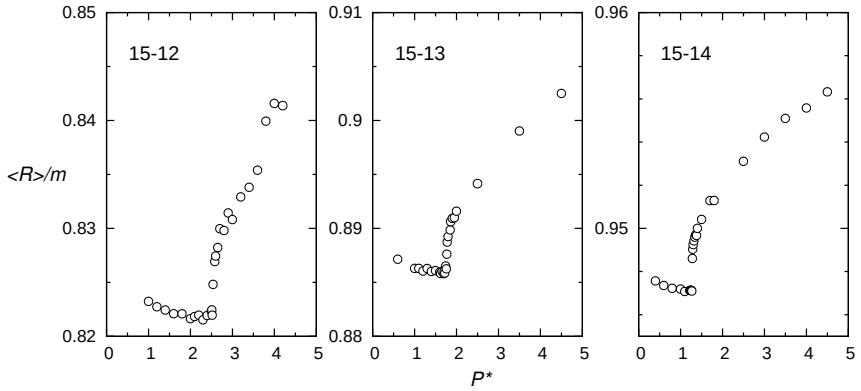

Figure 3.7: Average end-to-end length of partially-flexible hard-sphere 15-14-mer, 15-13-mer, 15-12-mer chain fluids. Results are shown relative to the total chain length 15-mer.

tendency of molecules to be more entangled at increased packing fractions. On the contrary, a step increase in the average end-to-end length occurs at the isotropic to nematic phase transition. This increased molecular elongation is a result of the orientational ordering in the nematic phase, forcing molecules to stretch along the phase director. Nevertheless, this step-difference in the average end-to-end length at coexistence is relatively small, varying from ∼0.2% for the partially-flexible 15-14-mer to ∼1% for the partially-flexible 15-12-mer. In the nematic region, the average end-to-end length increases asymptotically towards the total molecular length with increasing pressure. Although changes in the average end-to-end length are relatively small, Fig. 3.7 shows that the average molecular configuration of partially-flexible hard-sphere molecules varies with reduced pressure (packing fraction) and with molecular ordering, either isotropic and nematic. This change in the average molecular configuration may have an effect on the free volume of the fluid [157], influencing the solubility of hard spheres in hard-sphere fluids as it will be discussed in section 3.5.

Fig. 3.8 shows the liquid crystal phase behavior of the partially-flexible hard-sphere 14-13-mer, 14-12-mer and 14-10-mer chain fluids. A nematic phase is identified only for the partially-flexible 14-13-mer and 14-12-mer. Reduced pressures and packing fraction changes at the isotropic-nematic phase transition for these fluids are specified in Table 3.3. A transition to the smectic-A phase is identified at a reduced pressure in the range of 3.0−3.5 for the 14-13 fluid and 3.5 − 4.0 for the 14-12 fluid. The more flexible partially-flexible 14-10-mer does not show a nematic phase, experiencing a continuous transition from the isotropic to the smectic-A phase. The fact that for the partially-flexible 14-10-mer the isotropic to smectic phase transition is continuous is possibly a consequence of a negligible energy barrier between these phases due to the reduced system size as was already pointed out in section 3.3 for the linear hard-sphere 7-mer chain fluid. However, this premise was not tested here and simulations in larger systems would be required. A clear smectic-A phase could not be recognized for the partially-flexible hard-sphere 14-10-mer chain fluid, however partial smectic-A ordering was observed for reduced pressures of 5.0 and 5.2. A clear smectic-C phase is observed at a reduced pressure of 8.0 but partial smectic-C layering

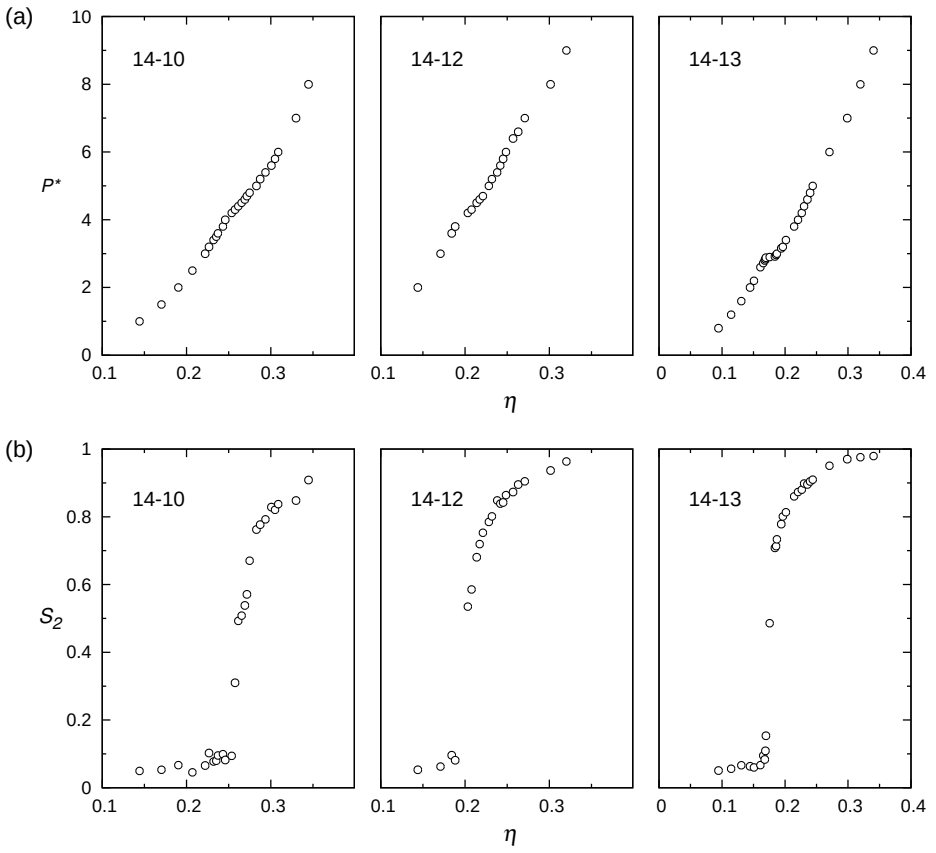

Figure 3.8: Liquid crystal phase behavior of partially-flexible hard-sphere 14-10-mer, 14-12-mer and 14-13-mer chain fluids: (a) reduced pressure P^*, (b) order parameter S_2 as a function of packing fraction η.

is already identified at reduced pressures between 5.4 and 7.0.

Fig. 3.9 shows the phase behavior of the partially-flexible hard-sphere 8-7-mer, 8-6-mer and 10-8-mer chain fluids. A continuous isotropic to smectic-A phase transition is observed for the partially-flexible 8-7-mer system in the reduced pressure range of 5.4 – 5.8 and clear smectic-A layers are identified at reduced pressures of 5.9 and higher. In the partially-flexible 8-6-mer system, clearly defined smectic-A layers could not be identified, however partial smectic ordering was observed at a reduced pressure of 14 and higher. For this system, a continuous phase transition from the isotropic to the smectic-A state was observed between reduced pressures of 9.4 and 10.4. Finally, the partially-flexible 10-8-mer shows a continuous phase transition from the isotropic to the smectic-A state between pressures of 4.7 and 5.6 and clear smectic-A layers at pressures of 5.8 and higher.

3.5 Solubility of hard spheres in hard-sphere chain fluids

The solubility of hard spheres in a hard-sphere chain fluid depends on the available free volume in the fluid, which is in principle determined by the molecular configuration, packing fraction, and orientation of all molecules in the fluid [157, 158]. Here, the relative importance of molecular configuration, *i.e.* connectivity and rigidity ,is investigated by means of relative Henry coefficients defined by Eq. 2.48. The residual chemical potential of a hard sphere in the monomer fluid, *i.e.* the hard-sphere fluid, H_k^0 is calculated from the Boublik-Mansoori-Carnahan-Starling-Leland equation of state [159–161]. The validity of this equation was verified with simulation results, showing an excellent agreement for the residual chemical potential of hard spheres in a hard sphere fluid.

Fig. 3.10 (a) shows relative Henry coefficients for the solubility of hard spheres in linear hard sphere chain fluids and Fig. 3.10 (b) shows the relative Henry coefficients for the solubility of hard spheres in partially-flexible hard sphere chain fluids. From Fig. 3.10 (a), a linear relationship between relative Henry coefficients and packing fraction can be identified for all linear fluids. A linear fit calculated from the results for linear hard-sphere 10-mer and longer chain fluids is included in Fig. 3.10 (a) and (b). This linearity seems to be independent of liquid crystal ordering and fairly independent of chain length for linear hard-sphere 10-mer and longer chain fluids.

In contrast to linear hard-sphere chain molecules, the average molecular configuration of partially-flexible hard-sphere molecules changes with packing fraction as it was shown in Fig. 3.7. It can be observed that at packing fractions lower than $\eta = 0.23$ the solubility of hard spheres in 15-14, 15-13, 15-12, 14-13 and 14-12 partially-flexible hard-sphere chain fluids follows the same linear relationship with packing fraction as for the linear hard-sphere chain fluids. As it is shown in Table 3.3, the isotropic-nematic phase transition of the nematic forming partially-flexible hard-sphere chain fluids takes place at packing fractions not higher than 0.2174, indicating that partial flexibility do not affect the relative behavior of solubility with packing fraction at the isotropic-nematic phase transition. The effect of larger flexibilities is also shown in Fig. 3.10 (b), which includes relative Henry coefficients calculated from literature data for the chemical potential of hard spheres in a freely-jointed hard-sphere 16-mer chain fluid [119, 163]. It can be observed that, at low packing fractions $\eta < 0.23$, relative Henry coefficients for the partially-flexible and fully flexible chain molecules do not appreciably deviate from the linear behavior derived from the linear hard-sphere chain fluids. At packing fractions higher than η=0.23, the solubility of hard spheres

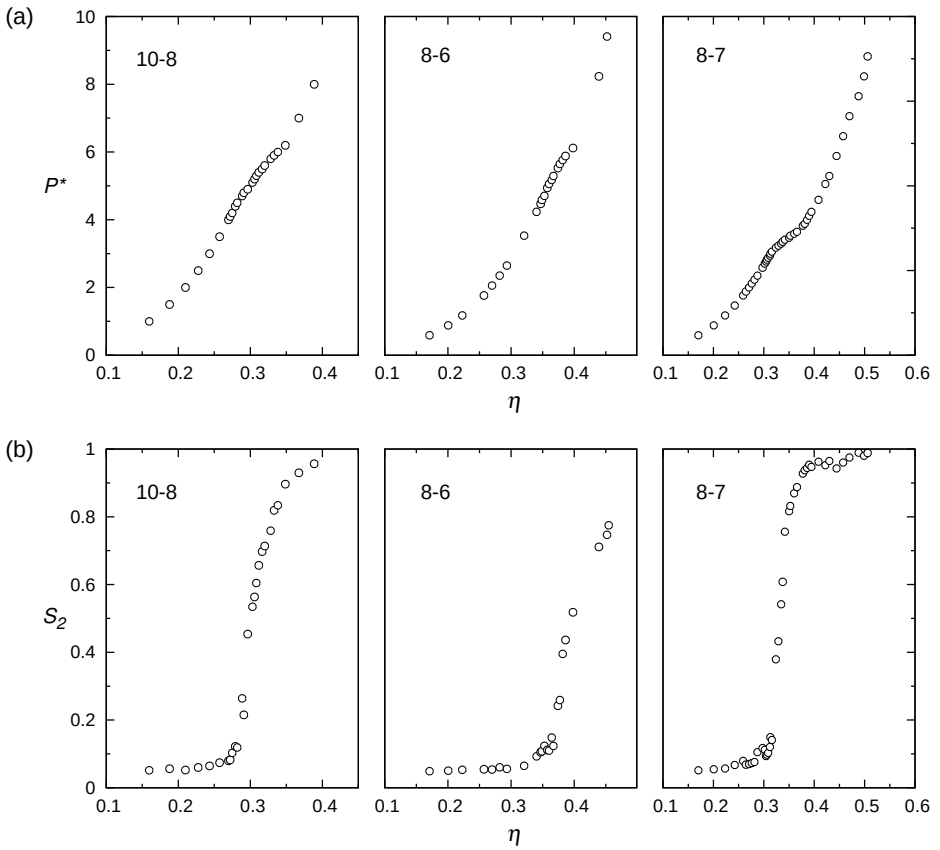

Figure 3.9: Liquid crystal phase behavior of partially-flexible hard-sphere 10-8-mer, 8-6-mer and 8-7-mer chain fluids: (a) reduced pressure P^*, (b) order parameter S_2 as a function of packing fraction η.

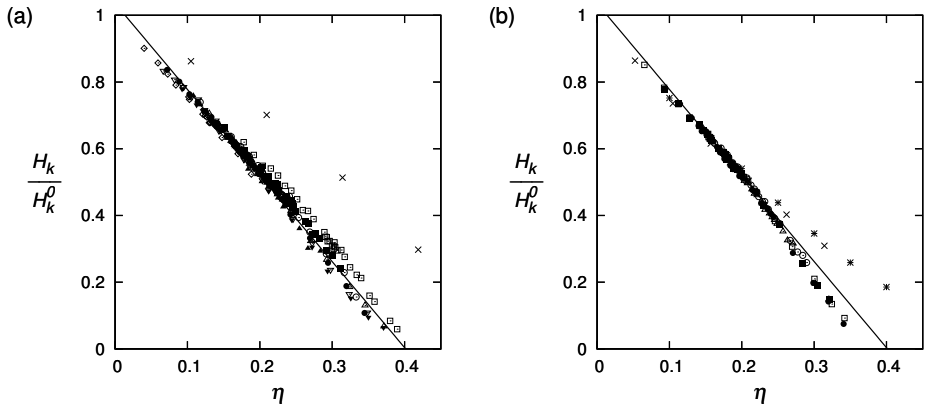

Figure 3.10: Relative Henry coefficients for the solubility of hard spheres in: (a) linear hard-sphere 7-mer (□), 9-mer (■), 10-mer (○), 11-mer (●), 12-mer (△), 13-mer (▲), 14-mer (▽), 15-mer (▼) and 20-mer (◇); (b) partially-flexible hard-sphere chain fluids 15-14-mer (□), 15-13 (■), 15-12 (○), 14-13 (●) and 14-12 (△). The solid line is a linear fit obtained with the data of the linear hard-sphere 10-mer and longer chain fluids, with slope -2.580 and intersection 1.036 (R^2=0.991). Relative Henry coefficients for hard spheres in a hard dumbbell fluid (×) were calculated from literature data for the chemical potential of hard spheres in a hard dumbbell fluid by Ben-Amotz and Omelyan [162]. Relative Henry coefficients for hard spheres in a freely-jointed hard-sphere 16-mer chain fluid were calculated from the data of Escobedo and de Pablo [119] (∗) and from the data of Kumar *et al.* [163] (×).

seems to increase for the partially-flexible hard-sphere chain fluids and to decrease for the freely-jointed hard-sphere chain fluid at the same packing fraction. A more clear insight to this effect is given in Fig. 3.11, where the effect of molecular flexibility in packing fraction is shown by the dimensionless rigidity parameter defined as the ratio between the number of rigid bonds angles to the total bond angles in the molecule [77, 157],

$$\chi_R = \begin{cases} \dfrac{m_R - 2}{m - 2} & ; \quad m > 2 \\ 1 & ; \quad m \leq 2 \end{cases} . \tag{3.1}$$

Fig. 3.11 (a) shows that at low packing fractions flexibility $\chi_R \rightarrow 0$ effectively increases the packing fraction of the fluid, reducing in principle the solubility of gases in the liquid crystal phase. However, this increment is relatively small (~4%), which explains together with the low values for the packing fraction the unnoticeable difference of relative Henry coefficients between linear and fully flexible chain fluids at low packing fractions. At high packing fractions, Fig. 3.11 (b), a minimum in packing fraction is observed as flexibility increases. For packing fractions below the value corresponding to χ_R=0, the same packing fraction value can be related to two different values of the rigidity parameter, one closer to the linear rigid chain χ_R=1 and one closer to the flexible chain χ_R=0. The same argument can be used for the behavior of solubility with flexibility at high packing fractions, *i.e.* two solubilities regimes, one closer to the linear chain fluid and one similar to the fully-flexible chain. For chain fluids with high flexibility, increasing rigidity reduces the packing fraction of the fluid with the consequence of a higher solubility compared to the fully-flexible case.

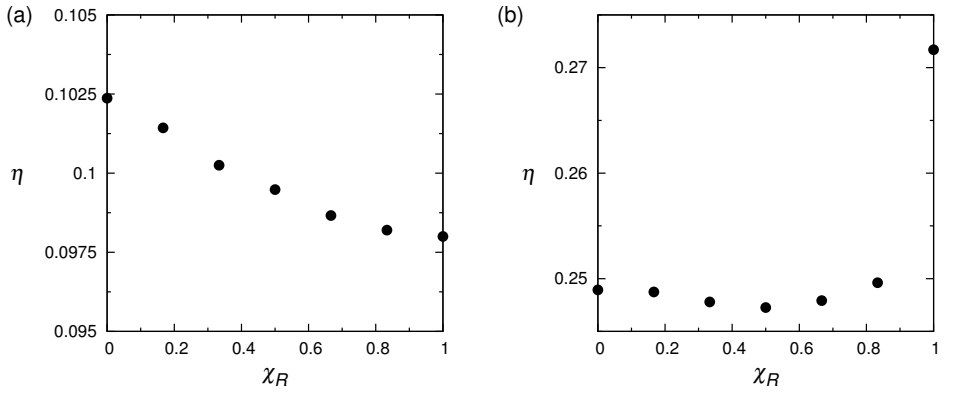

Figure 3.11: The effect of molecular rigidity χ_R on the packing fraction η of a hard-sphere 8-mer chain fluid at constant pressure: (a) $P^* = 0.3$, (b) $P^* = 2.7$.

For chain fluids with high rigidity, increasing flexibility reduces also the packing fraction of the fluid with the consequence of a higher solubility compared to the linear case. This behavior explains in principle the observed increase in solubility due to flexibility for the partially-flexible molecules shown in Fig. 3.10 (b).

To verify the independence of solubility with nematic ordering, constant volume Monte Carlo simulations at a packing fraction in-between the isotropic-nematic phase transition were performed using an umbrella sampling technique for the order parameter [80]. In these simulations, order parameter values were restricted to ranges of width 0.05 between 0 and 1. The simulation of every order parameter range was performed separately from an initial nematic configuration, which was allowed to freely evolve until a configuration with an order parameter value inside the desired range was obtained. From there on, trial moves that try to change the phase configuration to a new one with an order parameter outside the selected order parameter range were rejected. Fig. 3.12 shows the results for relative Henry coefficients as a function of order parameter for a linear hard-sphere 7-mer and 15-mer chain fluid at a constant packing fraction in-between the isotropic-nematic phase transition. From this figure, it can be clearly identified that relative Henry coefficients are independent of the nematic ordering, being a constant for a determined value of the packing fraction. This result indicates that at constant packing fraction the orientation of molecules does not influence the free volume between a hard sphere and a linear hard-sphere chain molecule. Although in the low packing fraction limit this result is expected due to a negligible interaction between fluid molecules, at finite values of the packing fraction this behavior could not be known *a priori* due to multi-body interactions in the fluid.

3.6 Conclusions

An extended description of the liquid crystal phase behavior of linear hard-sphere 7-mer to 16-mer, 18-mer and 20-mer chain fluids was obtained from constant pressure Monte Carlo simulations. For these systems, an accurate description of the isotropic to nematic phase transition was obtained, showing a decrease in the reduced transition pressure with increas-

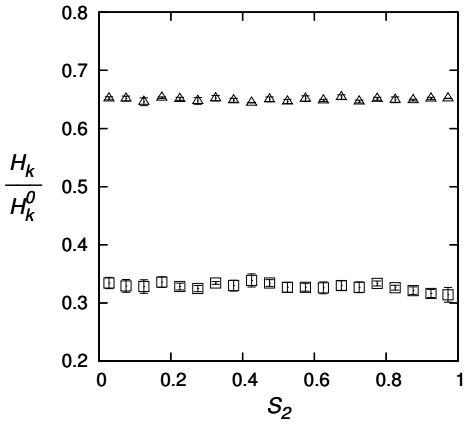

Figure 3.12: Relative Henry coefficients as a function of order parameter S_2 for the solubility of hard spheres in a linear hard-sphere 7-mer chain fluid at constant packing fraction $\eta = 0.295$ (□) and in a linear hard-sphere 15-mer chain fluid at constant packing fraction $\eta = 0.147$ (△).

ing chain length and a maximum in the isotropic to nematic packing fraction change for the linear 15-mer and 16-mer. The liquid crystal phase behavior of the partially-flexible hard-sphere 15-14-mer, 15-13-mer, 15-12-mer, 14-13-mer, 14-12-mer, 14-10-mer, 10-8-mer, 8-7-mer and 8-6-mer chain fluids was also determined. A nematic phase was only observed for the partially-flexible 15-14-mer, 15-13-mer, 15-12-mer, 14-13-mer, 14-12-mer chain fluids. Other partially-flexible fluids experienced a direct transition from the isotropic to the smectic state. Flexibility increases the transition pressures reducing the isotropic-nematic packing fraction difference. The infinite dilution solubility of hard spheres in linear and partially-flexible hard-sphere chain fluids was also studied. A linear relationship between relative Henry coefficients and packing fraction was observed for all linear hard-sphere chain fluids. Moreover, this linearity seems to be independent of chain length for the linear 10-mer and longer linear chains. The influence of molecular ordering on solubility was also investigated, showing that at constant packing fraction the nematic ordering does not influence the solubility of hard spheres in liquid crystal fluids. Results for the solubility of hard spheres in the nematic forming partially-flexible hard-sphere 15-14-mer, 15-13-mer, 15-12-mer, 14-13-mer and 14-12-mer chain fluids showed that in the isotropic-nematic transition region neither ordering or flexibility affected the linear behavior between relative Henry coefficients and packing fraction obtained from the linear fluids. However, it was observed that at higher packing fractions the solubility of hard spheres seems to increase for the low flexibilities of the nematic forming partially-flexible hard-sphere chain fluids and decrease for a freely-jointed hard-sphere chain fluid.

4

Isotropic-nematic phase equilibrium of hard-sphere chain fluids

The isotropic-nematic phase equilibria of single component linear hard-sphere chain fluids and binary mixtures of them are obtained from Monte Carlo simulations. In addition, the infinite dilution solubility of hard spheres in the coexisting isotropic and nematic phases is determined from the residual chemical potential of hard spheres in the fluid. Phase equilibria calculations are performed in an expanded formulation of the Gibbs ensemble. This method allows to carry out an extensive simulation study on the phase equilibria of pure linear hard-sphere 7-mer to 20-mer chain fluids and binary mixtures of an 8-mer with a 14-mer, a 16-mer and a 19-mer. The effect of molecular flexibility on the isotropic-nematic phase equilibria is assessed on the 8-mer+19-mer mixture by allowing one and two freely-jointed segments at the end of the longest molecule. Results for binary mixtures are compared with the theoretical predictions of van Westen et al. Ref. 78. Excellent agreement between theory and simulations is observed. The infinite dilution solubility of hard spheres in the hard-sphere fluids is obtained by the Widom test-particle insertion method. As in the previous chapter on single-component hard-sphere chains, a linear relationship between relative infinite dilution solubility (relative to that of hard spheres in a hard-sphere fluid) and packing fraction is found. It is observed that the solubility difference between coexisting isotropic and nematic phases is enhanced in binary mixtures compared to the pure components.

This chapter is based on:
B. Oyarzún, T. van Westen, and T.J.H. Vlugt *J. Chem. Phys.* **142** (2015) 064903 [164].

4.1 Introduction

Liquid crystal phases have been observed in molecular simulation studies of anisotropic hard molecules with diverse shapes [33–45]. From all possible anisotropic systems, tangent hard-sphere chains [46, 85, 88, 89] are the most simple segment-based model of liquid crystals. Segment-based molecules are relevant in the development of physically-based perturbation theories describing the behavior of liquid crystals [78, 83]. Linear and partially-flexible hard-sphere chains formed by a linear part and a freely-jointed part are used for studying the properties of liquid crystal fluids. Partial flexibility is introduced to reproduce the experimental observation that a certain degree of flexibility is required for the stability of liquid crystal phases over the crystal state [2, 165]. Flexibility is introduced to study its effect on the isotropic-nematic phase transition. Molecular simulation results for these systems are scarce, principally due to the difficulties on performing phase equilibria calculations of non-simple fluids with classical simulation techniques. In this work, an extended molecular simulation study on the isotropic-nematic phase equilibria of hard-sphere chain fluids is carried out. Furthermore, simulation results are compared with the theoretical predictions obtained from a recently developed equation of state [77, 78, 83].

In this chapter, simulation results for the isotropic-nematic phase transition of single-component and binary mixtures of hard-sphere chain fluids are presented. Details of the employed simulation technique are described in section 4.2. Simulation results for the isotropic-nematic phase equilibria of single-component linear hard-sphere chain fluids are reported in section 4.3. Simulation results for binary mixtures of linear hard-sphere chain fluids are presented in section 4.4. The effect of flexibility is studied in binary mixtures of linear and partially-flexible hard-sphere chain fluids is show in section 4.5. Results for the infinite dilution solubility of hard spheres in all studied systems are reported in section 4.6.

4.2 Simulation details

The isotropic-nematic phase equilibrium of linear and partially-flexible hard-sphere chain fluids was obtained by Monte Carlo simulations in an expanded version of the Gibbs ensemble [125]. The method is based on the gradual exchange of molecules by the coordinated coupling / decoupling of segments of a fractional molecule between phases as described in section 2.4. Constant volume *NVT* expanded Gibbs ensemble simulations are used for determining the phase equilibria of pure components, while constant pressure *NPT* expanded Gibbs ensemble simulations are used for the calculation of the phase equilibria of binary mixtures.

During a simulation the following trial moves are attempted: displacements, rotations, reptation, configurational-bias partial regrowths (only for partially-flexible molecules)[80], volume changes, identity exchanges [67, 166] (only for mixtures of linear chains), and coupling parameter changes. They are selected randomly but with a fixed probability proportional to the ratio 100:100:10:100:1:100:1000 respectively. Volume changes are performed isotropically in the logarithm of the volume (for simulations at constant pressure, volume changes are performed in one subsystem at a time). Simulation boxes for a starting isotropic configuration are defined cubic. A rectangular box with edge lengths with a ratio of 1:1.1:1.2 are used for initial nematic configurations. Periodic boundary conditions are used in all simulation boxes. Maximum displacement, rotation, volume, and coupling param-

eter changes are adjusted for a maximum acceptance ratio of 20%. A Monte Carlo cycle is defined by a number of trial moves equal to the number of molecules N in the system, typically in the order of $1{\times}10^3$. The number of Monte Carlo cycles required were typically $5{\times}10^6$ for equilibration and $2{\times}10^6$ cycles for production. Isotropic and nematic phases are identified by the order parameter S_2 defined by Eq 2.3. A value of S_2 close to 0 identifies the isotropic phase and a value close to 1 is related to the nematic phase. Configurations are sampled periodically independent of the fractional state. For the finite size systems studied here, it is observed that results obtained from end-state sampling do not differ significantly from those obtained from sampling regardless the fractional state. Therefore, all thermodynamic properties are calculated based on the number of whole molecules present in the system independent of the fractional state.

Simulations start with initial isotropic and nematic configurations. Initial configurations are obtained from independent constant pressure *NPT* ensemble simulations that approximate the volume of each phase at equilibrium. In the case of pure components, initial estimations of the packing fractions are taken from the previous section on pure linear hard-sphere chain fluids, section 3.3. For the case of mixtures, initial packing fractions, mole fractions, and equilibrium pressures are approximated from the theoretical work of van Westen *et al.* [83]. The initial size of the simulation boxes is dependent on chain length. The initial edge lengths of both simulation boxes are defined with a value that has to be larger than the length of the longest molecule in the system. Small systems sizes result in simulation boxes with at least one edge length close to the length of the molecule, inducing the formation of smectic phases due to restricted positional order perpendicular to the molecular length. An initial cubic box (isotropic phase) with a size of 25 was sufficient for all studied systems. For the rectangular box (nematic phase), an initial edge length of 25 (the shorter edge) for systems with molecules shorter than 17 beads, and a length of 27 for longer molecules was observed to be sufficient.

The solubility of gases is expressed in terms of dimensionless Henry coefficients Eq. 2.47. The infinite dilution residual chemical potential is obtained by the Widom test-particle insertion method as described in section 2.5.2. Equilibrium configurations are sampled every $1{\times}10^3$ Monte Carlo cycles and a total of 100 test-particle insertions are attempted for each sample. To identify the effect of connectivity and molecular anisotropy on solubility, relative Henry coefficients are used as defined by Eq. 2.48. The solubility of hard spheres in a hard-sphere chain fluid H_0 are calculated from the Boublik-Mansoori-Carnahan-Starling-Leland equation of state [159–161].

4.3 Linear hard-sphere chain molecules

The isotropic and nematic phase behavior of linear hard-sphere chain fluids of different lengths was reported in the previous section 3.3. There, the isotropic and nematic packing fractions at equilibrium were approximated from one-phase constant pressure *NPT* ensemble simulations. The isotropic and nematic packing fractions at equilibrium are directly calculated from two-phase simulations. In Table 4.1 the isotropic and nematic packing fractions at equilibrium for linear hard-sphere 7-mer to 20-mer chain fluids. Packing fraction is defined as $\eta = N_m v_m / V$, where N_m is the total number of segments, $v_m = \pi\sigma^3/6$ the volume of a single segment, and V the volume of the simulation box. It can be noticed that a maximum in the packing fraction difference exists for the 14-mer. However, due to

Table 4.1: Packing fraction of the isotropic η^I and nematic phase η^N, and packing fraction differences $\Delta\eta^{N-I}$ at equilibrium for linear 7-mer to 20-mer chain molecules. Mean values and standard deviations are obtained from at least 10 independent simulation runs.

m	η^I	η^N	$\Delta\eta^{N-I}$
7	0.2945 ± 0.0014	0.3033 ± 0.0010	0.0088 ± 0.0017
8	0.2548 ± 0.0011	0.2650 ± 0.0010	0.0102 ± 0.0015
9	0.2274 ± 0.0016	0.2391 ± 0.0009	0.0118 ± 0.0018
10	0.2066 ± 0.0009	0.2228 ± 0.0007	0.0162 ± 0.0011
11	0.1859 ± 0.0010	0.2000 ± 0.0008	0.0141 ± 0.0013
12	0.1722 ± 0.0008	0.1903 ± 0.0006	0.0181 ± 0.0010
13	0.1636 ± 0.0007	0.1859 ± 0.0006	0.0223 ± 0.0009
14	0.1530 ± 0.0009	0.1766 ± 0.0009	0.0236 ± 0.0013
15	0.1426 ± 0.0011	0.1657 ± 0.0011	0.0231 ± 0.0016
16	0.1344 ± 0.0008	0.1574 ± 0.0013	0.0230 ± 0.0015
17	0.1268 ± 0.0005	0.1497 ± 0.0009	0.0230 ± 0.0010
18	0.1192 ± 0.0004	0.1401 ± 0.0006	0.0209 ± 0.0007
19	0.1121 ± 0.0005	0.1311 ± 0.0008	0.0190 ± 0.0009
20	0.1072 ± 0.0008	0.1229 ± 0.0010	0.0157 ± 0.0013

numerical uncertainties, this maximum can be located between the 13-mer and the 17-mer. In section 3.3, this maximum was identified for a 15-mer and a 16-mer with a value of $\Delta\eta^{N-I} = 0.0220$. A large difference in the packing fraction between the isotropic and nematic phase is relevant for the solubility difference of hard spheres between both phases, as shown below in section 4.6.

4.4 Binary mixtures of linear hard-sphere chain fluids

In this section, results for the isotropic-nematic phase equilibria of binary mixtures of linear hard-sphere chains are presented. Tables 4.2 to 4.4 show the simulation results for binary mixtures of linear hard-sphere chains. Figs. 4.1, 4.2 and 4.3 show the reduced pressure P^* and packing fraction η *vs.* mole fraction of the largest component x_2, for mixtures of an 8-mer with a 14-mer, a 16-mer and a 19-mer, respectively. The plus sign is used to refer to a mixture, *e.g.* 8-mer+14-mer indicates a binary mixture of an 8-mer with a 14-mer. Reduced pressures are defined, relative to the molecular volume of the shortest component (in all cases the 8-mer), by $P^*{=}P\,v_{8-\mathrm{mer}}/k_BT$, where P is the pressure of the system, and $v_{8-\mathrm{mer}}$ is the molecular volume of an 8-mer. Simulation results are compared to theoretical predictions obtained from a Vega-Lago rescaled Onsager theory by van Westen *et al.* [78]. For the larger part of the phase diagrams, excellent agreement between theory and simulations is obtained, however, for systems very rich in the short component ($x_2 \approx 0$), a small overestimation of pressure by the theory is observed. The offset is a consequence of approximations of higher virial coefficients (which are treated by a Vega-Lago rescaling procedure). For smaller chain lengths, the phase transition is shifted to higher packing fractions. Therefore, any errors introduced by the approximate treatment of the higher virial coefficients become apparent, leading to somewhat larger deviations between theory

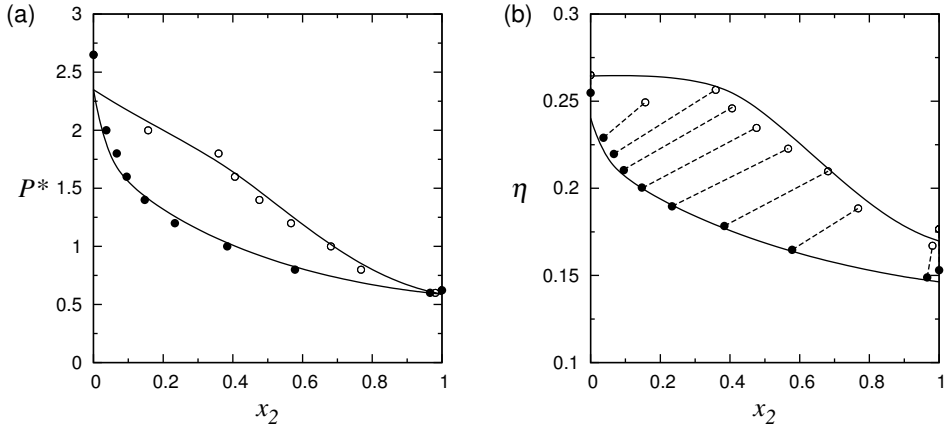

Figure 4.1: Isotropic-nematic phase equilibria for the binary mixture 8-mer+14-mer. (a) reduced pressure P^* *vs.* mole fraction of the largest component x_2, (b) packing fraction η *vs.* mole fraction of the largest component x_2. Black (•) and empty (◦) dots are simulation results for the isotropic and nematic phase respectively. Broken lines are constant pressure tie-lines. Solid lines are theoretical results obtained from a rescaled Onsager theory by van Westen *et al.* [78].

and simulations [78, 83]. The only available simulation data for the phase equilibria of mixtures of linear hard-sphere chains is that of Escobedo and de Pablo [94]. In Fig. 4.2, the simulation results of Escobedo and de Pablo are compared with the present ones and with the theoretical predictions of van Westen *et al.* [78]. All results are in good agreement with each other, validating previous results and the simulation technique presented here.

For all systems studied a phase split into an isotropic and a nematic phase is observed. This phase split is accompanied by a fractionation of the mixture into an isotropic phase richer in the short component and a nematic phase richer in the long component. Phase split and fractionation occurs as a consequence of maximizing the total entropy of the system, balancing orientational, translational, and mixing entropy. In hard systems this entropy maximum is associated to a maximization of the free volume or equivalently to a minimization of the excluded volume [167, 168]. For a mixture with a specific concentration, at pressures below the isotropic-nematic region, orientational and mixing entropy dominate and a one-phase isotropic system is observed. At higher pressures the translational entropy of the isotropic phase is reduced, and a further gain in total entropy is reached by phase split of the system into a nematic and an isotropic phase. The loss in orientational entropy due to the phase split and the loss of mixing entropy by the accompanying fractionation are more than compensated by the gain in translational entropy. Phase split from an isotropic to a nematic phase increases the translational entropy as a consequence of a reduced excluded volume in the nematic phase when chains lay fairly parallel [20, 169, 170]. Fractionation occurs due to a larger tendency to align of the long chains compared to the short chains [171, 172]. This tendency is a consequence of a larger excluded volume difference between the isotropic and nematic phase for the long chains than for the short chains [158]. This excluded volume difference increases with chain length, broadening the fractionation of the system into a nematic phase richer in long chains and an isotropic phase more depleted of them.

Table 4.2: Isotropic (I) and nematic (N) phase equilibria a binary mixture of linear 8-mer+14-mer hard-sphere chain fluids as a function of reduced pressure $P^* = P v_{8-\mathrm{mer}}/k_B T$. For each phase, mole fractions of the long chain x_2, packing fractions $\eta = N_m v_m/V = (N_1 * m_1 + N_2 * m_2) * v_m/V$, order parameters S_2, and reduced pressures P^*, are reported. Reported statistical uncertainties are equivalent to one standard deviation.

P^*	x_2^I	S_2^I	η^I	x_2^N	S_2^N	η^N
2.6500	0.0000 ± 0.0000	0.1940 ± 0.0552	0.2548 ± 0.0011	0.0000 ± 0.0000	0.6162 ± 0.0267	0.2650 ± 0.0010
2.0000	0.0370 ± 0.0031	0.0654 ± 0.0111	0.2290 ± 0.0007	0.1573 ± 0.0043	0.6824 ± 0.0452	0.2494 ± 0.0019
1.8000	0.0669 ± 0.0031	0.0583 ± 0.0077	0.2197 ± 0.0008	0.3593 ± 0.0100	0.8449 ± 0.0135	0.2565 ± 0.0025
1.6000	0.0951 ± 0.0032	0.0531 ± 0.0065	0.2104 ± 0.0005	0.4060 ± 0.0096	0.8305 ± 0.0116	0.2459 ± 0.0018
1.4000	0.1470 ± 0.0044	0.0664 ± 0.0054	0.2004 ± 0.0007	0.4764 ± 0.0114	0.8211 ± 0.0108	0.2347 ± 0.0016
1.2000	0.2336 ± 0.0047	0.0633 ± 0.0039	0.1897 ± 0.0007	0.5671 ± 0.0072	0.8143 ± 0.0087	0.2228 ± 0.0014
1.0000	0.3837 ± 0.0080	0.0772 ± 0.0086	0.1784 ± 0.0007	0.6815 ± 0.0106	0.8143 ± 0.0093	0.2098 ± 0.0018
0.8000	0.5780 ± 0.0051	0.0834 ± 0.0071	0.1647 ± 0.0004	0.7681 ± 0.0061	0.7625 ± 0.0122	0.1885 ± 0.0012
0.6000	0.9660 ± 0.0017	0.0970 ± 0.0124	0.1489 ± 0.0006	0.9812 ± 0.0009	0.7402 ± 0.0208	0.1671 ± 0.0017
0.6229	1.0000 ± 0.0000	0.1256 ± 0.0289	0.1530 ± 0.0009	1.0000 ± 0.0000	0.8078 ± 0.0113	0.1766 ± 0.0009

Table 4.3: Isotropic (I) and nematic (N) phase equilibria of binary mixture of linear 8-mer+16-mer hard-sphere chain fluids as a function of reduced pressure P^*. For each phase, mole fractions of the long chain x_2, packing fractions η, order parameters S_2, and reduced pressures P^*, are reported. Reported statistical uncertainties are equivalent to one standard deviation.

P^*	x_2^I	S_2^I	η^I	x_2^N	S_2^N	η^N
2.6500	0.0000 ± 0.0000	0.1940 ± 0.0552	0.2548 ± 0.0011	0.0000 ± 0.0000	0.6162 ± 0.0267	0.2650 ± 0.0010
2.4000	0.0064 ± 0.0010	0.1024 ± 0.0275	0.2461 ± 0.0017	0.0750 ± 0.0013	0.7734 ± 0.0141	0.2691 ± 0.0012
2.2000	0.0093 ± 0.0016	0.0735 ± 0.0129	0.2371 ± 0.0016	0.1802 ± 0.0033	0.8395 ± 0.0059	0.2716 ± 0.0013
2.0000	0.0157 ± 0.0014	0.0534 ± 0.0083	0.2284 ± 0.0009	0.3799 ± 0.0108	0.9139 ± 0.0035	0.2821 ± 0.0011
1.8000	0.0220 ± 0.0029	0.0484 ± 0.0053	0.2191 ± 0.0010	0.4197 ± 0.0136	0.9045 ± 0.0069	0.2725 ± 0.0016
1.6000	0.0398 ± 0.0025	0.0485 ± 0.0046	0.2093 ± 0.0011	0.5278 ± 0.0155	0.9171 ± 0.0055	0.2675 ± 0.0019
1.4000	0.0685 ± 0.0046	0.0565 ± 0.0059	0.1986 ± 0.0008	0.5804 ± 0.0147	0.9130 ± 0.0053	0.2551 ± 0.0016
1.2000	0.1173 ± 0.0083	0.0583 ± 0.0055	0.1878 ± 0.0006	0.6347 ± 0.0179	0.9023 ± 0.0050	0.2412 ± 0.0017
1.0000	0.1970 ± 0.0097	0.0556 ± 0.0032	0.1761 ± 0.0004	0.6782 ± 0.0174	0.8859 ± 0.0080	0.2236 ± 0.0015
0.8000	0.3205 ± 0.0103	0.0713 ± 0.0072	0.1625 ± 0.0003	0.6930 ± 0.0170	0.8294 ± 0.0127	0.1982 ± 0.0018
0.6000	0.6158 ± 0.0034	0.1362 ± 0.0239	0.1485 ± 0.0007	0.8356 ± 0.0055	0.8258 ± 0.0061	0.1777 ± 0.0012
0.4730	1.0000 ± 0.0000	0.1962 ± 0.2124	0.1344 ± 0.0005	1.0000 ± 0.0000	0.7932 ± 0.1317	0.1574 ± 0.0028

Table 4.4: Isotropic (I) and nematic (N) phase equilibria of binary mixture of linear 8-mer+19-mer hard-sphere chain fluids as a function of reduced pressure P^*. For each phase, mole fractions of the long chain x_2, packing fractions η, order parameters S_2, and reduced pressures P^*, are reported. Reported statistical uncertainties are equivalent to one standard deviation.

P^*	x_2^I	S_2^I	η^I	x_2^N	S_2^N	η^N
2.6500	0.0000 ± 0.0000	0.1940 ± 0.0552	0.2548 ± 0.0011	0.0000 ± 0.0000	0.6162 ± 0.0267	0.2650 ± 0.0010
2.2000	0.0023 ± 0.0010	0.0612 ± 0.0116	0.2360 ± 0.0015	0.1240 ± 0.0028	0.7473 ± 0.0403	0.2670 ± 0.0017
2.0000	0.0049 ± 0.0013	0.0586 ± 0.0062	0.2279 ± 0.0008	0.5240 ± 0.0098	0.9584 ± 0.0017	0.3115 ± 0.0022
1.8000	0.0067 ± 0.0016	0.0500 ± 0.0030	0.2189 ± 0.0007	0.6226 ± 0.0126	0.9655 ± 0.0025	0.3073 ± 0.0024
1.6000	0.0140 ± 0.0031	0.0464 ± 0.0039	0.2083 ± 0.0006	0.6967 ± 0.0146	0.9660 ± 0.0025	0.2987 ± 0.0023
1.4000	0.0317 ± 0.0008	0.0509 ± 0.0036	0.1989 ± 0.0011	0.7637 ± 0.0033	0.9685 ± 0.0013	0.2903 ± 0.0012
1.2000	0.0597 ± 0.0051	0.0462 ± 0.0015	0.1863 ± 0.0001	0.7936 ± 0.0046	0.9630 ± 0.0009	0.2717 ± 0.0001
1.0000	0.1051 ± 0.0044	0.0507 ± 0.0038	0.1749 ± 0.0004	0.7870 ± 0.0202	0.9484 ± 0.0065	0.2496 ± 0.0040
0.8000	0.1945 ± 0.0171	0.0600 ± 0.0041	0.1616 ± 0.0009	0.7904 ± 0.0365	0.9250 ± 0.0132	0.2238 ± 0.0065
0.6000	0.3552 ± 0.0111	0.0695 ± 0.0053	0.1455 ± 0.0006	0.7855 ± 0.0254	0.8744 ± 0.0169	0.1892 ± 0.0039
0.4000	0.7232 ± 0.0110	0.0939 ± 0.0116	0.1261 ± 0.0006	0.8809 ± 0.0210	0.8068 ± 0.0347	0.1527 ± 0.0052
0.3500	1.0000 ± 0.0000	0.1156 ± 0.0243	0.1192 ± 0.0004	1.0000 ± 0.0000	0.8068 ± 0.0072	0.1401 ± 0.0006

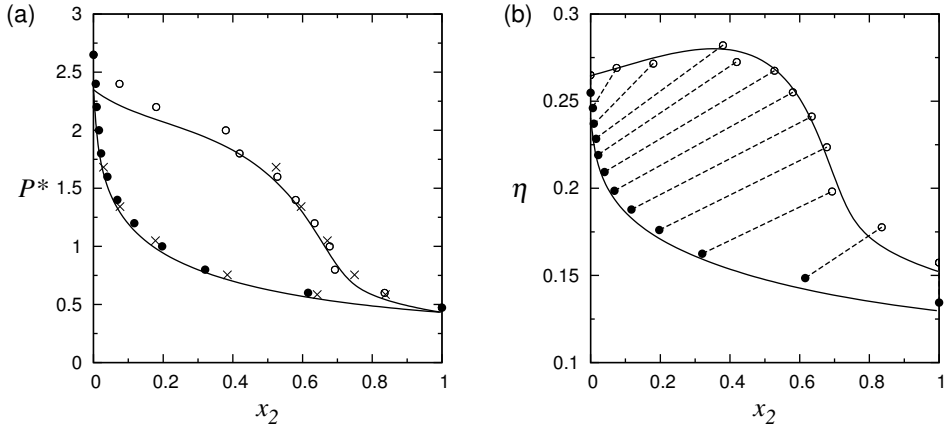

Figure 4.2: Isotropic-nematic phase equilibria for the binary mixture 8-mer+16-mer. (a) reduced pressure P^* *vs.* mole fraction of the largest component x_2, (b) packing fraction η *vs.* mole fraction of the largest component x_2. Symbols and lines as in Fig. 4.1. Crosses (×) are simulation results from Escobedo and de Pablo [94].

Increasing fractionation with the difference in molecular length was reported in previous studies [78, 173, 174] and is also observed in the results shown here.

Figs. 4.1 to 4.3 (a) show a broader isotropic-nematic region, in binary mixtures, as the length of the long chain (14-mer,16-mer and 19-mer) increases for a constant length of the short chain (8-mer). The behavior of packing fraction with mole fraction of the largest component is shown in Figs. 4.1 to 4.3 (b). It can be observed that the packing fraction of the isotropic phase at equilibrium decreases rapidly with mole fraction. This decrement is caused by the alignment potential that the long chains introduces in the fluid, facilitating the formation of the nematic phase at lower equilibrium pressures. In the nematic phase, at low concentrations of the long chains, the packing fraction remains fairly constant (Fig. 4.1) or increases with mole fraction (Figs. 4.2 and 4.3), although the coexistence pressure decreases. This behavior is a consequence of the "induced order" [78] introduced by the addition of a small amount of the long component to a fluid principally composed by short molecules. The long chain induce a larger pair excluded volume difference between the nematic and isotropic phase compared to the short chain [158]. This effect leads to a dramatic increase in the orientational order of the system and an increase in the density of the nematic phase. These two competing effects (reduced pressure *vs.* induced order) lead to the observed maximum in the packing fraction of the nematic phase in binary mixtures.

In the theoretical study of van Westen *et al.* [78], a nematic-nematic region was detected for binary mixtures at high reduced pressures. Specifically, it was shown that for the mixture 8-mer+19-mer a nematic-nematic region follows the isotropic-nematic equilibria after a triple point at a reduced pressure of 2.234 [78]. Here, phase equilibria simulations for the 8-mer+19-mer mixture are performed at high pressures to try to disclose the existence of the nematic-nematic region. Simulations at a reduced pressure of 2.4 show phase equilibrium between a nematic phase, concentrated in the short chains, and a smectic-A phase, concentrated in the long chains. The smectic phase is formed by a layer of short chain

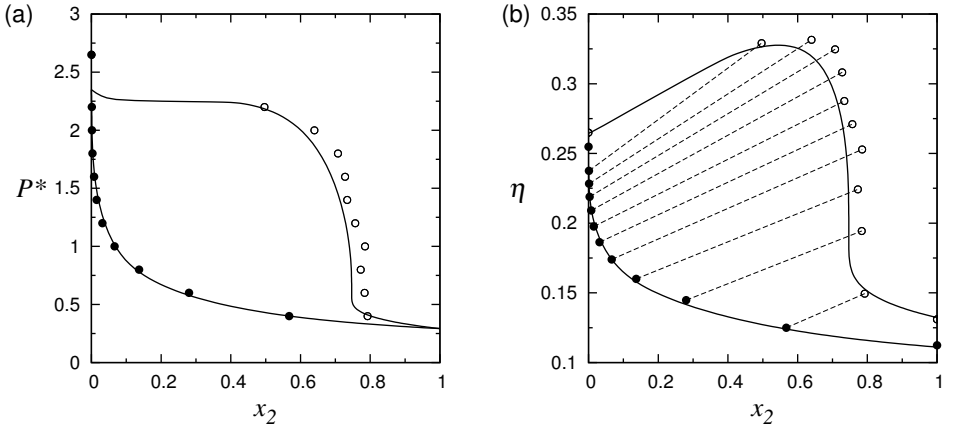

Figure 4.3: Isotropic-nematic phase equilibria for the binary mixture 8-mer+19-mer. (a) reduced pressure P^* *vs.* mole fraction of the largest component x_2, (b) packing fraction η *vs.* mole fraction of the largest component x_2. Symbols and lines as in Fig. 4.1.

molecules without clear positional order between two layers of long chain molecules with defined positional order. At a higher pressure of 3.0, the nematic phase is turned into a phase where long chains are locally clustered with a defined orientation and position surrounded by short chains oriented towards the nematic director but with no clear positional order. At this pressure, the smectic-A phase is clearly defined arranging a layer of short chains, formed by two consecutive layers of short chains, between two layers of long chains. These results are considered as preliminary since the systems and corresponding box sizes are too small to accommodate smectic phases without any influence of the periodic boundary conditions on the positional order of the system. Nevertheless, the theoretical existence of nematic and smectic phases in equilibrium at high pressures has been reported for the case of hard-spherocylinders [175–177]. And, although, the theoretical results of van Westen *et al.* do not consider the formation of smectic phases, Cinacchi *et al.* [178] showed that a metastable nematic-nematic region can precede the formation of stable nematic-smectic equilibria.

4.5 Binary mixtures of linear and partially-flexible hard-sphere chain fluids

Partially-flexible molecules are introduced to study the effect of molecular flexibility on the isotropic-nematic phase equilibria. A partially-flexible molecule is defined as a hard-sphere chain molecule with a linear part and a freely-jointed part. The effect of flexibility is investigated in two binary mixtures: a linear 8-mer with a 19-18-mer, and a linear 8-mer with a 19-17-mer. Figs. 4.4 and 4.5 show the results for the isotropic-nematic phase equilibria in these systems. Comparing these results with the fully linear case, Fig. 4.3, it is observed that flexibility has the effect of, first, increasing the pressure at which the two-phase region starts to appear, and second, reducing the degree of fractionation between coexisting

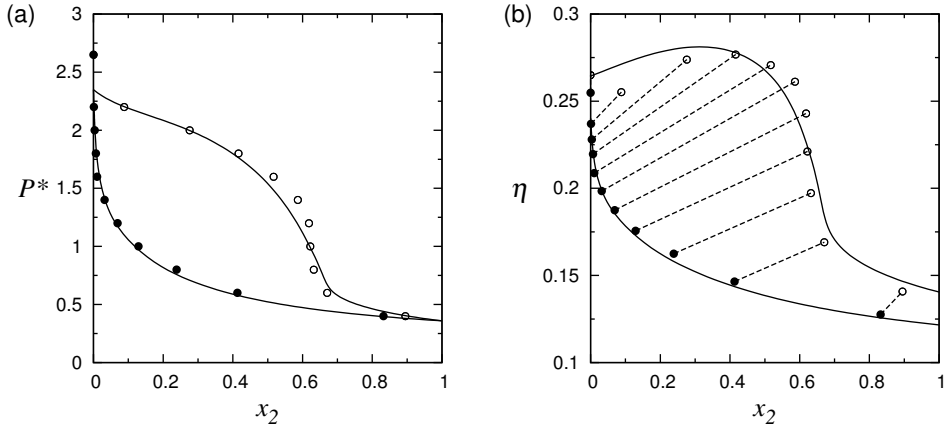

Figure 4.4: Isotropic-nematic phase equilibria for the binary mixture of a linear 8-mer with the partially-flexible 19-18-mer. (a) reduced pressure P^* *vs.* mole fraction of the largest component x_2, (b) packing fraction η *vs.* mole fraction of the largest component x_2. Symbols and lines as in Fig. 4.1.

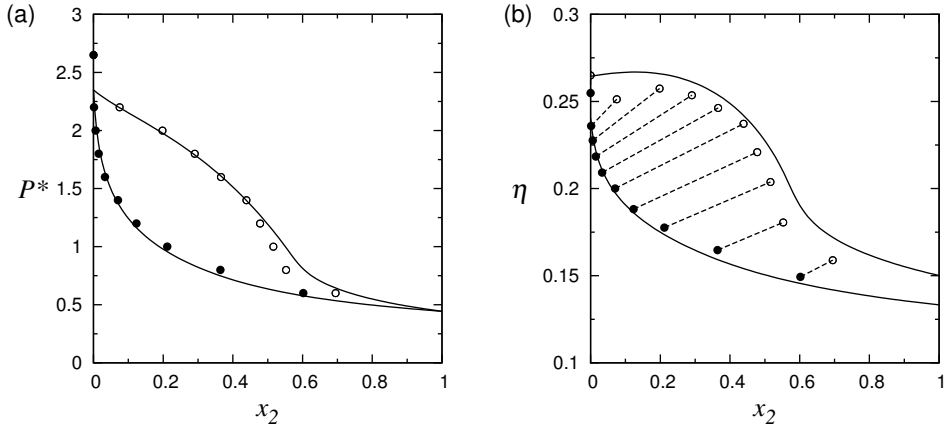

Figure 4.5: Isotropic-nematic phase equilibria for the binary mixture of a linear 8-mer with the partially-flexible 19-17-mer. (a) reduced pressure P^* *vs.* mole fraction of the largest component x_2, (b) packing fraction η *vs.* mole fraction of the largest component x_2. Symbols and lines as in Fig. 4.1.

phases. Flexibility decreases the anisotropy of the chain, diminishing the gain in translational entropy that can be obtained from a phase split into a nematic phase. Therefore, a closer packing is needed for the nematic phase to start to form, increasing the pressure at which the isotropic-nematic equilibria take place. The reduced fractionation is explained by a lower excluded volume difference between the isotropic and the nematic phase (lower tendency to align) for the partially-flexible chain compared to the linear case, as shown for the pair excluded volume of two partially-flexible molecules by van Westen *et al.* [157].

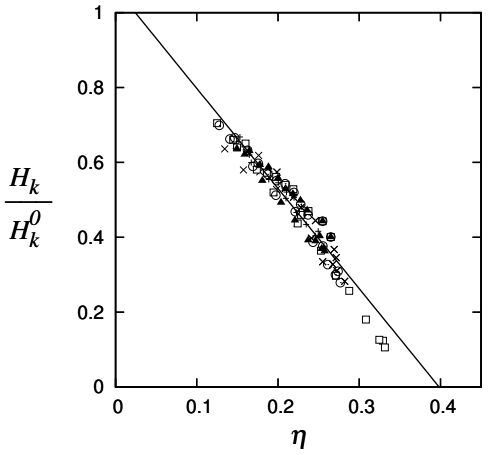

Figure 4.6: Relative infinite dilution solubility H_k/H_k^0 *vs.* packing fraction η for hard spheres in binary mixtures of linear and partially-flexible hard-sphere chains in the isotropic and nematic phase at equilibrium. (+) 8-mer+14-mer, (×) 8-mer+16-mer, (□) 8-mer+19-mer, (▲) 8-mer+19-18-mer, and (○) 8-mer+19-17-mer. The solid line is a linear regression calculated from all simulation data.

4.6 Solubility of hard spheres in hard-sphere chain fluids

In the previous chapter, it was showed that a linear relationship exists between relative infinite dilution solubility, defined by Eq. 2.48, with packing fraction. It was found that this relationship is practically independent of chain length for the linear hard-sphere 10-mer chain fluid and longer chains fluids. Moreover, it was demonstrated that this relationship does not depend on the liquid crystal state of the fluid, either isotropic or nematic, being only a function of packing fraction. In principle, the independence of relative solubility on chain length for long linear chains (longer than 10 segments) can be explained from pair excluded volume interactions. van Westen *et al.* [157] derived an expression for the dimensionless pair excluded volume between two linear chains of different length $V_{\text{ex}}^* = V_{\text{ex}}/V_{\bar{m}}$, where V_{ex} is the pair excluded volume and $V_{\bar{m}}$ is the volume of a chain of $\bar{m}$ hard spheres. Here $\bar{m} = (m_1 + m_2)/2$, with m_1 and m_2 as the lengths of the two linear chains. If one of the chains is considered just as a hard sphere, that expression reduces to $V_{\text{ex}}^* = (11\bar{m} - 3)/\bar{m}$. It can be observed that as $\bar{m}$ increases the value of the excluded volume approaches a limiting value. For the linear hard-sphere 10-mer chain fluid and longer chain fluids, changes in the relative excluded volume are progressively smaller, explaining in principle the unnoticeable effect of chain length on solubility reported in the previous chapter. It is remarkable that this argument taken from pair molecular interactions also holds for high packing fractions where multi-body interactions start to be relevant.

Fig. 4.6 shows the relative infinite dilution solubility of hard spheres in binary mixtures of linear, and linear with partially-flexible hard-sphere chains *vs.* packing fraction. It can be observed that, as for the pure component case (Ref. 46), a linear relationship of relative solubility with packing fraction independent of the mixture type is also obtained. Fig 4.6 includes a linear regression for all reported data. The slope and intercept of this regression are respectively -2.674±0.086 and 1.065±0.015, which are equivalent to the ones reported

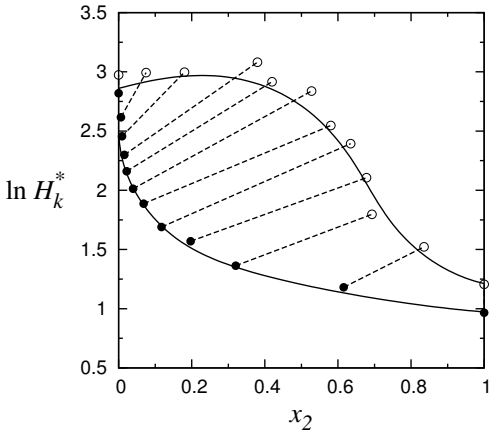

Figure 4.7: Dimensionless Henry's Law constants $\ln H_k^*$ *vs.* mole fraction of the longest component x_2 for the binary mixture 8-mer+16-mer in the isotropic and nematic phase at equilibrium. Symbols and lines as in Fig. 4.1.

in section 3.5. This result is coherent with the results of solubility in pure components, where for relatively long enough chains solubility seems to be independent of chain length. It has to be noticed that similarly to the pure component case, this linear relationship would eventually not be independent on chain length if one of the components forming the mixture becomes very small.

Finally, Fig. 4.7 shows dimensionless Henry coefficients, defined by Eq. 2.47, *vs.* mole fraction of long chains for the solubility of hard spheres in a mixture of linear chains, 8-mer+16-mer, at the isotropic-nematic coexistence. It can be observed that the solubility of hard spheres in the isotropic phase increases with mole fraction (indicated by a decrease in Henry's Law constants), showing a rapid increment at mole fractions close to the pure short chain fluid. The solubility in the nematic phase is fairly decreased at low values of the mole fraction showing a minimum after which it increases monotonically. This behavior is analogous to the changes in packing fraction observed in Fig. 4.2. A maximum in the solubility difference between the isotropic and the nematic phase is detected at a mole fraction of around 0.5, corresponding to the maximum in the packing fraction difference between both phases observed at the same concentration.

4.7 Conclusions

The isotropic-nematic phase equilibria of pure components and binary mixtures of linear and partially-flexible hard-sphere chains were directly calculated from expanded Gibbs ensemble simulations. For pure components, the packing fractions of the isotropic and nematic phases at equilibrium were obtained for linear hard-sphere 7-mer to 20-mer chain fluids. These results show a maximum in the packing fraction difference between both phases for a chain length between the 13-mer and the 17-mer. For binary mixtures, the packing fraction and mole fraction of the coexisting isotropic and nematic phases were obtained for mixtures of a linear 8-mer with a 14-, 16- and 19-mer. Phase split, between an isotropic and a nematic phase, and fractionation between an isotropic phase richer in the short component and a nematic phase richer in the large component, is observed for all binary mixtures. The degree of fractionation between both phases increases with the chain length of the largest component for a constant length of the short chain. The effect of molecular flexibility was studied in binary mixtures of an 8-mer with a partially-flexible 19-18-mer, and a 19-17-mer. Flexibility increases the isotropic-nematic equilibrium pressure and reduces the degree of fractionation between both phases. The relative infinite dilution solubility of hard spheres in the isotropic and nematic phases at equilibrium was obtained for all studied binary mixtures. A linear relationship between relative solubility and packing fraction is found. This linear relationship is equivalent to the one obtained in section 3.5. Binary mixtures show a larger packing fraction difference and, therefore, a larger hard sphere solubility difference between the isotropic and the nematic phase than the constituent pure components. This result shows that mixtures of liquid crystals have the potential of largely increasing the solubility difference of gases between the isotropic and the nematic phase. A large solubility difference is relevant for the use of liquid crystals as solvents for gas separation applications, as shown in studies that propose liquid crystals as novel solvents for CO_2 capture processes [6, 7].

5

Isotropic-nematic phase equilibrium of Lennard-Jones chain fluids

The liquid crystal phase equilibria of Lennard-Jones chain fluids and the solubility of a Lennard-Jones gas in the coexisting phases are calculated from Monte Carlo simulations. Direct phase equilibria calculations are performed using an expanded formulation of the Gibbs ensemble. Monomer densities, order parameters, and equilibrium pressures are reported for the coexisting isotropic and nematic phases of: (1) linear Lennard-Jones chains, (2) a partially-flexible Lennard-Jones chain, and (3) a binary mixture of linear Lennard-Jones chains. The effect of chain length is determined by calculating the isotropic-nematic coexistence of linear Lennard-Jones 8-mer, 10-mer, and 12-mer chain fluids. The effect of molecular flexibility on the isotropic-nematic equilibrium is studied in a Lennard-Jones 10-mer chain fluid with one freely-jointed segment at the end of the chain. Isotropic-nematic phase split and fractionation are observed for a binary mixture of linear 7-mer and 12-mer chains. Simulation results are compared with theoretical predictions as obtained from the analytical equation of state from the work of van Westen et al. [79]. Excellent agreement between theory and simulations is observed. The solubility of a monomer Lennard-Jones gas in the coexisting isotropic and nematic phases is estimated using the Widom test-particle insertion method. A linear relationship between solubility difference and density difference at the isotropic-nematic phase transition is observed. Furthermore, it is shown that gas solubility is independent of the nematic ordering of the fluid, at constant temperature and density conditions.

This chapter is based on:
B. Oyarzún, T. van Westen, and T.J.H. Vlugt accepted in *Molecular Physics* [179].

5.1 Introduction

In general, a certain degree of molecular anisotropy is required for the appearance of liquid crystal phases [1, 2]. Early theoretical work, *i.e.* the work of Onsager [20], Born [180], and Maier and Saupe [21–23], respectively, has shown that both repulsive and attractive interactions between molecules can drive the transition to a liquid crystal phase. Nowadays, it is well understood that anisotropic repulsive molecular interactions are a necessary condition for the appearance of ordered phases [29, 31, 32], while both repulsive and attractive interactions determine the rich phase behaviour observed in liquid crystal fluids [1, 2].

Simulation and theoretical studies of complex fluids are often based on a coarse-grained description of molecules. Coarse-grained models are used to reduce the information of molecular structure into main molecular properties, summarized by a small set of model parameters. Simulations based on coarse-grained models can access longer time and length scales than their atomistic counterparts, allowing a bulk description of fluids. Coarse-grained models are commonly used to represent a simplified picture of large molecules such as biomolecules [68, 181–184], polymers [110, 185–189], or liquid crystals [47, 48, 60, 62, 190, 191]. Moreover, simulation results obtained from coarse-grained models can be directly compared with theoretical predictions that are based on a well-defined Hamiltonian, such as the family of perturbation theories developed from the statistical association fluid theory (SAFT) [69–76]. Traditionally, this relation between fluid theories and molecular simulations was primarily used for the development of improved theories. More recent developments show that this is not a one-way street, as accurate SAFT-type theories also provide a very efficient means to derive coarse-grained force fields for use in molecular simulations [187, 189, 192–197] (see Ref. 188 for a recent review).

Typically, coarse-grained models use simple expressions for the interaction energies. Pair-interaction potentials as hard-sphere [46, 85, 88–90, 154, 164], hard-ellipsoid [35, 37, 38], hard-spherocylinders [39, 43, 44], and the Gay-Berne potential [51–55, 198] are popular for studying liquid crystals. Other more elaborated interaction models have been proposed, *e.g.* hard-spherocylinder with an attractive square-well potential [57–60], hard-disc with an anisotropic square-well attractive potential [62], hard-spherocylinder with an attractive Lennard-Jones potential [61], anisotropic soft-core spherocylinder potential [63, 199], and copolymers [64–66].

In this chapter, the isotropic-nematic phase behavior of linear and partially-flexible Lennard-Jones chain fluids is studied. Apart from our recent work [79, 179], there is no other study showing simulation results for the isotropic-nematic phase transition of Lennard-Jones chains. Galindo *et al.* [95] studied the phase behavior of linear Lennard-Jones chains of 3 and 5 segments; however, in that study, no liquid crystalline phases were observed due to the short length of the chains. In this sense, the importance of this chapter is twofold, first to determine the effect of main molecular characteristics (such as chain length, flexibility, attractive interactions and composition of mixtures) on the isotropic-nematic behavior of long Lennard-Jones chains, and second to validate the analytical equation of state presented by van Westen *et al.* [79] for Lennard-Jones chain fluids with variable degree of flexibility.

The equation of state of van Westen *et al.* was developed using a perturbation theory based on a reference fluid of hard-chain molecules. An important assumption in the development of the equation of state was that of orientation-independent attractive interac-

tions. As shown in Ref. 79, this assumption leads to a surprisingly good description of the isotropic-nematic phase behaviour of a linear Lennard-Jones 10-mer fluid. Here, a more elaborate evaluation of the equation of state is obtained by comparing it with simulation data, allowing further analysis on the effect of molecular orientation on attractive dispersion interactions.

An important property of liquid crystals, relevant for technological applications, is the solubility of gases in them. Recently, liquid crystals have been proposed as new solvents for CO_2 capture [6–10]. The principle behind this application is described in section 1.2 of this thesis. In this chapter, molecular simulations are used to analyze the effect of density, temperature, and composition of mixtures, on the solubility difference of gases between the coexisting isotropic and nematic phases.

Section 5.2 presents the simulation details for the phase equilibrium calculation of Lennard-Jones chains together with a brief description of the equation of state of van Westen *et al.*. Simulation results for the isotropic-nematic phase equilibria of linear Lennard-Jones chain fluids are presented in section 5.3. The effect of flexibility on the equilibrium properties is studied in section 5.4 for a partially-flexible Lennard-Jones chain fluid. The isotropic-nematic phase equilibria of a binary mixture of linear Lennard-Jones chains is shown in section 5.5. Solubility results for a Lennard-Jones gas in the coexisting isotropic and nematic phases are presented in section 5.6. Results are summarized in section 5.7.

5.2 Simulation details and theory

The isotropic-nematic phase equilibria of linear and partially-flexible Lennard-Jones chains is studied in this chapter. A chain molecule is defined as a molecule made of spherical segments connected by a rigid segment-to-segment bond length equal to the segment diameter σ. The pair potential between two segments i and j separated by a distance r_{ij} is defined by the Lennard-Jones potential, Eq. 2.2. The depth of the potential well ϵ and the segment diameter σ are constant and equal to 1 for all molecules and systems considered in this work. The pressure of the system is calculated by the molecular virial for chain molecules in a system with periodic boundaries as described by Theodorou *et al.* [200].

All magnitudes reported here are dimensionless with ϵ as the basis for energy and σ as the basis for length. Some of these magnitudes are: reduced temperature $T^*=k_BT/\epsilon$, where T is the temperature and k_B is the Boltzmann constant; reduced monomer density $\rho_m^*=mN\sigma^3/V$, where N is the number of molecules; and reduced pressure $P^*=P\sigma^3/k_BT$, where P is the pressure of the system. In a binary mixture, the reduced monomer density is defined as $\rho_m^*=(m_1x_1+m_2x_2)N\sigma^3/V$, where x_1 and x_2 are the mole fraction of the short and long chain respectively. Nematic phases are characterized by the order parameter S_2, defined as in Eq. 2.3.

Phase equilibria calculations are performed in an expanded version of the Gibbs ensemble, see section 2.4 and Refs. 120, 121, 164. Constant volume simulations are used for the calculation of single component systems, while constant pressure simulations are used in the case of mixtures. At every Monte Carlo step, one of the following trial moves is attempted: displacement, rotation, reptation, configurational-bias partial regrowth (only for partially-flexible molecules)[80], volume change, identity exchanges[166] (only for mixtures of linear chains), and coupling parameter change. Trial moves are selected randomly with a fixed probability proportional to the ratio 100:100:10:100:1:100:1000 respectively.

Volume changes are performed isotropically in the logarithm of the volume. Initial isotropic configurations are placed in a cubic box, while initial nematic configurations are placed in a rectangular box with an edge length ratio of 1:1.1:1.2. The maximum displacement, rotation, volume, and coupling parameter changes are adjusted for a maximum acceptance ratio of 20%. Periodic boundary conditions are used in all systems. The contribution of the fractional molecules to the tail corrections is neglected as this energy contribution is very small. A Monte Carlo cycle consists of a number of trial moves equal to the total number of molecules in the system ($\sim 1\times10^3$). Equilibration requires typically 3×10^6 cycles and averages were collected in 2×10^6 production cycles.

Infinity dilution solubility of gases is expressed as a dimensionless Henry coefficients defined by Eq. 2.42. Dimensionless Henry coefficients are related to the infinite dilution residual chemical potential of a gas in a solvent [146], which is calculated in constant pressure Monte Carlo simulations using the Widom test-particle insertion method as defined by Eq. 2.57 [148, 152]. The infinite dilution solubility of a single-segment Lennard-Jones gas molecule is measured in both the coexisting isotropic and nematic phase at equilibrium. Equilibrium configurations are sampled every 1×10^3 Monte Carlo cycles in which a total of 100 test-particle insertions are attempted.

The simulation results presented in this chapter are extensively compared to a recently developed analytical equation of state by van Westen *et al.* [79]. The equation of state was developed from a perturbation theory based on a hard-chain reference fluid. The Helmholtz energy as obtained from the equation of state can thus be written as a sum of different contributions according to,

$$\frac{A}{Nk_\mathrm{B}T} = \frac{A^\mathrm{id}}{Nk_\mathrm{B}T} + \frac{A^\mathrm{hc}}{Nk_\mathrm{B}T} + \frac{A^\mathrm{disp}}{Nk_\mathrm{B}T} \tag{5.1}$$

Here, A^id is an ideal gas contribution, A^hc is a Helmholtz energy due to chain formation, and A^disp is a contribution due to attractive dispersion interactions. The hard-chain term was obtained from a rescaled Onsager theory, based on the Onsager trial function for describing the orientational distribution function of the molecules. The dispersion term was developed using a second order Barker-Henderson theory [201, 202], based on the radial distribution function of hard-chain molecules in the isotropic phase. The dispersion contribution is therefore independent on the orientation of the molecules. For details on the equations for calculating the different contributions, the reader is referred to the work of van Westen *et al.* [79]. Details on the development of the different contributions to the equation of state can be found elsewhere [77, 78, 83, 84, 157].

5.3 Linear Lennard-Jones chains

The liquid crystal phase equilibria of linear Lennard-Jones 8-, 10- and 12-mers were calculated from constant volume expanded Gibbs ensemble simulations. Initial estimates of densities in the coexisting isotropic and nematic phases were obtained from the equation of state of van Westen *et al.* [79]. Reduced monomer densities, order parameters, and reduced pressures at the isotropic-nematic coexistence are shown in Table 5.1 as a function of reduced temperature. Temperature-density phase diagrams are shown in Fig. 5.1 together with theoretical results obtained from the equation of state. It can be observed that for

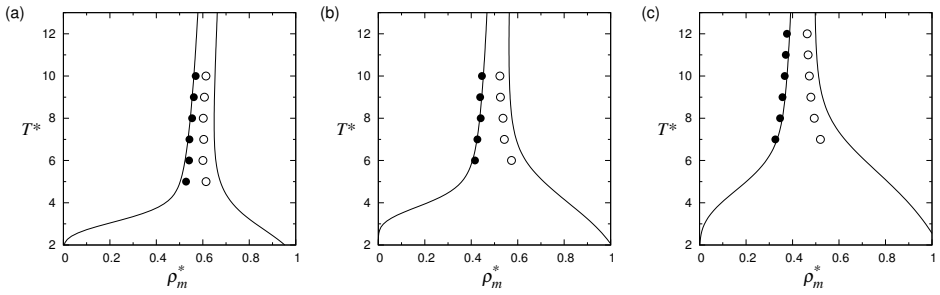

Figure 5.1: Isotropic-nematic phase equilibria of linear Lennard-Jones chain fluids: (a) 8-mer, (b) 10-mer, and (c) 12-mer. Reduced temperature T^* *vs.* reduced monomer density ρ_m^*. Filled (•) and open (◦) symbols are simulation results for the isotropic and nematic phase respectively. Solid lines are theoretical results obtained from the analytical equation of state of van Westen *et al.* [79].

longer chains, the isotropic-nematic equilibrium is shifted towards lower densities while the density difference between both coexisting phases is increased. Lower equilibrium densities and larger density differences are a consequence of larger excluded volume differences between the isotropic and the nematic phase as the chain length increases [158]. For longer chains, the pair-excluded volume is more anisotropic than for shorter chains, resulting in a larger driving force for the isotropic-nematic transition.

As it is shown in Fig. 5.1, the theoretical results as obtained from the perturbation theory of van Westen *et al.* provide an overall excellent description of the isotropic-nematic phase diagram. Nevertheless, some minor deviations can be observed. The small but systematic overestimation of nematic equilibrium densities is expected, since densities in the nematic phase are already overestimated in the description of the hard-chain reference fluid [83]. These small overestimations are a result of the approximations made for describing higher (third, fourth, etc.) virial coefficients in the rescaled Onsager approach for hard chain fluids. Equilibrium densities of the isotropic phase are slightly different from simulation results, with an increasing deviation for longer chain lengths. Albeit the deviations are small, the increasing deviation with chain length cannot be explained from the behavior of the reference fluid [83], since the description of the hard-chain reference system improves for longer chain lengths. Fig. 5.2 shows the reduced pressure *vs.* reduced temperature diagram at isotropic-nematic coexistence for linear Lennard-Jones chain fluids. In this figure, it can be clearly identified that the theoretical description of the isotropic-nematic phase equilibria is less accurate as the chain length increases. Figs. 5.1 and 5.2 suggest that the theoretical description misses a small (positive) contribution to the driving force for the isotropic to nematic phase transition. van Westen *et al.* assumed that no explicit orientation dependent contribution in the dispersive Helmholtz energy was required for a reliable description of the isotropic-nematic phase equilibria of Lennard-Jones chain fluids [79]. The results shown here indicate that this assumption may be less justified for longer chains, wherefore a stronger effect of anisotropic interactions is expected. Another theoretical assumption that could explain the observed deviations is the use of a fixed temperature-independent aspect ratio of the molecules. This assumption is typically needed in a perturbed-chain approach [84]; however, it reduces the driving force for the isotropic to nematic phase tran-

Table 5.1: Isotropic (I) and nematic (N) phase equilibria of linear Lennard-Jones m-mer chain fluids as a function of reduced temperatures T^*. For each phase, reduced monomer densities ρ_m^*, order parameters S_2, and reduced pressures P^*, are reported. Reported statistical uncertainties are equivalent to one standard deviation.

T^*	$\rho_m^{*,I}$	S_2^I	$P^{*,I}$	$\rho_m^{*,N}$	S_2^N	$P^{*,N}$
			$m = 8$			
10	0.569 ± 0.005	0.132 ± 0.059	4.809 ± 0.062	0.614 ± 0.004	0.685 ± 0.051	4.810 ± 0.065
9	0.561 ± 0.004	0.168 ± 0.053	4.026 ± 0.058	0.607 ± 0.003	0.689 ± 0.051	4.030 ± 0.059
8	0.554 ± 0.004	0.196 ± 0.060	3.269 ± 0.031	0.602 ± 0.003	0.709 ± 0.018	3.269 ± 0.030
7	0.542 ± 0.004	0.141 ± 0.041	2.562 ± 0.025	0.604 ± 0.003	0.747 ± 0.023	2.561 ± 0.026
6	0.541 ± 0.005	0.262 ± 0.078	1.881 ± 0.033	0.600 ± 0.004	0.744 ± 0.030	1.881 ± 0.033
5	0.528 ± 0.007	0.243 ± 0.082	1.202 ± 0.018	0.614 ± 0.005	0.813 ± 0.021	1.201 ± 0.018
			$m = 10$			
10	0.446 ± 0.002	0.144 ± 0.042	2.275 ± 0.114	0.523 ± 0.002	0.789 ± 0.009	2.275 ± 0.112
9	0.438 ± 0.002	0.138 ± 0.046	1.919 ± 0.017	0.526 ± 0.003	0.801 ± 0.011	1.919 ± 0.015
8	0.441 ± 0.006	0.198 ± 0.081	1.567 ± 0.025	0.537 ± 0.004	0.828 ± 0.009	1.566 ± 0.024
7	0.427 ± 0.004	0.192 ± 0.070	1.168 ± 0.016	0.542 ± 0.004	0.849 ± 0.005	1.165 ± 0.015
6	0.416 ± 0.007	0.225 ± 0.052	0.805 ± 0.012	0.573 ± 0.006	0.893 ± 0.008	0.803 ± 0.013
			$m = 12$			
12	0.376 ± 0.004	0.081 ± 0.021	1.825 ± 0.044	0.463 ± 0.011	0.820 ± 0.023	1.823 ± 0.045
11	0.371 ± 0.004	0.085 ± 0.017	1.577 ± 0.036	0.467 ± 0.010	0.834 ± 0.015	1.576 ± 0.036
10	0.366 ± 0.002	0.087 ± 0.015	1.337 ± 0.012	0.472 ± 0.006	0.846 ± 0.014	1.335 ± 0.013
9	0.357 ± 0.004	0.085 ± 0.023	1.078 ± 0.023	0.479 ± 0.007	0.862 ± 0.008	1.077 ± 0.023
8	0.347 ± 0.005	0.085 ± 0.018	0.833 ± 0.026	0.493 ± 0.011	0.882 ± 0.011	0.831 ± 0.026
7	0.326 ± 0.004	0.072 ± 0.007	0.579 ± 0.014	0.520 ± 0.011	0.909 ± 0.010	0.576 ± 0.015

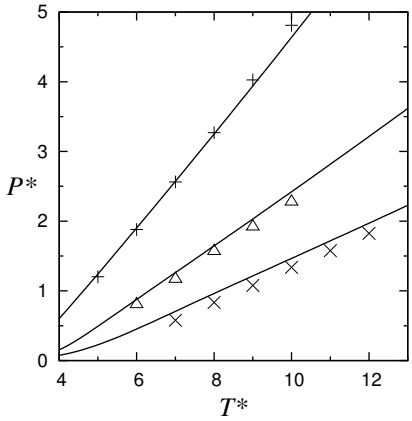

Figure 5.2: Reduced temperature T^* *vs.* reduced pressure P^* at the isotropic-nematic coexistence for linear Lennard-Jones 8-mer (+), 10-mer (△), and 12-mer (×) chain fluids. Solid lines are theoretical results obtained from the analytical equation of state of van Westen *et al.* [79].

sition as the aspect ratio should slightly increase with temperature (see *e.g.* Ref. 199). An increased aspect ratio would lead to a more anisotropic molecule and therefore a higher driving force for the phase transition. In summary, the systematic but small deviations between theory and simulations could be caused by the assumption of orientation-independent attractions or a fixed aspect ratio of the molecules. However, it is clear that this assumption do not diminish an accurate description of the phase equilibrium.

Fig. 5.2 shows a linear relationship between pressure and temperature at the isotropic-nematic coexistence for linear Lennard-Jones chain fluids. Further analysis is obtained considering the Clapeyron equation, $dP/dT = \Delta h^{\mathrm{I-N}}/(T\Delta v^{\mathrm{I-N}})$, where $\Delta h^{\mathrm{I-N}}$ is the enthalpy change at the isotropic-nematic phase transition, and $\Delta v^{\mathrm{I-N}}$ is the molar volume change between both phases at coexistence. A constant slope dP^*/dT^* indicates a proportional relationship between enthalpy change and volume change. It is remarkable that energetic and density effects at the isotropic-nematic phase transition are directly coupled, suggesting that any energetic change at the phase transition can be described from the isotropic-nematic density change and vice versa.

At temperatures lower than the ones reported in Fig. 5.1 and Table 5.1, isotropic-smectic and isotropic-solid phase coexistence is found. Fig. 5.3 shows typical snapshots for a sequence of nematic, smectic-C, and crystal phases for a linear 10-mer fluid as temperature decreases. A similar picture of crystal and smectic-C phases of a 10-mer fluid at a constant monomer density of $\rho_m^* = 0.8$ was reported by Affouard *et al.* [203]. In the smectic-C phase, molecules are positioned in layers and oriented with the nematic director tilted with respect to the normal of the layers. Smectic phases were detected by the smectic order parameter (Eq. 2.4) and identified as smectic-C phases by inspecting snapshots of final configurations. Table 5.2 shows the results for the observed coexistence between isotropic and smectic-C phases. These data should be considered only as preliminary due to small differences (∼5%) in the calculated pressure of both coexisting phases. This difference is a conse-

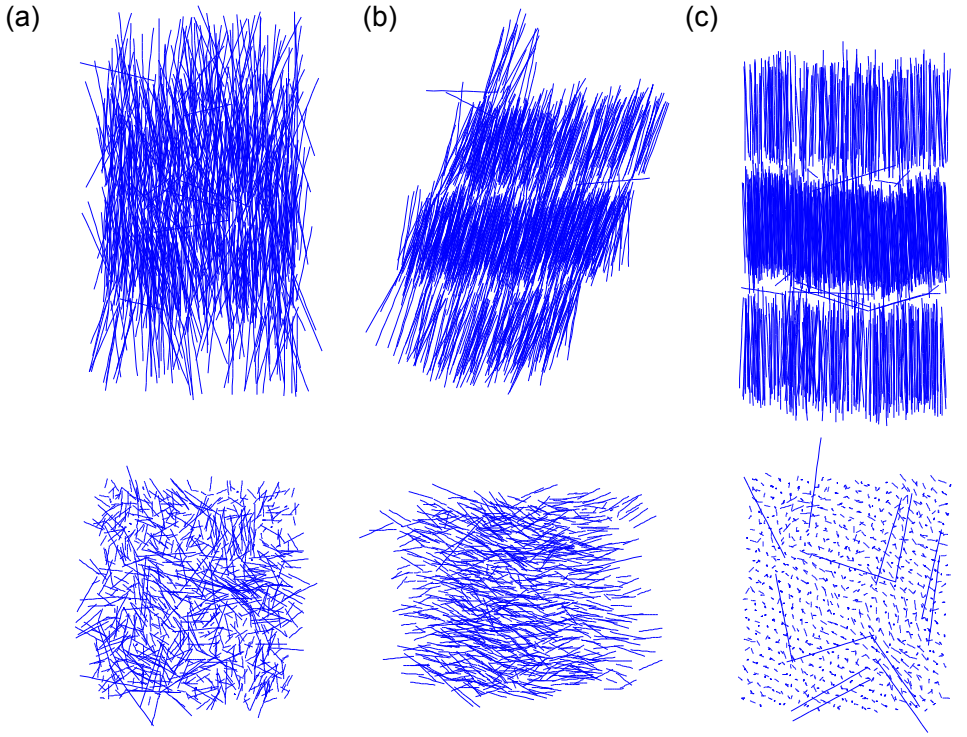

Figure 5.3: Typical snapshots of ordered phases for a linear Lennard-Jones 10-mer chain fluid at coexistence between an isotropic phase and: (a) a nematic phase at $T^* = 6$, (b) a smectic-C phase at $T^* = 5$, and (c) a crystal phase at $T^* = 4$. The top row shows parallel views and the bottom row shows perpendicular views to the largest axis of the simulation box.

quence of the difficulties in arranging the tilted oriented layers in the periodically repeating rectangular box. In the crystal phases, molecules are arranged in layers with the molecular axis pointing in the direction of the normal of the layers. Vega *et al.* [86] described the possible crystal phases of hard-sphere dumbbells from closest packing considerations. These authors identified that dumbbells should be arranged in layers with their axis parallel but tilted from the normal layer by approximately 35°. In that study, the stacking of layers was considered in three different ways, forming an ABAB (hexagonal close packed), or an ABC (face-centered cubic) sequence, or a sequence where layers are stacked alternating the tilted angles between successive layers. Galindo *et al.* [95] considered the ABC sequence in the solid phases of linear Lennard-Jones chains, while Polson *et al.* [204] suggested that an AAA (body-centered cubic) stacking with a tilt angle of approximately 33° is the stable configuration for the crystal phase of a 6-mer Lennard-Jones fluid with finite bending potential. Simulations showing crystal phases are considered only as an indication of the formation of solid phases. This is because of large pressure differences observed between both coexisting phases and the known difficulties in performing direct phase equilibrium calculations of systems including solids [80, 204–206].

Table 5.2: Isotropic (I) and smectic-C (SmC) phase equilibria of linear Lennard-Jones m-mer chain fluids.

m	T^*	$\rho_m^{*,I}$	S_2^I	$P^{*,I}$	$\rho_m^{*,SmC}$	S_2^{SmC}	$P^{*,SmC}$
8	4	0.468 ± 0.021	0.178 ± 0.101	0.471 ± 0.026	0.699 ± 0.031	0.924 ± 0.021	0.447 ± 0.032
10	5	0.335 ± 0.007	0.101 ± 0.009	0.338 ± 0.015	0.688 ± 0.010	0.965 ± 0.005	0.309 ± 0.015
12	6	0.308 ± 0.015	0.087 ± 0.016	0.372 ± 0.030	0.673 ± 0.032	0.977 ± 0.007	0.348 ± 0.024

Table 5.3: Isotropic (I) and nematic (N) phase equilibria of the partially-flexible Lennard-Jones 10-9-mer chain fluid.

T^*	$\rho_m^{*,I}$	S_2^I	$P^{*,I}$	$\rho_m^{*,N}$	S_2^N	$P^{*,N}$
10	0.568 ± 0.007	0.227 ± 0.120	4.558 ± 0.048	0.597 ± 0.002	0.601 ± 0.035	4.562 ± 0.045
9	0.564 ± 0.006	0.283 ± 0.123	3.823 ± 0.033	0.599 ± 0.002	0.685 ± 0.021	3.824 ± 0.036
8	0.559 ± 0.004	0.171 ± 0.061	3.187 ± 0.029	0.600 ± 0.002	0.710 ± 0.019	3.189 ± 0.023
7	0.560 ± 0.005	0.265 ± 0.102	2.518 ± 0.021	0.600 ± 0.002	0.726 ± 0.020	2.519 ± 0.022
6	0.555 ± 0.010	0.295 ± 0.060	1.831 ± 0.013	0.601 ± 0.002	0.745 ± 0.007	1.828 ± 0.016
5	0.543 ± 0.006	0.294 ± 0.108	1.101 ± 0.032	0.605 ± 0.002	0.781 ± 0.013	1.105 ± 0.028

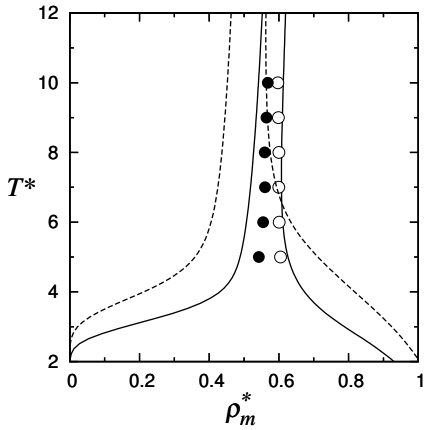

Figure 5.4: Isotropic-nematic phase equilibria of the partially-flexible Lennard-Jones 10-9-mer compared to the linear Lennard-Jones 10-mer chain fluid. Reduced temperature T^* *vs.* reduced monomer density ρ_m^*. Symbols and solid lines for the partially-flexible 10-9-mer fluid as in Fig. 5.1. Dashed lines are theoretical results for the linear 10-mer fluid.

5.4 Partially-flexible Lennard-Jones chains

The effect of molecular flexibility on the isotropic-nematic phase equilibria of Lennard-Jones chain fluids is studied for a partially-flexible 10-9-mer fluid. Table 5.3 reports the simulation data and Fig. 5.4 compares the isotropic-nematic coexistence densities of the partially-flexible 10-9-mer to those of the linear 10-mer fluid. It can be observed that the effect of flexibility is twofold: (1) it increments the densities at which the phase transition takes place, and (2) it reduces the density difference between both phases. These observations can be explained from the fact that the pair-excluded volume of partially flexible chains is less anisotropic than that of linear chains [157], thereby constituting a smaller driving force for the isotropic to nematic phase transition.

Another effect of flexibility is the appearance of smectic phases at a temperature lower than the one observed for the linear chain fluid. At T^*=5, isotropic-nematic equilibrium is observed for the 10-9-mer fluid while isotropic-smectic coexistence was found for the linear 10-mer fluid at the same temperature. Our observations suggest that the temperature of the isotropic-nematic-smectic triple point of Lennard-Jones chain fluids decreases with increasing flexibility, *i.e.* decreasing molecular anisotropy. A similar behavior was observed in the case of Gay-Berne fluids with different shape anisotropy [56, 207, 208]. At reduced temperatures lower than the ones reported in Fig. 5.4 and Table 5.3, smectic and crystal phases were observed, similarly as described in the previous section.

5.5 Binary mixture of linear Lennard-Jones chains

Constant pressure expanded Gibbs-ensemble simulations are performed for determining the isotropic-nematic phase equilibria of a binary mixture of linear Lennard-Jones 7-mer and 12-mer chains (7-mer+12-mer). Table 5.4 reports numerical results and Fig. 5.5 shows a comparison between simulation results and theoretical predictions obtained from the ana-

Table 5.4: Isotropic (I) and nematic (N) phase equilibria of the binary mixture of linear Lennard-Jones 7-mer and 12-mer chains at $P^* = 2.535$. x_2 is the mole fraction of the long chain (12-mer).

T^*	x_2^I	$\rho_m^{*,I}$	S_2^I	x_2^N	$\rho_m^{*,N}$	S_2^N
14	0.971 ± 0.001	0.402 ± 0.012	0.143 ± 0.081	0.988 ± 0.001	0.489 ± 0.000	0.844 ± 0.002
13	0.766 ± 0.011	0.407 ± 0.003	0.157 ± 0.052	0.904 ± 0.007	0.505 ± 0.001	0.837 ± 0.010
12	0.606 ± 0.011	0.418 ± 0.002	0.098 ± 0.009	0.845 ± 0.008	0.530 ± 0.001	0.857 ± 0.006
11	0.463 ± 0.018	0.431 ± 0.003	0.092 ± 0.020	0.787 ± 0.013	0.556 ± 0.002	0.874 ± 0.008
10	0.338 ± 0.015	0.449 ± 0.003	0.065 ± 0.010	0.767 ± 0.023	0.603 ± 0.003	0.907 ± 0.010
9	0.222 ± 0.017	0.467 ± 0.003	0.065 ± 0.006	0.716 ± 0.040	0.637 ± 0.004	0.920 ± 0.014
8	0.124 ± 0.010	0.491 ± 0.002	0.062 ± 0.008	0.668 ± 0.041	0.680 ± 0.002	0.938 ± 0.011
7	0.050 ± 0.001	0.522 ± 0.001	0.063 ± 0.008	0.521 ± 0.009	0.706 ± 0.001	0.938 ± 0.004
6	0.014 ± 0.004	0.566 ± 0.001	0.092 ± 0.023	0.402 ± 0.041	0.788 ± 0.048	0.959 ± 0.013
5.397	0.000 ± 0.000	0.606 ± 0.004	0.156 ± 0.040	0.000 ± 0.000	0.631 ± 0.004	0.517 ± 0.081

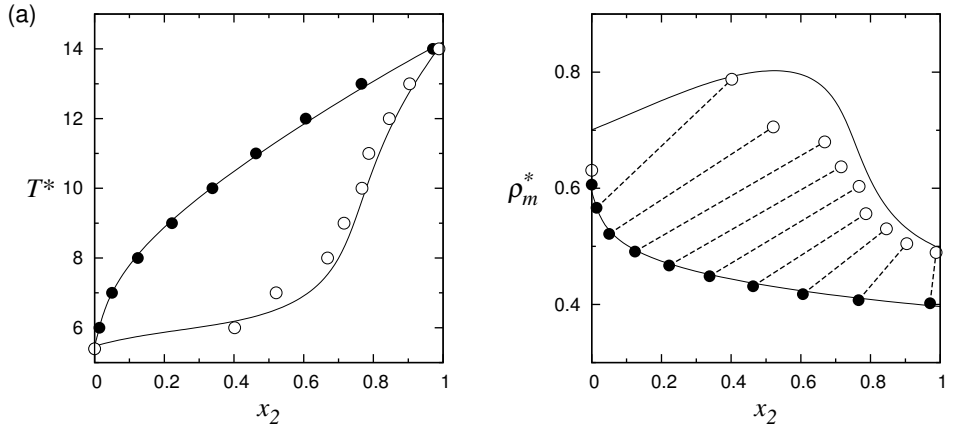

Figure 5.5: Isotropic-nematic phase equilibria for a binary mixture of linear Lennard-Jones 7-mer and 12-mer chains at a reduced pressure of $P^* = 2.535$. (a) Reduced temperature T^* and (b) reduced monomer density ρ_m^* *vs.* mole fraction of the largest component x_2. Symbols and solid lines as in Fig. 5.1. Dashed lines are constant temperature tie-lines as reported in Table 5.4. Pure component simulation data for the 7-mer fluid are calculated from constant volume expanded Gibbs-ensemble simulations at temperatures close to the equilibrium temperature. Equilibrium temperature and isotropic-nematic coexisting densities at the specified pressure of the mixture are determined by interpolation from the closest calculated equilibrium pressures.

lytical equation of state of van Westen *et al.* [79]. Phase split between an isotropic and a nematic phase and fractionation of the fluid between both phases is observed. Fractionation of the mixture into an isotropic phase richer in the short chains and a nematic phase richer in the long chains is a consequence of the more anisotropic pair-excluded volume interactions of the long chains. Fig. 5.5 (a) shows the mole fraction of the long chain x_2 in the isotropic and nematic phases at different equilibrium temperatures. An accurate description of fractionation between both phases is obtained from theoretical calculations. Fig. 5.5 (b) compares simulation results for the isotropic and nematic coexistence monomer densities with theoretical results from the equation of state. At constant mole fraction, a maximum in the density of the nematic phase and a maximum in the isotropic-nematic density difference is observed in the range x_2=0.4–0.6 from simulation results and at x_2=0.5 from the theoretical results. Previously, a similar behavior was found for binary mixtures of linear hard-sphere chains [78, 164]. With increasing mole fraction of the long component, the driving force for the phase transition increases, which leads to lower coexistence densities. However, the addition of a small amount of the long component to a pure fluid of the short component leads to a dramatic increase in the orientational order of the system (due to induced order [78]). As a result, the density of the nematic phase increases. These two competing effects lead to the observed maximum. Overall, comparison between theory and simulations is accurate. A slight overestimation of the isotropic and nematic monomer densities is observed, with larger deviations at lower temperatures corresponding to a larger concentration of the short chains. This effect is expected since the description of the hard-chain reference fluid that underlies the perturbation theory becomes less accurate for shorter chain lengths [78].

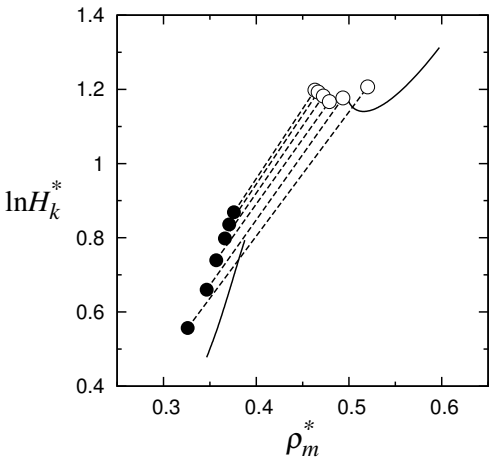

Figure 5.6: Infinite dilution solubility of a Lennard-Jones gas in the coexisting isotropic and nematic phases of a linear Lennard-Jones 12-mer chain fluid. Symbols and solid lines as in Fig. 5.1. Dashed lines are constant temperature tie-lines as reported in Table 5.1.

5.6 Solubility of gases in Lennard-Jones chains

In this section, the infinite dilution solubility of a Lennard-Jones gas in the coexisting isotropic and nematic phases of Lennard-Jones chain fluids is studied. Solubility is described by the dimensionless Henry coefficient as defined by Eq. 2.47.

In Fig. 5.6, simulation results for the solubility of a Lennard-Jones gas in the coexisting isotropic and nematic phases of a linear Lennard-Jones 12-mer chain fluid are reported as a function of monomer density. A decrease in solubility with density is observed in the isotropic phase, while first an increasing and then a decreasing solubility is identified in the nematic phase. As temperature increases (see Fig. 5.1 (c)), decreasing solubilities in the isotropic phase are caused by both larger equilibrium temperatures and higher equilibrium densities, while the increasing/decreasing behavior in the nematic phase is the consequence of a balance between larger temperatures accompanied by lower equilibrium densities. Larger solubility differences between both coexisting phases are observed at lower equilibrium temperatures.

Fig. 5.7 shows the infinite dilution solubility of a Lennard-Jones gas in the coexisting isotropic and nematic phases of a binary mixture of linear 7- and 12-mer at constant pressure. It can be identified that the solubility difference between both phases is always larger in the mixture than in the pure components. A maximum in the isotropic-nematic solubility difference is observed at a mole fraction in the range $x_2 = 0.4 - 0.6$ from simulations and $x_2 = 0.5$ from theoretical results. This maximum is directly related to the maximum density difference shown in the previous section, see Fig. 5.5 (b).

Fig. 5.8 shows the isotropic-nematic solubility difference as a function of the density difference at coexistence for the linear Lennard-Jones chain fluids. A linear relationship between solubility difference and density difference is identified in all cases. This result indicates the central role that density has in solubility, which seems to be independent of the

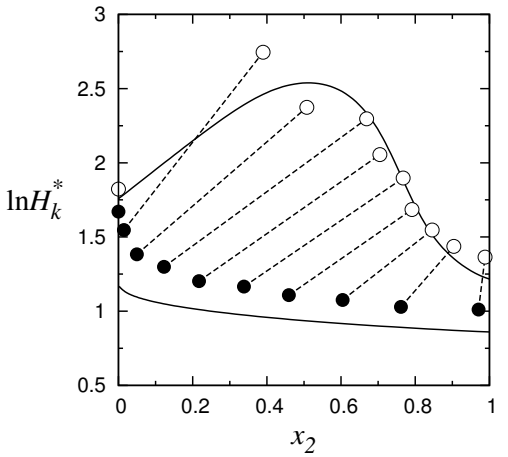

Figure 5.7: Infinite dilution solubility of a Lennard-Jones gas in the coexisting isotropic and nematic phases of a binary mixture of linear Lennard-Jones 7-mer and 12-mer chains. Logarithm of dimensionless Henry's coefficient $\ln H_k^*$ *vs* mole fraction of the long chain x_2. Symbols and solid lines as in Fig. 5.1. Dashed lines are constant temperature tie-lines as reported in Table 5.4.

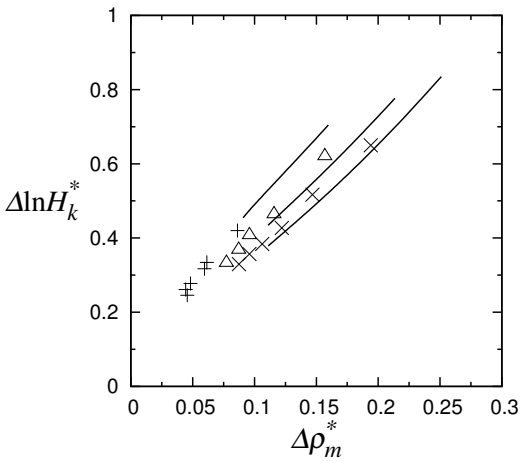

Figure 5.8: Solubility difference $\Delta \ln H_k^*$ as a function of reduced monomer density difference $\Delta\rho_m^*$ at the isotropic-nematic phase transition for linear Lennard-Jones 8-mer (+), 10-mer (△) and 12-mer (×) chain fluids. Solid lines are theoretical results obtained from the analytical equation of state of van Westen *et al.* [79].

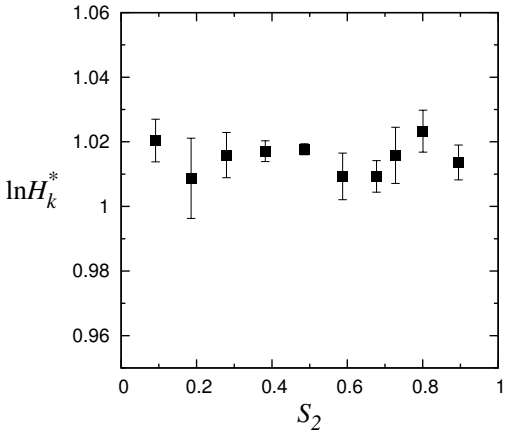

Figure 5.9: Infinite dilution solubility of a Lennard-Jones gas in a linear 12-mer fluid at the isotropic-nematic phase transition as a function of nematic ordering. Logarithm of dimensionless Henry's coefficient $\ln H_k^*$ *vs.* order parameter S_2. Results are obtained at constant temperature $T^* = 10$ and monomer density $\rho_m^* = 0.42$. Error bars represent one standard deviation.

nematic ordering of the fluid. To confirm this supposition, simulations at constant number of molecules, volume, and temperature, in the *NVT* ensemble, but restricting the nematic ordering of the system are performed, similarly as in section 3.5. Fig. 5.9 shows the solubility of gases in a 12-mer for different values of the order parameter at constant temperature and density. From these results, it can be concluded that the solubility of a Lennard-Jones gas molecule is independent of the nematic ordering of the fluid at constant density and temperature conditions.

Figs. 5.6 and 5.7 include theoretical results obtained from the equation of state of van Westen *et al.* for the same temperature range considered in the simulations (see Tables 5.1 and 5.4). These results indicate that the theory systematically underestimates the Henry coefficient. In Fig. 5.8, we show the isotropic-nematic solubility difference as a function of density difference. It can be observed, that theory and simulations follow the same linear relationship. This underlines the fact that the differences between simulations and theory are systematic. Unfortunately, we have not found the underlying reason for these systematic differences. In Fig. 5.8, it can be observed that density differences are overestimated by the theory, with the consequence of a higher solubility difference between the isotropic and nematic phase. The overestimation of the density difference at the isotropic-nematic transition is a common flaw of rescaled Onsager theories of the type examined in the work of van Westen *et al.*, and is expected to become less pronounced for longer chain lengths.

5.7 Conclusions

The isotropic-nematic phase equilibria of Lennard-Jones chain fluids were determined from direct phase equilibria calculations using an expanded version of the Gibbs ensemble. Results for linear Lennard-Jones chain fluids showed that increasing chain length leads to a

decrease of the isotropic-nematic coexistence densities and an increase of the isotropic-nematic density difference. These results are explained from a more anisotropic pair-excluded volume of longer chains, which constitutes a larger driving force for the isotropic to nematic transition. A linear relationship between coexistence pressure and temperature was found, indicating a proportional relationship between energetic and volume effects at the isotropic-nematic phase transition. We found evidence of the formation of smectic-C and crystal phases. However, these results are not conclusive due to the difficulties of the current simulation technique in representing the bulk behaviour of highly structured phases. The effect of flexibility was studied by means of partially flexible chains, consisting of a rigid linear part, and a freely-jointed part. It was found that flexibility shifts the isotropic-nematic equilibrium to larger densities and pressures, reducing at the same time the isotropic-nematic density difference. This can be explained from the fact that flexibility reduces the anisotropy of molecules, and thereby lowers the driving force for the isotropic-nematic transition. Results for the isotropic-nematic coexistence of a binary mixture showed fractionation of the fluid into an isotropic phase richer in the short chains and a nematic phase richer in the long chains. For this mixture, a maximum in the density of the nematic phase and a maximum in the isotropic-nematic density difference at coexistence were identified. This maximum appears as a balance between a larger potential for the phase transition as the mole fraction of the long component increases (reducing the coexisting isotropic density), and the order induced in the nematic phase by a larger presence of the long component (increasing the coexisting nematic density).

Simulation results were extensively compared to theoretical results as obtained from a recently developed equation of state of van Westen *et al.* [79]. It was found that the equation of state provides an excellent description of phase equilibria. The equation of state was developed based on the assumption that attractive dispersive interactions between Lennard-Jones chains do not depend on their relative orientations. The good comparison to simulation results therefore suggests that the effect of anisotropic dispersion interactions is small, and that a faithful description of real nematic liquid crystals could well be developed without it.

The infinite dilution solubility of a Lennard-Jones gas in Lennard-Jones chain fluids was estimated by the Widom test-particle insertion method. Pure components showed an increasing solubility difference between coexisting isotropic and nematic phases as temperature decreases. A linear relationship between solubility difference and density difference at coexistence was identified for all linear Lennard-Jones systems. In the binary mixture, a maximum in the isotropic-nematic solubility difference as a function of mole fraction was observed. This maximum is directly related to the observed maximum in the density difference between both phases. Simulations at constant temperature and density but with restricted values of the order parameter showed that the solubility of a Lennard-Jones gas is independent of the nematic ordering of the fluid.

Bibliography

[1] P. G. de Gennes, *The Physics of Liquid Crystals* (Oxford University Press, New York, 1974).

[2] G. R. Luckhurst and G. W. Gray, *Molecular Physics of Liquid Crystals* (Academic Press, London, 1979).

[3] G. W. Gray and M. S. Kelly, Liquid Crystals for Twisted Nematic Display Devices, Journal of Materials Chemistry **9**, 2037 (1999).

[4] K. Sun, Z. Xiao, S. Lu, W. Zajaczkowski, W. Pisula, E. Hanssen, J. M. White, R. M. Williamson, J. Subbiah, J. Ouyang, A. B. Holmes, W. W. H. Wong, and D. J. Jones, A Molecular Nematic Liquid Crystalline Material for High-Performance Organic Photovoltaics, Nature Communications **6**, 1 (2015).

[5] N. W. Schmidt, F. Jin, R. Lande, T. Curk, W. Xian, C. Lee, L. Frasca, D. Frenkel, J. Dobnikar, M. Gilliet, and G. C. L. Wong, Liquid-Crystalline Ordering of Antimicrobial Peptide-DNA Complexes Controls TLR9 Activation, Nature Materials **14**, 696 (2015).

[6] J. Gross and P. J. Jansens, WO2008147181-A1/NL2000654-C2 (2008).

[7] M. de Groen, T. J. H. Vlugt, and T. W. de Loos, Phase Behavior of Liquid Crystals with CO_2, The Journal of Physical Chemistry B **116**, 9101 (2012).

[8] M. de Groen, H. Matsuda, T. J. H. Vlugt, and T. W. de Loos, Phase Behaviour of the System 4'-Pentyloxy-4-cyanobiphenyl+CO_2, The Journal of Chemical Thermodynamics **59**, 20 (2013).

[9] M. de Groen, B. C. Ramaker, T. J. H. Vlugt, and T. W. de Loos, Phase Behavior of Liquid Crystal + CO_2 Mixtures, Journal of Chemical & Engineering Data **59**, 1667 (2014).

[10] M. de Groen, T. J. H. Vlugt, and T. W. de Loos, Binary and Ternary Mixtures of Liquid Crystals with CO_2, AIChE Journal (2015).

[11] T. Brückert, D. Büsing, A. Würflinger, and S. Urban, Differential Thermal Analysis (DTA) and Dielectric Studies on 4-(Trans-4-Pentyl-Cyclohexyl)-Benzonitrile (PCH-5) Under High Pressure, Molecular Crystals and Liquid Crystals Science and Technology. Section A. Molecular Crystals and Liquid Crystals **262**, 209 (1995).

[12] D. S. Chen, G. H. Hsiue, J. D. Schultze, B. Song, and J. Springer, Gas Sorption Properties and Molecular States of a Liquid Crystal, Molecular Crystals and Liquid Crystals Science and Technology. Section A. Molecular Crystals and Liquid Crystals **237**, 85 (1993).

[13] G.-H. Chen and J. Springer, Sorption and Diffusion of Gases in Liquid Crystalline Substances, Molecular Crystals and Liquid Crystals Science and Technology. Section A. Molecular Crystals and Liquid Crystals **339**, 31 (2000).

[14] W. E. Acree and J. S. Chickos, Phase Change Enthalpies and Entropies of Liquid Crystals, Journal of Physical and Chemical Reference Data **35**, 1051 (2006).

[15] J. Deschamps, J. P. M. Trusler, and G. Jackson, Vapor Pressure and Density of Thermotropic Liquid Crystals: MBBA, 5CB, and Novel Fluorinated Mesogens, The Journal of Physical Chemistry B **112**, 3918 (2008).

[16] J. E. Bara, D. E. Camper, D. L. Gin, and R. D. Noble, Room-Temperature Ionic Liquids and Composite Materials: Platform Technologies for CO_2 Capture, Accounts of Chemical Research **43**, 152 (2010).

[17] B. R. Anand and S. R. Edward, A Technical, Economic, and Environmental Assessment of Amine-Based CO_2 Capture Technology for Power Plant Greenhouse Gas Control, Environmental Science & Technology **36**, 4467 (2002).

[18] G. T. Rochelle, Amine Scrubbing for CO_2 Capture, Science **325**, 1652 (2009).

[19] B. Oyarzún, A. Bardow, and J. Gross, Integration of Process and Solvent Design Towards a Novel Generation of CO_2 Absorption Capture Systems, Energy Procedia **4**, 282 (2011).

[20] L. Onsager, The Effects of Shape on the Interaction of Colloidal Particles, Annals of the New York Academy of Sciences **51**, 627 (1949).

[21] W. Maier and A. Saupe, Eine einfache molekulare Theorie des nematischen kristallinflüssigen Zustandes, Zeitschrift Naturforschung Teil A **13**, 564 (1958).

[22] W. Maier and A. Saupe, Eine einfache molekularstatistische Theorie der nematischen kristallinflüssigen Phase. Teil I, Zeitschrift Naturforschung Teil A **14**, 882 (1959).

[23] W. Maier and A. Saupe, Eine einfache molekularstatistische Theorie der nematischen kristallinflüsign Phase. Teil II, Zeitschrift Naturforschung Teil A **15**, 287 (1960).

[24] T. D. Schultz, On the Validity of the Maier-Saupe Theroy of the Nematic Transition, Molecular Crystals and Liquid Crystals **14**, 147 (1971).

[25] R. L. Humphries, P. G. James, and G. R. Luckhurst, Molecular Field Treatment of Nematic Liquid Crystals, Journal of the Chemical Society, Faraday Transactions 2 **68**, 1031 (1972).

[26] A. Wulf, Difficulties with the Maier–Saupe Theory of Liquid Crystals, The Journal of Chemical Physics **64**, 104 (1976).

[27] G. R. Luckhurst and C. Zannoni, Why is the Maier-Saupe Theory of Nematic Liquid Crystals so Successful?, Nature **267**, 412 (1977).

[28] W. H. D. Jeu, On the Role of Spherical Symmetry in the Maier-Saupe Theory, Molecular Crystals and Liquid Crystals Science and Technology. Section A. Molecular Crystals and Liquid Crystals **292**, 13 (1997).

[29] M. A. Cotter, Hard Spherocylinders in an Anisotropic Mean Field: A Simple Model for a Nematic Liquid Crystal, The Journal of Chemical Physics **66**, 1098 (1977).

[30] G. J. Vroege and H. N. W. Lekkerkerker, Phase Transitions in Lyotropic Colloidal and Polymer Liquid Crystals, Reports on Progress in Physics **55**, 1241 (1992).

[31] D. Frenkel, Entropy-Driven Phase Transitions, Physica A: Statistical Mechanics and its Applications **263**, 26 (1999), proceedings of the 20th IUPAP International Conference on Statistical Physics.

[32] M. Franco-Melgar, A. J. Haslam, and G. Jackson, Advances in Generalised van der Waals Approaches for the Isotropic-Nematic Fluid Phase Equilibria of Thermotropic Liquid Crystals-An Algebraic Equation of State for Attractive Anisotropic Particles with the Onsager Trial Function, Molecular Physics **107**, 2329 (2009).

[33] D. Frenkel and R. Eppenga, Monte Carlo Study of the Isotropic-Nematic Transition in a Fluid of Thin Hard Disks, Physical Review Letters **49**, 1089 (1982).

[34] R. Eppenga and D. Frenkel, Monte Carlo Study of the Isotropic and Nematic Phases of Infinitely Thin Hard Platelets, Molecular Physics **52**, 1303 (1984).

[35] D. Frenkel, B. M. Mulder, and J. P. McTague, Phase Diagram of a System of Hard Ellipsoids, Physical Review Letters **52**, 287 (1984).

[36] D. Frenkel and B. M. Mulder, The Hard Ellipsoid-of-Revolution Fluid, Molecular Physics **55**, 1171 (1985).

[37] M. P. Allen, Computer Simulation of a Biaxial Liquid Crystal, Liquid Crystals **8**, 499 (1990).

[38] A. Samborski, G. T. Evans, C. P. Mason, and M. P. Allen, The Isotropic to Nematic Liquid Crystal Transition for Hard Ellipsoids: An Onsager-Like Theory and Computer Simulations, Molecular Physics **81**, 263 (1994).

[39] A. Stroobants, H. N. W. Lekkerkerker, and D. Frenkel, Evidence for One-, Two-, And Three-Dimensional Order in a System of Hard Parallel Spherocylinders, Physical Review A **36**, 2929 (1987).

[40] D. Frenkel, Structure of Hard-Core Models for Liquid Crystals, The Journal of Physical Chemistry **92**, 3280 (1988).

[41] A. Stroobants, H. N. W. Lekkerkerker, and D. Frenkel, Evidence for Smectic Order in a Fluid of Hard Parallel Spherocylinders, Physical Review Letters **57**, 1452 (1986).

[42] D. Frenkel, H. N. W. Lekkerkerker, and A. Stroobants, Thermodynamic Stability of a Smectic Phase in a System of Hard Rods, Nature **332**, 822 (1988).

[43] J. A. C. Veerman and D. Frenkel, Phase Diagram of a System of Hard Spherocylinders by Computer Simulation, Physical Review A **41**, 3237 (1990).

[44] P. Bolhuis and D. Frenkel, Tracing the Phase Boundaries of Hard Spherocylinders, The Journal of Chemical Physics **106**, 666 (1997).

[45] J. A. C. Veerman and D. Frenkel, Phase Behavior of Disklike Hard-Core Mesogens, Physical Review A **45**, 5632 (1992).

[46] B. Oyarzún, T. van Westen, and T. J. H. Vlugt, The Phase Behavior of Linear and Partially Flexible Hard-Sphere Chain Fluids and the Solubility of Hard Spheres in Hard-Sphere Chain Fluids, The Journal of Chemical Physics **138**, 204905 (2013).

[47] D. Frenkel, Computer Simulation of Hard-Core Models for Liquid Crystals, Molecular Physics **60**, 1 (1987).

[48] M. P. Allen, Simulations Using Hard Particles, Philosophical Transactions of the Royal Society of London. Series A: Physical and Engineering Sciences **344**, 323 (1993).

[49] A. Saupe, On Molecular Structure and Physical Properties of Thermotropic Liquid Crystals, Molecular Crystals **7**, 59 (1969).

[50] L. F. Rull, Phase Diagram of a Liquid Crystal Model: A Computer Simulation Study, Physica A: Statistical Mechanics and its Applications **220**, 113 (1995).

[51] B. J. Berne and P. Pechukas, Gaussian Model Potentials for Molecular Interactions, The Journal of Chemical Physics **56**, 4213 (1972).

[52] J. G. Gay and B. J. Berne, Modification of the Overlap Potential to Mimic a Linear Site–Site Potential, The Journal of Chemical Physics **74**, 3316 (1981).

[53] D. Adams, G. Luckhurst, and R. Phippen, Computer Simulation Studies of Anisotropic Systems, Molecular Physics **61**, 1575 (1987).

[54] E. de Miguel, L. F. Rull, M. K. Chalam, and K. E. Gubbins, Liquid Crystal Phase Diagram of the Gay-Berne Fluid, Molecular Physics **74**, 405 (1991).

[55] M. Bates and G. Luckhurst, Computer Simulation of Liquid Crystal Phases Formed by Gay-Berne Mesogens, in *Liquid Crystals I*, Structure and Bonding, Vol. 94, edited by D. Mingos and P. Michael (Springer Berlin Heidelberg, 1999) pp. 65–137.

[56] E. de Miguel and C. Vega, The Global Phase Diagram of the Gay–Berne Model, The Journal of Chemical Physics **117**, 6313 (2002).

[57] D. C. Williamson and F. del Rio, The Isotropic–Nematic Phase Transition in a Fluid of Square Well Spherocylinders, The Journal of Chemical Physics **109**, 4675 (1998).

[58] B. Martínez-Haya, L. F. Rull, A. Cuetos, and S. Lago, Gibbs Ensemble Simulation of the Vapour-Liquid Equilibrium of Square Well Spherocylinders, Molecular Physics **99**, 509 (2001).

[59] A. Cuetos, B. Martínez-Haya, L. F. Rull, and S. Lago, Monte Carlo Study of Liquid Crystal Phases of Hard and Soft Spherocylinders, The Journal of Chemical Physics **117**, 2934 (2002).

[60] L. Wu, E. A. Müller, and G. Jackson, Understanding and Describing the Liquid-Crystalline States of Polypeptide Solutions: A Coarse-Grained Model of PBLG in DMF, Macromolecules **47**, 1482 (2014).

[61] A. Cuetos, B. Martínez-Haya, S. Lago, and L. F. Rull, Liquid Crystal Behavior of the Kihara Fluid, Physical Review E **68**, 011704 (2003).

[62] L. Wu, G. Jackson, and E. A. Müller, Liquid Crystal Phase Behaviour of Attractive Disc-Like Particles, International Journal of Molecular Sciences **14**, 16414 (2013).

[63] J. S. Lintuvuori and M. R. Wilson, A New Anisotropic Soft-Core Model for the Simulation of Liquid Crystal Mesophases, The Journal of Chemical Physics **128**, 044906 (2008).

[64] M. R. Wilson, Molecular Dynamics Simulations of Flexible Liquid Crystal Molecules Using a Gay-Berne/Lennard-Jones Model, The Journal of Chemical Physics **107**, 8654 (1997).

[65] Z. E. Hughes, L. M. Stimson, H. Slim, J. S. Lintuvuori, J. M. Ilnytskyi, and M. R. Wilson, An Investigation Of Soft-Core Potentials for the Simulation of Mesogenic Molecules and Molecules Composed of Rigid and Flexible Segments, Computer Physics Communications **178**, 724 (2008).

[66] J. S. Lintuvuori and M. R. Wilson, A Coarse-Grained Simulation Study of Mesophase Formation in a Series of Rod-Coil Multiblock Copolymers, Physical Chemistry Chemical Physics **11**, 2116 (2009).

[67] M. G. Martin and J. I. Siepmann, Transferable Potentials for Phase Equilibria. 1. United-Atom Description of n-Alkanes, The Journal of Physical Chemistry B **102**, 2569 (1998).

[68] S. J. Marrink, H. J. Risselada, S. Yefimov, D. P. Tieleman, and A. H. de Vries, The MARTINI Force Field: Coarse Grained Model for Biomolecular Simulations, The Journal of Physical Chemistry B **111**, 7812 (2007).

[69] W. G. Chapman, K. E. Gubbins, G. Jackson, and M. Radosz, SAFT: Equation-of-State Solution Model for Associating Fluids, Fluid Phase Equilibria **52**, 31 (1989).

[70] W. G. Chapman, K. E. Gubbins, G. Jackson, and M. Radosz, New Reference Equation of State for Associating Liquids, Industrial & Engineering Chemistry Research **29**, 1709 (1990).

[71] A. Gil-Villegas, A. Galindo, P. J. Whitehead, S. J. Mills, G. Jackson, and A. N. Burgess, Statistical Associating Fluid Theory for Chain Molecules with Attractive Potentials of Variable Range, The Journal of Chemical Physics **106**, 4168 (1997).

[72] F. J. Blas and L. F. Vega, Improved Vapor-Liquid Equilibria Predictions for Lennard-Jones Chains from the Statistical Associating Fluid Dimer Theory: Comparison with Monte Carlo Simulations, The Journal of Chemical Physics **115**, 4355 (2001).

[73] J. Gross and G. Sadowski, Perturbed-Chain SAFT: An Equation of State Based on a Perturbation Theory for Chain Molecules, Industrial & Engineering Chemistry Research **40**, 1244 (2001).

[74] E. A. Müller and K. E. Gubbins, Molecular-Based Equations of State for Associating Fluids: A Review of SAFT and Related Approaches, Industrial & Engineering Chemistry Research **40**, 2193 (2001).

[75] S. Tamouza, J. P. Passarello, P. Tobaly, and J. C. de Hemptinne, Group Contribution Method with SAFT EOS Applied to Vapor Liquid Equilibria of Various Hydrocarbon Series, Fluid Phase Equilibria **222–223**, 67 (2004).

[76] A. Lymperiadis, C. S. Adjiman, A. Galindo, and G. Jackson, A Group Contribution Method for Associating Chain Molecules Based on the Statistical Associating Fluid Theory (SAFT-γ), The Journal of Chemical Physics **127**, 234903 (2007).

[77] T. van Westen, B. Oyarzún, T. J. H. Vlugt, and J. Gross, An Equation of State for the Isotropic Phase Of Linear, Partially Flexible and Fully Flexible Tangent Hard-Sphere Chain Fluids, Molecular Physics **112**, 919 (2014).

[78] T. van Westen, T. J. H. Vlugt, and J. Gross, The Isotropic-Nematic And Nematic-Nematic Phase Transition of Binary Mixtures of Tangent Hard-Sphere Chain Fluids: An Analytical Equation of State, The Journal of Chemical Physics **140**, 034504 (2014).

[79] T. van Westen, B. Oyarzún, T. J. H. Vlugt, and J. Gross, An Analytical Equation of State for Describing Isotropic-Nematic Phase Equilibria of Lennard-Jones Chain Fluids with Variable Degree of Molecular Flexibility, The Journal of Chemical Physics **142**, 244903 (2015).

[80] D. Frenkel and B. Smit, *Understanding Molecular Simulations*, 2nd ed. (Academic Press, London, 2002).

[81] N. Metropolis, A. W. Rosenbluth, M. N. Rosenbluth, A. H. Teller, and E. Teller, Equation of State Calculations by Fast Computing Machines, The Journal of Chemical Physics **21**, 1087 (1953).

[82] V. I. Manousiouthakis and M. W. Deem, Strict Detailed Balance is Unnecessary in Monte Carlo Simulation, The Journal of Chemical Physics **110**, 2753 (1999).

[83] T. van Westen, B. Oyarzún, T. J. H. Vlugt, and J. Gross, The Isotropic-Nematic Phase Transition of Tangent Hard-Sphere Chain Fluids—Pure Components, The Journal of Chemical Physics **139**, 034505 (2013).

[84] T. van Westen, T. J. H. Vlugt, and J. Gross, On the Vapor-Liquid Equilibrium of Attractive Chain Fluids with Variable Degree of Molecular Flexibility, The Journal of Chemical Physics **142**, 224504 (2015).

[85] C. Vega, C. McBride, and L. G. MacDowell, Liquid Crystal Phase Formation for the Linear Tangent Hard Sphere Model from Monte Carlo Simulations, The Journal of Chemical Physics **115**, 4203 (2001).

[86] C. Vega, E. P. A. Paras, and P. A. Monson, Solid–Fluid Equilibria for Hard Dumbbells via Monte Carlo Simulation, The Journal of Chemical Physics **96**, 9060 (1992).

[87] W. G. Hoover and F. H. Ree, Melting Transition and Communal Entropy for Hard Spheres, The Journal of Chemical Physics **49**, 3609 (1968).

[88] D. C. Williamson and G. Jackson, Liquid Crystalline Phase Behavior in Systems of Hard-Sphere Chains, The Journal of Chemical Physics **108**, 10294 (1998).

[89] A. Yethiraj and H. Fynewever, Isotropic to Nematic Transition in Semiflexible Polymer Melts, Molecular Physics **93**, 693 (1998).

[90] M. Whittle and A. Masters, Liquid Crystal Formation in a System of Fused Hard Spheres, Molecular Physics **72**, 247 (1991).

[91] C. McBride, C. Vega, and L. G. MacDowell, Isotropic-Nematic Phase Transition: Influence of Intramolecular Flexibility Using a Fused Hard Sphere Model, Physical Review E **64**, 011703 (2001).

[92] C. McBride and C. Vega, A Monte Carlo Study of the Influence of Molecular Flexibility on the Phase Diagram of a Fused Hard Sphere Model, The Journal of Chemical Physics **117**, 10370 (2002).

[93] C. Vega, C. McBride, and L. G. MacDowell, The Effect of Flexibility on the Phase Diagram of Simple Molecular Models, Physical Chemistry Chemical Physics **4**, 853 (2002).

[94] F. A. Escobedo and J. J. de Pablo, Monte Carlo Simulation of Athermal Mesogenic Chains: Pure Systems, Mixtures, and Constrained Environments, The Journal of Chemical Physics **106**, 9858 (1997).

[95] A. Galindo, C. Vega, E. Sanz, L. G. MacDowell, E. de Miguel, and F. J. Blas, Computer Simulation Study of the Global Phase Behavior of Linear Rigid Lennard-Jones Chain Molecules: Comparison with Flexible Models, The Journal of Chemical Physics **120**, 3957 (2004).

[96] S. S. Turzi, On the Cartesian Definition of Orientational Order Parameters, Journal of Mathematical Physics **52**, 053517 (2011).

[97] R. B. Meyer and T. C. Lubensky, Mean-Field Theory of the Nematic-Smectic-*A* Phase Change in Liquid Crystals, Physical Review A **14**, 2307 (1976).

[98] J. M. Polson and D. Frenkel, First-Order Nematic-Smectic Phase Transition for Hard Spherocylinders in the Limit of Infinite Aspect Ratio, Physical Review E **56**, R6260 (1997).

[99] J. I. Siepmann, A Method for the Direct Calculation of Chemical Potentials for Dense Chain Systems, Molecular Physics **70**, 1145 (1990).

[100] J. I. Siepmann and D. Frenkel, Configurational Bias Monte Carlo: A New Sampling Scheme for Flexible Chains, Molecular Physics **75**, 59 (1992).

[101] D. Frenkel, G. C. A. M. Mooij, and B. Smit, Novel Scheme to Study Structural and Thermal Properties of Continuously Deformable Molecules, Journal of Physics: Condensed Matter **4**, 3053 (1992).

[102] M. Laso, J. J. de Pablo, and U. W. Suter, Simulation of Phase equilibria for Chain Molecules, The Journal of Chemical Physics **97**, 2817 (1992).

[103] A. Z. Panagiotopoulos, Direct Determination of Phase Coexistence Properties of Fluids by Monte Carlo Simulation in a New Ensemble, Molecular Physics **61**, 813 (1987).

[104] A. Z. Panagiotopoulos, N. Quirke, M. Stapleton, and D. J. Tildesley, Phase Equilibria by Simulation in the Gibbs Ensemble, Molecular Physics **63**, 527 (1988).

[105] L. F. Rull, G. Jackson, and B. Smit, The Condition of Microscopic Reversibility in Gibbs Ensemble Monte Carlo Simulations of Phase Equilibria, Molecular Physics **85**, 435 (1995).

[106] A. Z. Panagiotopoulos, Molecular Simulation of Phase equilibria: Simple, Ionic and Polymeric Fluids, Fluid Phase Equilibria **76**, 97 (1992).

[107] J. J. de Pablo, M. Laso, and U. W. Suter, Estimation of the Chemical Potential of Chain Molecules by Simulation, The Journal of Chemical Physics **96**, 6157 (1992).

[108] J. I. Siepmann, S. Karaborni, and B. Smit, Vapor-Liquid Equilibria of Model Alkanes, Journal of the American Chemical Society **115**, 6454 (1993).

[109] J. I. Siepmann, S. Karaborni, and B. Smit, Simulating the Critical Behaviour of Complex Fluids, Nature **365**, 330 (1993).

[110] B. Smit, S. Karaborni, and J. I. Siepmann, Computer Simulations of Vapor-Liquid Equilibria of n-Alkanes, The Journal of Chemical Physics **102**, 2126 (1995).

[111] S. T. Cui, P. T. Cummings, and H. D. Cochran, Configurational Bias Gibbs Ensemble Monte Carlo Simulation of Vapor-Liquid Equilibria of Linear and Short-Branched Alkanes, Fluid Phase Equilibria **141**, 45 (1997).

[112] J. I. Siepmann and M. G. Martin, Intermolecular Potentials for Branched Alkanes and the Vapour-Liquid Phase Equilibria of n-Heptane, 2-Methylhexane, and 3-Ethylpentane, Molecular Physics **90**, 687 (1997).

[113] T. J. H. Vlugt, M. G. Martin, B. Smit, J. I. Siepmann, and R. Krishna, Improving the Efficiency of the Configurational-Bias Monte Carlo Algorithm, Molecular Physics **94**, 727 (1998).

[114] T. J. H. Vlugt, Efficiency of Parallel CBMC Simulations, Molecular Simulation **23**, 63 (1999).

[115] S. Consta, T. J. H. Vlugt, J. W. Hoeth, B. Smit, and D. Frenkel, Recoil Growth Algorithm for Chain Molecules with Continuous Interactions, Molecular Physics **97**, 1243 (1999).

[116] S. Consta, N. B. Wilding, D. Frenkel, and Z. Alexandrowicz, Recoil Growth: An Efficient Simulation Method for Multi-Polymer Systems, The Journal of Chemical Physics **110**, 3220 (1999).

[117] A. P. Lyubartsev, A. A. Martsinovski, S. V. Shevkunov, and P. N. Vorontsov-Velyaminov, New Approach to Monte Carlo Calculation of the Free Energy: Method of Expanded Ensembles, The Journal of Chemical Physics **96**, 1776 (1992).

[118] N. B. Wilding and M. Müller, Accurate Measurements of the Chemical Potential of Polymeric Systems by Monte Carlo Simulation, The Journal of Chemical Physics **101**, 4324 (1994).

[119] F. A. Escobedo and J. J. de Pablo, Monte Carlo Simulation of the Chemical Potential of Polymers in an Expanded Ensemble, The Journal of Chemical Physics **103**, 2703 (1995).

[120] F. A. Escobedo and J. J. de Pablo, Expanded Grand Canonical and Gibbs Ensemble Monte Carlo Simulation of Polymers, The Journal of Chemical Physics **105**, 4391 (1996).

[121] W. Shi and E. J. Maginn, Improvement in Molecule Exchange Efficiency in Gibbs Ensemble Monte Carlo: Development and Implementation of the Continuous Fractional Component Move, Journal of Computational Chemistry **29**, 2520 (2008).

[122] B. A. Berg and T. Neuhaus, Multicanonical Algorithms for First Order Phase Transitions, Physics Letters B **267**, 249 (1991).

[123] N. B. Wilding, Computer Simulation of Fluid Phase Transitions, American Journal of Physics **69**, 1147 (2001).

[124] C. R. A. Abreu and F. A. Escobedo, A General Framework for Non-Boltzmann Monte Carlo Sampling, The Journal of Chemical Physics **124**, 054116 (2006).

[125] A. Z. Panagiotopoulos, Direct Determination of Fluid Phase Equilibria by Simulation in the Gibbs Ensemble: A Review, Molecular Simulation **9**, 1 (1992).

[126] A. P. Lyubartsev, A. Laaksonen, and P. N. Vorontsov-Velyaminov, Free Energy Calculations for Lennard-Jones Systems and Water Using the Expanded Ensemble Method A Monte Carlo and Molecular Dynamics Simulation Study, Molecular Physics **82**, 455 (1994).

[127] A. P. Lyubartsev, A. Laaksonen, and P. N. Vorontsov-velyaminov, Determination of Free Energy from Chemical Potentials: Application of the Expanded Ensemble Method, Molecular Simulation **18**, 43 (1996).

[128] W. Shi and E. J. Maginn, Continuous Fractional Component Monte Carlo: An Adaptive Biasing Method for Open System Atomistic Simulations, Journal of Chemical Theory and Computation **3**, 1451 (2007).

[129] E. J. Maginn, Atomistic Simulation of the Thermodynamic and Transport Properties of Ionic Liquids, Accounts of Chemical Research **40**, 1200 (2007).

[130] W. Shi and E. J. Maginn, Atomistic Simulation of the Absorption of Carbon Dioxide and Water in the Ionic Liquid 1-n-Hexyl-3-methylimidazolium Bis(trifluoromethylsulfonyl)imide ([hmim][Tf_2N], The Journal of Physical Chemistry B **112**, 2045 (2008).

[131] X. Zhang, F. Huo, Z. Liu, W. Wang, W. Shi, and E. J. Maginn, Absorption of CO_2 in the Ionic Liquid 1-n-Hexyl-3-methylimidazolium Tris(pentafluoroethyl)trifluorophosphate ([hmim][FEP]): A Molecular View by Computer Simulations, The Journal of Physical Chemistry B **113**, 7591 (2009).

[132] E. J. Maginn, Molecular Simulation of Ionic Liquids: Current Status and Future Opportunities, Journal of Physics: Condensed Matter **21**, 373101 (2009).

[133] T. W. Rosch and E. J. Maginn, Reaction Ensemble Monte Carlo Simulation of Complex Molecular Systems, Journal of Chemical Theory and Computation **7**, 269 (2011), http://dx.doi.org/10.1021/ct100615j .

[134] A. Torres-Knoop, S. P. Balaji, T. J. H. Vlugt, and D. Dubbeldam, A Comparison of Advanced Monte Carlo Methods for Open Systems: CFCMC vs CBMC, Journal of Chemical Theory and Computation **10**, 942 (2014).

[135] M. Ramdin, S. Prasaad Balaji, J. M. Vicent-Luna, J. J. Gutiérrez-Sevillano, S. Calero, T. W. de Loos, and T. J. H. Vlugt, Solubility of the Precombustion Gases CO_2, CH_4, CO, H_2, N_2, and H_2S in the Ionic Liquid [bmim][Tf_2N] from Monte Carlo Simulations, The Journal of Physical Chemistry C **118**, 23599 (2014).

[136] Q. Chen, S. Prasaad Balaji, M. Ramdin, J. J. Gutiérrez-Sevillano, A. Bardow, E. Goetheer, and T. J. H. Vlugt, Validation of the CO_2/N_2O Analogy Using Molecular Simulation, Industrial & Engineering Chemistry Research **53**, 18081 (2014).

[137] S. P. Balaji, S. Gangarapu, M. Ramdin, A. Torres-Knoop, H. Zuilhof, E. L. Goetheer, D. Dubbeldam, and T. J. H. Vlugt, Simulating the Reactions of CO_2 in Aqueous Monoethanolamine Solution by Reaction Ensemble Monte Carlo Using the Continuous Fractional Component Method, Journal of Chemical Theory and Computation **11**, 2661 (2015).

[138] M. Ramdin, S. Prasaad Balaji, A. Torres-Knoop, D. Dubbeldam, T. W. de Loos, and T. J. H. Vlugt, Solubility of Natural Gas Species in Ionic Liquids and Commercial Solvents: Experiments and Monte Carlo Simulations, Journal of Chemical & Engineering Data **60**, 3039 (2015).

[139] M. Ramdin, Q. Chen, S. Prasaad Balaji, J. M. Vicent-Luna, A. Torres-Knoop, D. Dubbeldam, S. Calero, T. W. de Loos, and T. J. H. Vlugt, Solubilities of CO_2, CH_4, C_2H_6, and SO_2 in Ionic Liquids and Selexol from Monte Carlo Simulations, Journal of Computational Science (2015), 10.1016/j.jocs.2015.09.002, in press.

[140] M. Ramdin, S. Prasaad Balaji, J. M. Vicent-Luna, A. Torres-Knoop, Q. Chen, D. Dubbeldam, S. Calero, T. W. de Loos, and T. J. H. Vlugt, Computing Bubble-Points of CO_2/CH_4 Gas Mixtures in Ionic Liquids from Monte Carlo Simulations, Fluid Phase Equilibria (2015), 10.1016/j.Fluid.2015.09.041, in press.

[141] F. A. Escobedo, Optimized Expanded Ensembles for Simulations Involving Molecular Insertions and Deletions. II. Open Systems, The Journal of Chemical Physics **127**, 174104 (2007).

[142] F. Wang and D. P. Landau, Efficient, Multiple-Range Random Walk Algorithm to Calculate the Density of States, Physical Review Letters **86**, 2050 (2001).

[143] F. Wang and D. P. Landau, Determining the Density of States for Classical Statistical Models: A Random Walk Algorithm to Produce a Flat Histogram, Physical Review E **64**, 056101 (2001).

[144] M. S. Shell, P. G. Debenedetti, and A. Z. Panagiotopoulos, Generalization of the Wang-Landau Method for Off-Lattice Simulations, Physical Review E **66**, 056703 (2002).

[145] S. I. Sandler, *Chemical, Biochemichal, and Engineering Thermodynamics*, 4th ed. (John Willey & Sons, Inc., Hoboken, 2006).

[146] K. S. Shing and K. E. Gubbins, The Chemical Potential in Dense Fluids and Fluid Mixtures via Computer Simulation, Molecular Physics **46**, 1109 (1982).

[147] D. Ghonasgi, M. Llano-Restrepo, and W. G. Chapman, Henry's Law Constant for Diatomic and Polyatomic Lennard-Jones Molecules, The Journal of Chemical Physics **98**, 5662 (1993).

[148] B. Widom, Some Topics in the Theory of Fluids, The Journal of Chemical Physics **39**, 2808 (1963).

[149] D. A. Kofke and P. T. Cummings, Quantitative Comparison and Optimization of Methods for Evaluating the Chemical Potential by Molecular Simulation, Molecular Physics **92**, 973 (1997).

[150] K. Shing and K. Gubbins, The Chemical Potential in Non-Ideal Liquid Mixtures, Molecular Physics **49**, 1121 (1983).

[151] K. S. Shing, K. E. Gubbins, and K. Lucas, Henry Constants in Non-Ideal Fluid Mixtures, Molecular Physics **65**, 1235 (1988).

[152] J. K. Shah and E. J. Maginn, Monte Carlo Simulations of Gas Solubility in the Ionic Liquid 1-n-Butyl-3-methylimidazolium Hexafluorophosphate, The Journal of Physical Chemistry B **109**, 10395 (2005).

[153] M. Wilson, Molecular Dynamics Simulation of Semi-Flexible Mesogens, Molecular Physics **81**, 675 (1994).

[154] M. R. Wilson and M. P. Allen, Computer Simulation Study of Liquid Crystal Formation in a Semi-Flexible System of Linked Hard Spheres, Molecular Physics **80**, 277 (1993).

[155] J. J. de Pablo, M. Laso, and U. W. Suter, Simulation of Polyethylene Above and Below the Melting Point, The Journal of Chemical Physics **96**, 2395 (1992).

[156] H. Fynewever and A. Yethiraj, Phase Behavior of Semiflexible Tangent Hard Sphere Chains, The Journal of Chemical Physics **108**, 1636 (1998).

[157] T. van Westen, T. J. H. Vlugt, and J. Gross, An Analytical Approximation for the Orientation-Dependent Excluded Volume of Tangent Hard Sphere Chains of Arbitrary Chain Length and Flexibility, The Journal of Chemical Physics **137**, 044906 (2012).

[158] D. C. Williamson and G. Jackson, Excluded Volume for a Pair of Linear Chains of Tangent Hard Spheres with an Arbitrary Relative Orientation, Molecular Physics **86**, 819 (1995).

[159] T. Boublík, Hard-Sphere Equation of State, The Journal of Chemical Physics **53**, 471 (1970).

[160] G. A. Mansoori, N. F. Carnahan, K. E. Starling, and J. T. W. Leland, Equilibrium Thermodynamic Properties of the Mixture of Hard Spheres, The Journal of Chemical Physics **54**, 1523 (1971).

[161] L. E. S. de Souza, A. Stamatopoulou, and D. Ben-Amotz, Chemical Potentials of Hard Sphere Solutes in Hard Sphere Solvents. Monte Carlo Simulations and Analytical Approximations, The Journal of Chemical Physics **100**, 1456 (1994).

[162] D. Ben-Amotz and I. P. Omelyan, Cavity Formation Energies for Diatomic and Spherical Solutes in a Diatomic Hard Body Fluid, The Journal of Chemical Physics **113**, 4349 (2000).

[163] S. K. Kumar, I. Szleifer, C. K. Hall, and J. M. Wichert, Computer Simulation Study of the Approximations Associated with the Generalized Flory Theories, The Journal of Chemical Physics **104**, 9100 (1996).

[164] B. Oyarzún, T. van Westen, and T. J. H. Vlugt, Isotropic-Nematic Phase Equilibria of Hard-Sphere Chain Fluids – Pure Components and Binary Mixtures, The Journal of Chemical Physics **142**, 064903 (2015).

[165] H. Finkelmann and H. J. Wendorff, *Polymeric Liquid Crystals*, edited by A. Blumstein, Polymer Science and Technology, Vol. 28 (Springer US, 1985) pp. 295–302.

[166] C. M. Wijmans, B. Smit, and R. D. Groot, Phase Behavior of Monomeric Mixtures and Polymer Solutions with Soft Interaction Potentials, The Journal of Chemical Physics **114**, 7644 (2001).

[167] M. Adams, Z. Dogic, S. L. Keller, and S. Fraden, Entropically Driven Microphase Transitions in Mixtures of Colloidal Rods and Spheres, Nature **393**, 349 (1998).

[168] H. N. W. Lekkerkerker and A. Stroobants, Colloids: Ordering Entropy, Nature **393**, 305 (1998).

[169] D. Frenkel, Onsager's Spherocylinders Revisited, The Journal of Physical Chemistry **91**, 4912 (1987).

[170] M. Franco-Melgar, A. J. Haslam, and G. Jackson, A Generalisation of the Onsager Trial-Function Approach: Describing Nematic Liquid Crystals with an Algebraic Equation of State, Molecular Physics **106**, 649 (2008).

[171] T. Odijk and H. N. W. Lekkerkerker, Theory of the Isotropic-Liquid Crystal Phase Separation for a Solution of Bidisperse Rodlike Macromolecules, The Journal of Physical Chemistry **89**, 2090 (1985).

[172] S. Varga, A. Galindo, and G. Jackson, New Types of Phase Behaviour in Binary Mixtures of Hard Rod-Like Particles, Molecular Physics **101**, 817 (2003).

[173] H. N. W. Lekkerkerker, P. Coulon, R. Van Der Haegen, and R. Deblieck, On the Isotropic-Liquid Crystal Phase Separation in a Solution of Rodlike Particles of Different Lengths, The Journal of Chemical Physics **80**, 3427 (1984).

[174] T. Odijk, Theory of Lyotropic Polymer Liquid Crystals, Macromolecules **19**, 2313 (1986).

[175] G. Cinacchi, L. Mederos, and E. Velasco, Liquid–Crystal Phase Diagrams of Binary Mixtures of Hard Spherocylinders, The Journal of Chemical Physics **121**, 3854 (2004).

[176] G. Cinacchi, E. Velasco, and L. Mederos, Entropic Segregation in Smectic Phases of Hard-Body Mixtures, Journal of Physics: Condensed Matter **16**, S2003 (2004).

[177] G. Cinacchi, Y. Martínez-Ratón, L. Mederos, and E. Velasco, Binary Mixtures of Hard Rods: A Short Account, Molecular Crystals and Liquid Crystals **465**, 121 (2007).

[178] G. Cinacchi, Y. Martínez-Ratón, L. Mederos, and E. Velasco, Smectic, Nematic, and Isotropic Phases in Binary Mixtures of Thin and Thick Hard Spherocylinders, The Journal of Chemical Physics **124**, 234904 (2006).

[179] B. Oyarzún, T. van Westen, and T. J. H. Vlugt, Liquid-Crystal Phase Equilibria of Lennard-Jones Chains, Molecular Physics (2015), accepted.

[180] M. Born, Elektronentheorie des natürlichen optischen Drehungsvermögens isotroper und anisotroper Flüssigkeiten, Annalen der Physik **360**, 177 (1918).

[181] S. J. Marrink, A. H. de Vries, and A. E. Mark, Coarse Grained Model for Semiquantitative Lipid Simulations, The Journal of Physical Chemistry B **108**, 750 (2004).

[182] W. G. Noid, Perspective: Coarse-Grained Models for Biomolecular Systems, The Journal of Chemical Physics **139**, 090901 (2013).

[183] W. G. Noid, Systematic Methods for Structurally Consistent Coarse-Grained Models, in *Biomolecular Simulations*, Methods in Molecular Biology, Vol. 924, edited by L. Monticelli and E. Salonen (Humana Press, , 2013) pp. 487–531.

[184] M. G. Saunders and G. A. Voth, Coarse-Graining Methods for Computational Biology, Annual Review of Biophysics **42**, 73 (2013).

[185] S. C. Glotzer and W. Paul, Molecular and Mesoscale Simulation Methods for Polymer Materials, Annual Review of Materials Research **32**, 401 (2002).

[186] F. Müller-Plathe, Coarse-Graining in Polymer Simulation: From the Atomistic to the Mesoscopic Scale and Back, ChemPhysChem **3**, 754 (2002).

[187] C. Avendaño, T. Lafitte, C. S. Adjiman, A. Galindo, E. A. Müller, and G. Jackson, SAFT-γ Force Field for the Simulation of Molecular Fluids: 2. Coarse-Grained Models of Greenhouse Gases, Refrigerants, and Long Alkanes, The Journal of Physical Chemistry B **117**, 2717 (2013).

[188] E. A. Müller and G. Jackson, Force-Field Parameters from the SAFT-γ Equation of State for Use in Coarse-Grained Molecular Simulations, Annual Review of Chemical and Biomolecular Engineering **5**, 405 (2014).

[189] T. van Westen, T. J. H. Vlugt, and J. Gross, Determining Force Field Parameters Using a Physically Based Equation of State, The Journal of Physical Chemistry B **115**, 7872 (2011).

[190] C. M. Care and D. J. Cleaver, Computer Simulation of Liquid Crystals, Reports on Progress in Physics **68**, 2665 (2005).

[191] M. R. Wilson, Molecular Simulation of Liquid Crystals: Progress Towards a Better Understanding of Bulk Structure and the Prediction of Material Properties, Chemical Society Reviews **36**, 1881 (2007).

[192] C. S. Schacht, T. J. H. Vlugt, and J. Gross, Using an Analytic Equation of State to Obtain Quantitative Solubilities of CO_2 by Molecular Simulation, The Journal of Physical Chemistry Letters **2**, 393 (2011).

[193] C. Avendaño, T. Lafitte, A. Galindo, C. S. Adjiman, G. Jackson, and E. A. Müller, SAFT-γ Force Field for the Simulation of Molecular Fluids. 1. A Single-Site Coarse Grained Model of Carbon Dioxide, The Journal of Physical Chemistry B **115**, 11154 (2011).

[194] T. Lafitte, C. Avendaño, V. Papaioannou, A. Galindo, C. S. Adjiman, G. Jackson, and E. A. Müller, SAFT-γ Force Field for the Simulation of Molecular Fluids: 3. Coarse-Grained Models of Benzene and Hetero-Group Models of n-Decylbenzene, Molecular Physics **110**, 1189 (2012).

[195] O. Lobanova, C. Avendaño, T. Lafitte, E. A. Müller, and G. Jackson, SAFT-γ Force Field for the Simulation of Molecular Fluids: 4. A Single-Site Coarse-Grained model of Water Applicable over a Wide Temperature Range, Molecular Physics **113**, 1228 (2015).

[196] A. Hemmen, A. Z. Panagiotopoulos, and J. Gross, Grand Canonical Monte Carlo Simulations Guided by an Analytic Equation of State—Transferable Anisotropic Mie Potentials for Ethers, The Journal of Physical Chemistry B **119**, 7087 (2015), http://dx.doi.org/10.1021/acs.jpcb.5b01806 .

[197] A. Hemmen and J. Gross, Transferable Anisotropic United-Atom Force Field Based on the Mie Potential for Phase Equilibrium Calculations: n-Alkanes and n-Olefins, The Journal of Physical Chemistry B **119**, 11695 (2015).

[198] C. Zannoni, Molecular Design and Computer Simulations of Novel Mesophases, Journal of Materials Chemistry **11**, 2637 (2001).

[199] A. Cuetos and B. Martínez-Haya, Liquid Crystal Phase Diagram of Soft Repulsive Rods and its Mapping on the Hard Repulsive Reference Fluid, Molecular Physics **113**, 1137 (2015).

[200] D. N. Theodorou, T. D. Boone, L. R. Dodd, and K. F. Mansfield, Stress Tensor in Model Polymer Systems with Periodic Boundaries, Macromolecular Theory and Simulations **2**, 191 (1993).

[201] J. A. Barker and D. Henderson, Perturbation Theory and Equation of State for Fluids: The Square-Well Potential, The Journal of Chemical Physics **47**, 2856 (1967).

[202] J. A. Barker and D. Henderson, Perturbation Theory and Equation of State for Fluids. II. A Successful Theory of Liquids, The Journal of Chemical Physics **47**, 4714 (1967).

[203] F. Affouard, M. Kröger, and S. Hess, Molecular Dynamics of Model Liquid Crystals Composed of Semiflexible Molecules, Physical Review E **54**, 5178 (1996).

[204] J. M. Polson and D. Frenkel, Calculation of Solid-Fluid Phase Equilibria for Systems of Chain Molecules, The Journal of Chemical Physics **109**, 318 (1998).

[205] R. Agrawal and D. A. Kofke, Thermodynamic and Structural Properties of Model Systems at Solid-Fluid Coexistence, Molecular Physics **85**, 23 (1995).

[206] M. B. Sweatman, New Techniques for Simulating Crystals, Molecular Simulation **35**, 897 (2009).

[207] P. Mishra and J. Ram, Effect of Shape Anisotropy on the Phase Diagram of the Gay-Berne Fluid, The European Physical Journal E **17**, 345 (2005).

[208] B. Martínez-Haya and A. Cuetos, Stability of Nematic and Smectic Phases in Rod-Like Mesogens with Orientation-Dependent Attractive Interactions, The Journal of Physical Chemistry B **111**, 8150 (2007).

Summary

The liquid crystal phase behavior of chain fluids and the solubility of gases in them was determined using Monte Carlo simulations. The effect of molecular properties such as elongation and flexibility was studied using linear and partially-flexible chain molecules. Linear chain molecules are rigid molecules with all segments aligned on the same molecular axis, while partially-flexible molecules are made of a linear and a freely-jointed part that provide a certain degree of flexibility to the molecule. Volumetric and thermal effects are studied independently by hard-sphere and Lennard-Jones potentials. Molecular simulations were performed for hard-sphere and Lennard-Jones chain fluids with a focus on the isotropic-nematic phase transition. The solubility of gases in liquid crystal phases and specially the solubility change at the isotropic-nematic transition is of interest for gas separation applications. This was studied using a single-segment gas molecule at the infinite dilution limit.

Monte Carlo simulations were performed in the *NPT* ensemble and in an expanded version of the Gibbs ensemble. The phase behavior of single-phase hard-sphere chain fluids was determined using *NPT* ensemble simulations, while the isotropic-nematic phase equilibrium of single-component and binary mixtures of hard-sphere and Lennard-Jones fluids was calculated using expanded Gibbs ensemble simulations. Fluid properties such as packing fractions (hard-sphere fluids), densities and temperatures (Lennard-Jones fluids), order parameters, pressures, and gas solubilities (Henry coefficients) were obtained for chain fluids with different degrees of elongation and flexibility.

The study of single-component athermal (hard-sphere) systems showed that larger chain lengths increase the potential for the formation of nematic phases, decreasing monotonically the pressure and packing fractions at which the isotropic-nematic phase transition takes place. However, a maximum in the isotropic-nematic packing fraction difference was observed as a function of chain length. Flexibility reduces the anisotropy of the molecule, which increases the isotropic-nematic transition pressure and decreases the packing fraction difference between both phases. It was shown that the solubility of a single-segment hard-sphere gas molecule does not depend on molecular order, being determined only by the packing fraction of the system. The solubility difference at the isotropic-nematic phase transition is therefore determined by the packing fraction difference at coexistence. The effect of connectivity was studied by considering relative Henry coefficients, defined as the Henry coefficient of the gas in the chain fluid divided by the Henry coefficient of the gas in the monomer fluid at same density. A linear relationship between relative Henry coefficients and packing fraction was obtained.

Binary mixtures of hard-sphere chain fluids showed a phase split and fractionation between a nematic phase concentrated in the longest component and an isotropic phase richer in the shortest component. Fractionation is a consequence of the larger tendency to align of the long chains compared to the short chains. This tendency increases with the difference in chain length between both components forming the mixture. A larger fractionation leads to a larger isotropic-nematic packing fraction difference, which was found to be always larger for the mixture than for the constituting pure components. Flexibility of the

longest component reduces fractionation, increasing the pressure and packing fraction at which the isotropic-nematic transition takes place for a specific composition of the fluid. As in the case of pure components, a linear relationship between relative Henry coefficients and packing fraction independent of the molecular order was observed.

The isotropic-nematic phase equilibria of Lennard-Jones chains was determined for: linear chain molecules with different lengths, a partially-flexible chain molecule, and a binary mixture of linear chains. Increasing chain lengths displaces the isotropic-nematic coexistence of linear Lennard-Jones chain fluids to larger equilibrium densities and lower equilibrium pressures, increasing at the same time the isotropic-nematic density difference. Flexibility reduces the anisotropy of the molecule shifting the isotropic-nematic equilibrium to larger pressures and densities, reducing at the same time the density difference between both phases. In a binary mixture of linear Lennard-Jones chains, fractionation between an isotropic phase richer in the short chains and a nematic phase richer in the long chains was observed. The isotropic-nematic density difference was found to be always larger in the mixture than for pure components, with a maximum at a certain mole fraction. The solubility of a single-segment Lennard-Jones gas molecule was calculated for linear Lennard-Jones chain fluids and for a binary mixture of them. A linear relationship between solubility difference and density difference at coexistence was identified for all linear chain systems. Furthermore, it was shown that the solubility of a Lennard-Jones gas in linear Lennard-Jones chain fluids is independent of the molecular order of the fluid at coexistence. The isotropic-nematic solubility difference in the binary mixture was observed to be always larger in the mixture than for the pure components, with an observed maximum at the mole fraction corresponding to the maximum in the isotropic-nematic density difference.

Simulation results for the isotropic-nematic transition were compared to theoretical predictions obtained from the analytical equation of state developed by van Westen *et al.*, (Refs. 77–79, 83, 84). Excellent agreement between simulation and theoretical results were observed. A rescaled Onsager theory was used in the description of hard-sphere systems showing an accurate prediction compared to simulation results. A perturbed theory approach was used in the treatment of Lennard-Jones fluids, whereby orientation dependent attractions were not considered explicitly in the development of the dispersion term. A reliable description of the isotropic-nematic phase equilibrium of Lennard-Jones fluids was obtained using this approach.

The simulation data presented in this work represents a large contribution to the liquid crystal phase behavior of chain fluids. The effect of molecular properties on the phase behavior of liquid crystals was determined using linear and partially-flexible molecules with different elongations and flexibility, for purely repulsive (hard-sphere) and soft-attractive (Lennard-Jones) interactions. Predictions obtained from the equation of state of van Westen *et al.* showed an excellent agreement with simulation data, validating the assumptions made in the development of this theory.

Samenvatting

Het vloeibaar-kristallijne fasegedrag van 'fluids' bestaande uit ketenmoleculen, alsmede de oplosbaarheid van gassen in deze 'fluids', is verkregen uit Monte Carlo simulaties. Het effect van moleculaire eigenschappen zoals elongatie en flexibiliteit is bestudeerd door middel van lineaire en deels flexibele ketenmoleculen. Lineaire ketenmoleculen zijn rigide, met alle segmenten uitgelijnd op dezelfde moleculaire as. Deels flexibele ketenmoleculen zijn opgebouwd uit een lineair- en volledig flexibel deel. Het laatste deel verschaft een zekere maat van flexibiliteit aan het molecuul. Volumetrische en thermische effecten zijn onafhankelijk van elkaar bestudeerd door middel van respectievelijk, een 'harde-bollen' en 'Lennard-Jones' potentiaal. Monte Carlo simulaties zijn uitgevoerd voor zowel ketens van harde segmenten als segmenten met Lennard-Jones interacties; de focus hierbij was op de isotroop-nematische faseovergang. De oplosbaarheid van gassen in vloeibare kristallen - vooral het oplosbaarheidsverschil tussen twee co-existerende isotrope en nematische fasen - is van belang voor gasabsorptie. Deze oplosbaarheid is bestudeerd voor een oneindig verdunde oplossing van gasmoleculen bestaande uit een enkel segment.

Monte Carlo simulaties zijn uitgevoerd in het *NPT* ensemble en in een 'expanded' versie van het Gibbs ensemble. De *NPT* simulaties zijn gebruikt om het één-fasegedrag van harde ketens te bepalen. De simulaties in het Gibbs ensemble zijn gebruikt om de isotroop-nematische faseovergang van zowel pure componenten als mengsels van harde ketens en Lennard-Jones ketens te bepalen. Vloeistofeigenschappen zoals pakkingsfracties (harde ketens), dichtheden en temperatuur (Lennard-Jones ketens), orde parameters, druk en oplosbaarheden van gassen (Henry coëfficiënten), zijn verkregen voor ketenfluids van variërende elongatie en flexibiliteit.

De studie van athermische (hardebollenpotentiaal) pure systemen, laat zien dat een toenemende ketenlengte resulteert in een grotere drijvende kracht voor de isotroop-nematisch-overgang, wat leidt tot een lagere druk en pakkingsfractie bij de faseovergang. Echter, het dichtheidsverschil tussen beide fasen toont een maximum als functie van ketenlengte. Flexibiliteit verkleint de anisotroopheid van een molecuul. Dit leidt tot een hogere overgangsdruk en een kleiner dichtheidsverschil tussen beide fasen. We tonen aan dat de oplosbaarheid van een gasmolecuul bestaande uit een enkel segment volledig wordt bepaald door pakkingsfractie van het systeem en dus niet afhangt van moleculaire ordening. Het oplosbaarheidsverschil bij de isotroop-nematisch-overgang wordt daarom uitsluitend bepaald door het dichtheidsverschil tussen beide fasen. Het effect van ketenconnectiviteit is bepaald door relatieve Henrycoëfficiënten te beschouwen, gedefinieerd als de Henrycoëfficiënt van het gas in de ketenfluid gedeeld door de Henrycoëfficiënt van het gas in een fluid van losse segmenten bij dezelfde dichtheid. We vinden een lineaire verband tussen relatieve Henry coëfficiënten en de pakkingsfractie.

Binaire systemen van fluids bestaande uit harde ketenmoleculen tonen een faseschei-ding en fractionering tussen een nematische fase geconcentreerd in de lange component en een isotrope fase geconcentreerd in de korte component. Fractionering is een gevolg van het feit dat langere moleculen een grotere neiging hebben tot ordenen van de moleculaire as. Deze neiging wordt groter naarmate het verschil in ketenlengte groter wordt. Een grotere

fractionering leidt tot een groter dichtheidsverschil bij de isotroop-nematisch-overgang. Dit dichtheidsverschil is altijd groter dan dat voor de pure componenten. Flexibiliteit van de langste component verkleint de fractionering, wat leidt tot een hogere druk en dichtheid bij de faseovergang. Voor pure systemen vinden we een linear verband tussen relatieve Henry-coëfficiënten en pakkingsfractie. Deze relatie is onafhankelijk van moleculaire ordening.

Het evenwicht tussen isotrope en nematische fasen van Lennard-Jones ketenmoleculen is uitgerekend voor de volgende systemen: lineaire (rigide) ketens van verschillende lengte, een deels flexibel ketenmolecuul, en een binair mengsel van lineaire ketens. Een grotere ketenlengte leidt tot (1) een verschuiving van de isotroop-nematisch-overgang naar lagere dichtheid en druk, en (2) een kleiner dichtheidsverschil tussen beide fasen. Een grotere flexibiliteit resulteert in een kleinere anisotroopheid van de moleculen. Dit leidt tot (1) een verschuiving van de isotroop-nematisch-overgang naar hogere druk en dichtheid, en (2) een afname van het dichheidsverschil tussen de isotrope en nematische fase. In een binair mengsel van lineaire Lennard-Jones ketens is een fractionering van de componenten tussen beide fasen vastgesteld. Het dichtheidsverschil tussen de isotrope en nematische fasen is altijd groter dan dat voor de pure componenten. Het oplosbaarheidsverschil van een Lennard-Jones gasmolecuul is berekend voor een oplosmiddel van lineaire Lennard-Jones ketenmoleculen en voor een binair mengsel van deze moleculen. Voor alle bestudeerde systemen is een lineaire relatie tussen het oplosbaarheidsverschil en het dichtheidsverschil bij de faseovergang verkregen. Het is aangetoond dat de oplosbaarheid onafhankelijk is van de moleculaire ordening bij de faseovergang. Het isotroop-nematisch oplosbaarheidsverschil in het binaire systeem is altijd groter dan dat voor de pure componenten.

Simulatieresultaten voor de isotroop-nematisch-overgang zijn vergeleken met theoretische voorspellingen verkregen uit de analytische toestandsvergelijking van van Westen *et al.*, (Refs. 77–79, 83, 84). We vinden een nauwkeurige overeenstemming tussen simulaties en theorie. De theorie is gebaseerd op een geschaalde Onsager theorie voor harde ketens, uitgebreid met een perturbatieterm voor het beschrijven van Lennard-Jones ketens. Orientatie-afhankelijke attractieve interacties tussen de moleculen zijn niet meegenomen in de perturbatieterm. Zowel voor harde- als Lennard-Jones ketenmoleculen leidt deze aanpak tot een goede beschrijving van het isotroop-nematische fasegedrag.

De simulatiedata zoals gepresenteerd in dit werk levert een grote bijdrage aan het begrip van het vloeibaar-kristallijne fasegedrag van ketenmoleculen. Het effect van moleculaire eigenschappen op het fasegedrag van vloeibare kristallen is bepaald door gebruik te maken van lineaire en deels flexibele moleculen van variërende lengte en flexibiliteit. Zowel ketens met repulsieve- (gemaakt uit harde bollen) en zacht-attractieve (Lennard-Jones) interacties tussen de segmenten zijn beschouwd. Voorspellingen verkregen uit de toestandsvergelijking van van Westen *et al.* komen uitstekend overeen met de resultaten uit de simulaties. Deze goede overeenstemming valideert de benaderingen die gemaakt zijn in de ontwikkeling van de toestandsvergelijking.

Curriculum Vitæ

Bernardo Andrés Oyarzún Rivera
16-12-1979, born in Viña del Mar, Chile

EDUCATION

Dates:	October 2007 - October 2009
Title:	Master in Process and Energy Engineering (Dipl.-Ing.)
Thesis:	Simulation and economic evaluation of cryogenic CO_2 capture
Institution:	Technische Universität Berlin
City/Country:	Berlin, Germany

Dates:	March 1999 - September 2007
Title:	Bachelor and Master in Chemical Engineering (Ing.-Civ.)
Thesis:	Lycopene extraction with supercritical CO_2
Institution:	Universidad Técnica Federico Santa María
City/Country:	Valparaíso, Chile

Dates:	October 1995 - July 1997
Title:	Secondary Education
Institution:	Colegio Alemán Quito
City/Country:	Quito, Ecuador

PROFESSIONAL EXPERIENCE

Internships

Dates:	July 2006 - March 2007
Project:	Modelling of CO_2 scrubbing by enhanced potash solutions
Employer:	BASF S.E.
City/Country:	Ludwigshafen, Germany

Dates:	January 2004 - February 2004
Project:	Estimation of critical production parameters in the salmon industry
Employer:	Salmones Multiexport Ltda.
City/Country:	Puerto Montt, Chile

Dates:	January 2003 - February 2003
Project:	Technical-economical study of a wastewater treatment plant
Employer:	Oxiquim S.A.
City/Country:	Viña del Mar, Chile

Research Assistant

Dates:	November 2009 - January 2011
Project:	Integrated solvent and process design
Employer:	Delft University of Technology
City/Country:	Delft, The Netherlands

Dates:	February 2008 - March 2009
Project:	Design and development of experimental assets for basic studies on the coalescence of water/oil/water emulsions
Employer:	Technische Universität Berlin - Sulzer Chemtech Ltd.
City/Country:	Berlin, Germany

Dates:	October 2005 - July 2006
Project:	Simulation of thermal separation processes
Employer:	Technische Universität Berlin
City/Country:	Berlin, Germany

OTHER

Workshops

- Advanced Course on Thermodynamic Models - Fundamentals & Computational Aspects, by Michel Michelsen, Technical University of Denmark, Lyngby, Denmark, January 2014.
- MolSim 2011: Understanding Molecular Simulation, by Daan Frenkel (Cambridge University) and Berend Smit (Berkeley University), University of Amsterdam, Amsterdam, The Netherlands, January 2011.

Prizes and Awards

- DPTI 2nd Annual Event, Poster award: “The effect of molecular shape on the infinite dilution solubility of gases in liquid crystals", Rotterdam, The Netherlands, November 2014.
- DAAD (German Academic Exchange Service), fellow for engineering studies in Germany, Berlin, Germany, July 2005 - June 2006.
- Universidad Técnica Federico Santa María, member of the university’s honour’s list for outstanding academic performance, Valparaíso, Chile, 2002 - 2007.

List of Journal Publications

6. **Oyarzún, B.**; van Westen, T.; Vlugt, T. J. H., *Liquid-crystal phase equilibria of Lennard-Jones chains*, accepted in Mol. Phys.

5. **van Westen, T.**; Oyarzún, B.; Vlugt, T. J. H.; Gross, J., *An analytical equation of state for describing isotropic-nematic phase equilibria of Lennard-Jones chain fluids with variable degree of molecular flexibility*, J. Chem. Phys. **142**, 244903 (2015)

4. **Oyarzún, B.**; van Westen, T.; Vlugt, T. J. H., *Isotropic-Nematic Phase Equilibria of Hard-Sphere Chain Fluids - Pure Components and Binary Mixtures*, J. Chem. Phys. **142**, 064903 (2015)

3. **van Westen, T.**; Oyarzún, B.; Vlugt, T. J. H.; Gross, J., *An equation of state for the isotropic phase of linear, partially flexible and fully flexible tangent hard-sphere chain fluids*, Mol. Phys. **112**, 919–928 (2014)

2. **Oyarzún, B.**; van Westen, T.; Vlugt, T. J. H., *The phase behavior of linear and partially flexible hard-sphere chain fluids and the solubility of hard spheres in hard-sphere chain fluids*, J. Chem. Phys. **138**, 204905 (2013)

1. **van Westen, T.**; Oyarzún, B.; Vlugt, T. J. H.; Gross, J., *The isotropic-nematic phase equilibrium of tangent hard-sphere chain fluids - Pure components*, J. Chem. Phys. **139**, 034505 (2013)

Acknowledgement

The decision of starting a PhD is usually a choice driven by curiosity in science connected with a personal commitment on understanding reality in its organic form. This romantic vision is confronted with the "reality" of science that reduces scientific progress to relevance and quantity of the scientific output. Luckily, doing a PhD was for me the result of a healthy balance between both, a romantic vision that transforms curiosity into understanding and a large amount of work that converts findings into a consistent scientific contribution.

The book that you are having now on your hands is the result of multiple hours of programming (mostly finding the bug!) and simulation runs that made possible the numerical results presented in the main part of the text. Nevertheless, the meaning of these results would not be complete without the input, discussion and contribution of the exceptional individuals that enriched the vision and work presented here.

The relevance of this scientific work was mainly possible due to the input and experience of my supervisor Thijs Vlugt. ThijsV, your absolute commitment to science was a decisive factor on making progress. I felt very lucky of having the advice (and here I have to emphasize, almost immediate advice!) of somebody that knew precisely what to do at bifurcations and dead-end roads.

Coherence in this book is, in a large part, a consequence of the collaboration with Thijs van Westen. ThijsvW, many of the conclusions that appear in this thesis are a result of our discussions (after polishing some stubbornness from both sides). Comparing simulation results with theoretical predictions did not only "match the lines with the points" but also gave us a deeper understanding of the physics of fluids.

Programming and performing simulations have many tricks and ways or, better to say, elegant solutions to specific requirements. I would like to thank Sayee Prasaad Balaji and Sondre Kvalvåg Schnell for their help in making the coding and simulation work much simpler.

I would also like to thank all the people involved in the liquid crystals project, specially Mariëtte de Groen and Theo de Loos for all the discussions about experiments and the behavior or real liquid crystal fluids.

The vision and motivation that made this book possible is strongly related to all the people with which I have shared this PhD path. I find very difficult now to write one name before another, because everybody had a special contribution in shaping this work and I hope to find the words for expressing my gratitude to all of you (including the ones that are not named here):

Irina, you are the person that has been closer to me during this process. You know the difficulties and rewards that came across, and I had the fortune to be accompanied by you during this time. Your presence gave me the energy to bring this book to an end, and it is also the inspiration for the dreams and facts that have came, and will come, along. I appreciate all your patience and efforts while this thesis was taking form, while, somehow, everything else was taking form. *Sunt foarte bucuros că suntem aici unul pentru celălalt!*. I am very thankful to you for the design of the cover (I feel that you read my mind!), making a beautiful and meaningful image for presenting this work.

ThijsvW, apart from all the science related work said above, I have to say that it was great to have you as a colleague. From the first talk that we had that influenced me in taking the decision of joining this project, until the last discussions about "... and now what?", I found always a good person to talk and to be listen. Trips were amazing, beer was refreshing, and always with fine music.

Sara, Jorge, Marta, I think that you are the ones that I know since my very first days in Holland. Marta, many thanks for all the favors including letting me to be inscribed at your place when I was starting to deal with the dutch bureaucracy. I am very happy that I could showed you the place where I come from (including an earthquake magnitude 8.2 and many 7+, which in any case are definitely an experience to remember!). Sara and Jorge, many thanks for all the talks, dinners, bike trips and specially for had taking part of your wonderful wedding. Sara, Jorge and Marta, many thanks for your friendship.

Alex, you have been always been there, man. It is difficult to find somebody that it is willing to meet or have a beer just after a call. Thanks for all the talking and joking around.

Shouruk (Su), I am very happy that we were flat-mates keeping always good spirits at home. Many thanks for watering the plants :p and all the other things that I could have not done just by myself.

Dragos, without you I could have not met the girl that I love!. Many thanks for all the time spent together, and for being always available when your help was needed.

Stevia, I want to thank you for your humor and advices. I will always admire your capacity of knowing what-to-do as cheaper-as-possible.

Sebastián, many thanks for all the talks with some "chelitas" at the side. I was happy of meeting somebody with who I could share the feeling of coming from the middle of the world.

I would also like to thank everybody in the office, the old and new generations: Sayee (the boss!), Samir (life is complicated), Albert (lunch!), Lawien, Carsten, Mahinder, Emiliano, Alondra/Timo, Sergio, Stephanie, Tim, Karsten, Julia, Dion and Daniel. Marloes, you and your social skills are definitely an important contribution to the department.

I would also like to thank Brian Tighe with who I had the privilege to work as teaching assistant during the Thermodynamics for Process & Energy course.

And also, I would like to thank all of you that have been far but at the same time very close, Katharina, Diego, José, Marta, María, Sebastián/Simona, Steffi, Andrea, Nico, Dieguito, Sandra and Juanito.

Y finalmente, Papá/mamá/ñaña, esta tesis está dedicada a ustedes. El que haya llegado a seguir y a terminar un programa de doctorado es todo consecuencia del apoyo incondicional de su parte. Ustedes siempre creyeron en mi y que podría cumplir cualquier proyecto con el que soñara. A ustedes le debo la visión y las ganas de explorar que me han llevado a sitios tan lejanos. Y aunque la distancia siempre nos ha dolido, creo que hemos podido encontrar la manera de estar cerca en todos estos años.